

# Journal of Materials Chemistry A

Materials for energy and sustainability

Accepted Manuscript

This article can be cited before page numbers have been issued, to do this please use: F. Baskoro, S. U. Sharma, A. L. Lubis and H. Yen, *J. Mater. Chem. A*, 2024, DOI: 10.1039/D4TA06028H.



This is an Accepted Manuscript, which has been through the Royal Society of Chemistry peer review process and has been accepted for publication.

Accepted Manuscripts are published online shortly after acceptance, before technical editing, formatting and proof reading. Using this free service, authors can make their results available to the community, in citable form, before we publish the edited article. We will replace this Accepted Manuscript with the edited and formatted Advance Article as soon as it is available.

You can find more information about Accepted Manuscripts in the [Information for Authors](#).

Please note that technical editing may introduce minor changes to the text and/or graphics, which may alter content. The journal's standard [Terms & Conditions](#) and the [Ethical guidelines](#) still apply. In no event shall the Royal Society of Chemistry be held responsible for any errors or omissions in this Accepted Manuscript or any consequences arising from the use of any information it contains.

## ARTICLE

# Recent Advances p-type Polymeric Electrode Materials towards High-Voltage 4.0 V-class Organic Lithium-ion Batteries

Febri Baskoro,<sup>\*‡<sup>a</sup></sup> Santosh U. Sharma,<sup>‡<sup>a</sup></sup> Andre Lammiduk Lubis,<sup>a</sup> Hung-Ju Yen<sup>\*<sup>a,b</sup></sup>

Received 00th January 20xx,  
Accepted 00th January 20xx

DOI: 10.1039/x0xx00000x

Lithium-ion batteries stand at the forefront of energy storage technologies, facilitating the transition towards sustainable and electrified systems. To meet the increasing demands for energy density, safety, and longevity, the development of high-performance electrode materials is paramount. Although inorganic materials have been dominated in the current lithium-ion battery cathodes, the widely utilized inorganic cathode materials suffer from drawbacks such as limited capacity, high energy consumption during production, safety hazards associated with toxic metals (Li, Co, Mn, Ni), and high raw material costs due to the limited or localized resource distributions. Alternatively, polymeric materials have been seen and considered as a promising candidate to replace conventional inorganic materials, due to their advantages such as abundance and environmentally friendly resources, structural diversity, ease of functionalization, fabrication, and recycling, high capacity and rate capability, and excellent flexibility. This review article explores the strategic design principles underlying the synthesis and optimization of p-type polymeric electrode materials for next-generation 4.0 V-class batteries. Through a comprehensive analysis of recent advancements, morphology control, and interface engineering, this review elucidates the key strategies employed to achieve high-energy-density electrodes. Additionally, this review discusses the fundamental mechanisms governing the electrochemical performance of p-type polymeric electrodes and highlights emerging trends and future directions in the field. By integrating insights from materials science, electrochemistry, and engineering, this paper provides a roadmap for the rational design and development of p-type polymeric electrode materials towards the realization of high-performance 4.0 V-class lithium-ion batteries.

## 1. Introduction

In today's fast-paced and interconnected world, lithium-ion batteries (LIBs) have emerged as the linchpin of modern society, powering a vast array of devices that have become essential to our daily lives. From smartphones and laptops to electric vehicles (EVs) and renewable energy storage grids, LIBs serve as the backbone of our digital economy and the catalyst for the transition towards a sustainable energy future.<sup>1-3</sup> As the world's dependency on LIBs continues to deepen, driven by advancements in technology, evolving consumer preferences, and global efforts to combat climate change, it becomes increasingly imperative to understand their significance, challenges, and prospects. However, the reliance on LIBs also presents challenges, including the need for improved safety, the environmental impact of raw material extraction, and the development of effective recycling strategies to manage end-of-life batteries.<sup>4</sup> These challenges must be addressed to ensure the sustainable growth of LIB technology. In this regards,

innovations in battery chemistry, design, and manufacturing processes are expected to further improve the energy density, safety, and lifecycle of LIBs, contributing to their continued importance in a low-carbon future.<sup>5</sup>

Generally, a conventional LIB cell consists of a positive electrode (cathode), negative electrode (anode), and non-aqueous electrolyte system as well as a separator to prevent physical contact between those two electrodes (Fig. 1a). In principle, when the battery is being charged, the Li<sup>+</sup> moves from the cathode to the anode through the electrolyte; vice versa, during discharge, the Li<sup>+</sup> will move back from the anode to cathode and release electrical current. As cathode materials, typical Li-intercalated materials, such as LiCoO<sub>2</sub> (a lithium metal oxide with layered structure), have been widely used as lithium-ion source. Meanwhile, graphite has been widely utilized as the anode material to store Li<sup>+</sup> in its layers via intercalation process. Notably, both cathode and anode materials should be reversibly

<sup>a</sup> Institute of Chemistry, Academia Sinica, Taipei 115, Taiwan. E-mail: [febri\\_baskoro@yahoo.co.id](mailto:febri_baskoro@yahoo.co.id); [hjyen@gate.sinica.edu.tw](mailto:hjyen@gate.sinica.edu.tw)

<sup>b</sup> Sustainable Chemical Science and Technology Program, Taiwan International Graduate Program (TIGP), Academia Sinica and National Taiwan University, Taipei 11529, Taiwan

‡ These authors contributed equally.

See DOI: 10.1039/x0xx00000x



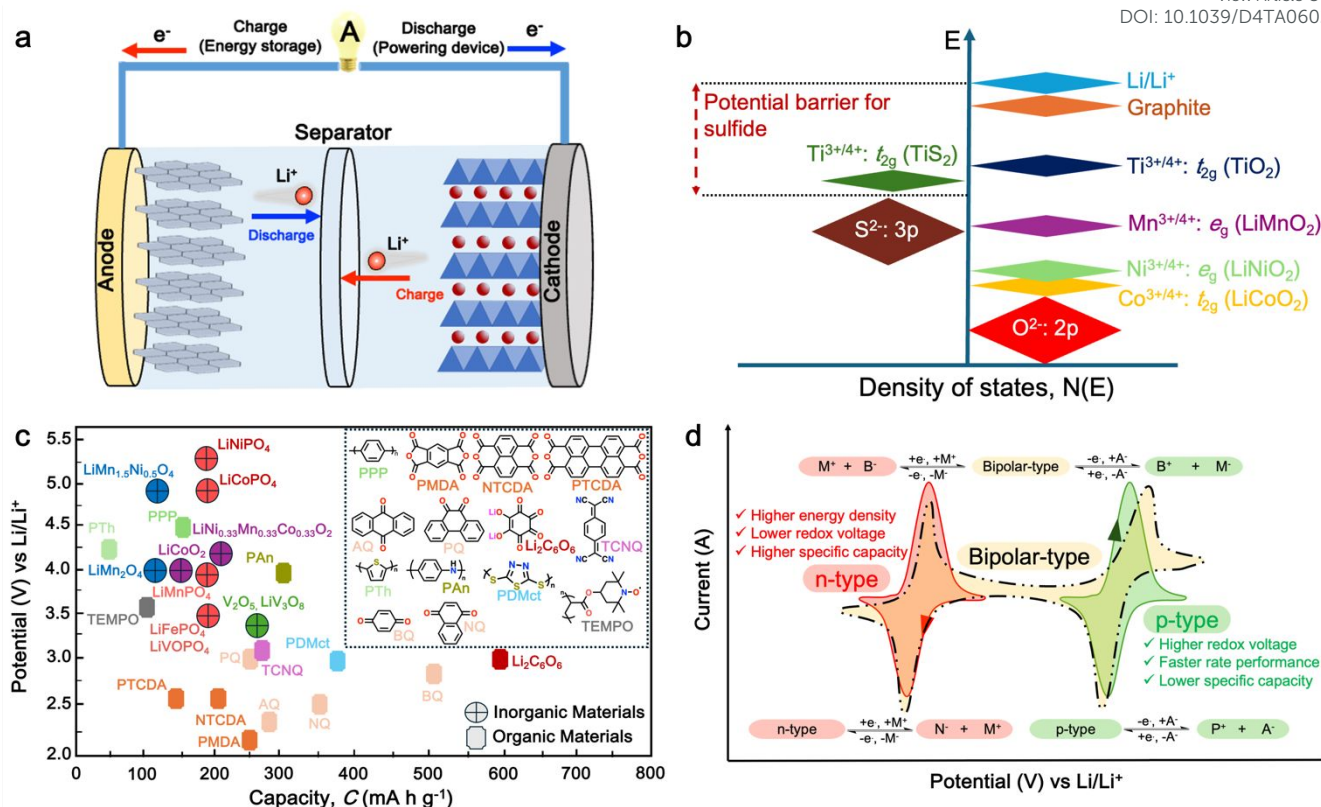


Fig. 1 (a) Schematic of a full cell Li-ion battery. (b) Positions of the redox energies relative to the top of the anion: p bands. The top of the  $S^{2-}$ : 3p band lying at a higher energy limits the cell voltage to  $<2.5$  V with a sulfide cathode. In contrast, the top of the  $O^{2-}$ : 2p band lying at a lower energy enables access to lower-lying energy bands with higher oxidation states and increases the cell voltage substantially to  $\sim 4$  V. Reproduced from ref. 6. (c) Recent cathode materials development for LIBs. (d) The redox behavior of organic molecules in electrochemical processes.

inserted and removed the  $Li^+$  from its respective structure.<sup>7</sup> Furthermore, since cell voltage is established by the energy difference between the anode and cathode, thus, cathode energy should lie as low as possible, and the anode must lie as high as possible. This implies that cathode materials would require the stabilization of higher oxidative states with a lower-lying energy band, while the anode materials would require the stabilization of lower oxidative states with a higher-lying energy band.<sup>6, 8, 9</sup> The electrolyte is the third component of LIB that serves as a medium to transport  $Li^+$  ions involved during charging/discharging process of the LIBs.<sup>10</sup> Although the role of electrolytes is often considered trivial, the choice of electrolyte system is crucial depending on the compatibility with both electrodes.<sup>11</sup> Besides the importance and technological advancement in the LIB components, development in cathode materials has been attracted research interests since it plays important role in defining the working potential of LIB cell, thus gives significant impact on the energy density of the battery.

### 1.1 Current-status of cathode materials for LIBs

Since the cathode materials are key in determining the cells' voltage and, consequently, its energy density, the high-energy-density batteries require high working potential cathodes,

paired with anodes that can provide a high specific capacity.<sup>2</sup> In early study of LIB cathode, Goodenough employed the basic understanding that the top of the  $S^{2-}$ : 3p band lies at a higher energy than the top of the  $O^{2-}$ : 2p band to design oxide cathodes (Fig. 1b). This means that the access to lower-lying energy bands with higher oxidation states such as  $Co^{3+/4+}$  and hence the higher cell voltage will be limited by the top of the  $S^{2-}$ : 3p band and attempts to lower the cathode redox energy by accessing higher oxidation states in a sulfide will result in an oxidation of  $S^{2-}$  ions to molecular disulfide ions  $(S_2)^{2-}$ . In contrast, in an oxide, the cathode redox energy can be significantly lowered by accessing lower-lying energy bands such as  $Co^{3+/4+}$  and hence the cell voltage can be increased to as high as 4 V as the top of the  $O^{2-}$ : 2p band lies at a lower energy compared to the top of the  $S^{2-}$ : 3p band. This basic idea led to the discovery of oxide cathodes materials such as layered oxide, spinel oxide, and polyanion cathodes.<sup>6, 8, 9</sup>



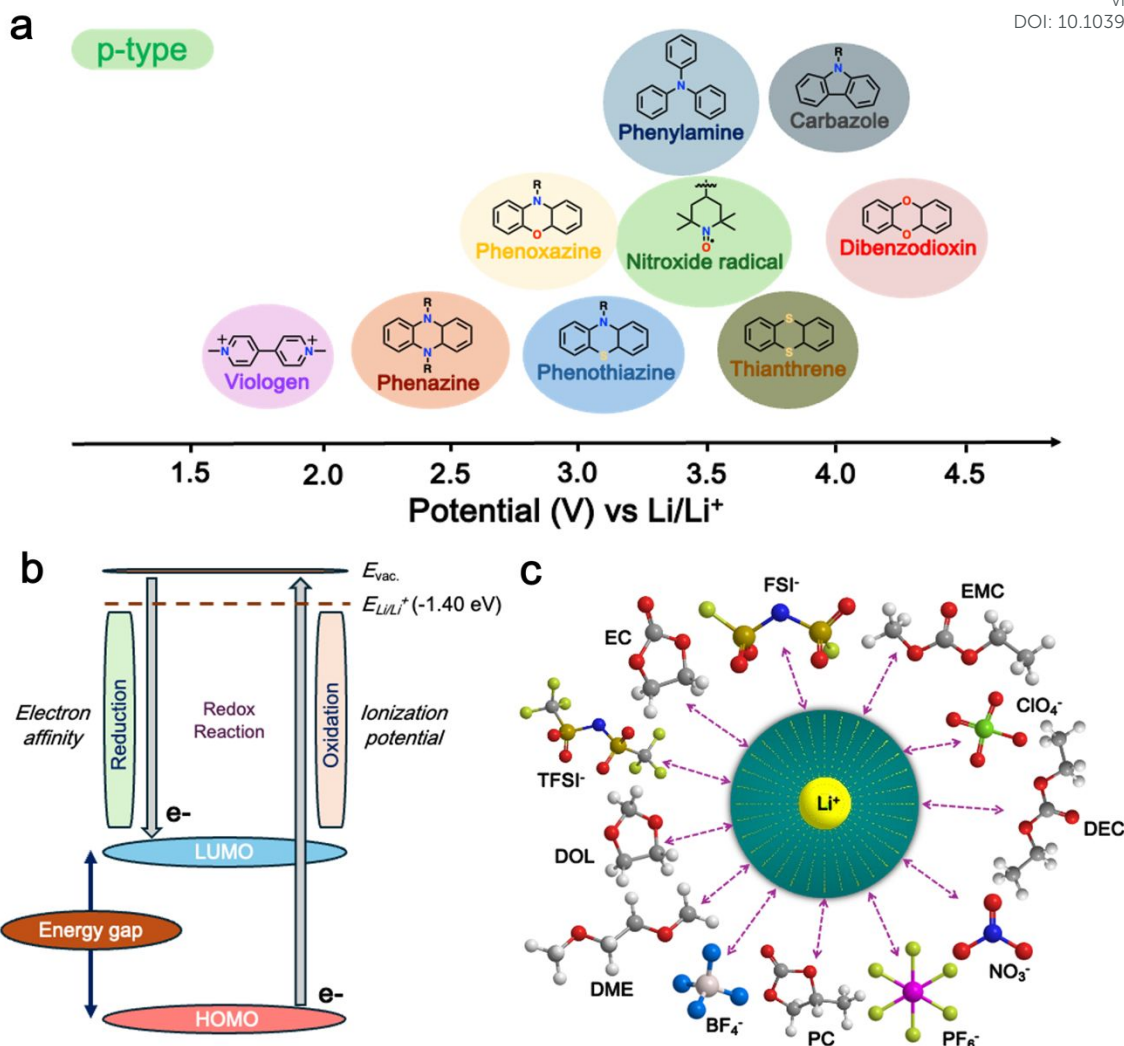


Fig. 2 (a) Different p-type organic materials along with their average redox voltages. (b) Frontier molecular orbitals (FMOs) relevant to the redox reactions of redox-active organic materials. (c) Schematic representation showing a solvated anion and cation within the electrolyte. Reproduced from ref. 12.

In general, the most common cathode materials used in commercial LIBs are based on transition metal oxides (Fig. 1c), such as lithium cobalt oxide (LiCoO<sub>2</sub>),<sup>13</sup> lithium manganese oxide (LiMn<sub>2</sub>O<sub>4</sub>),<sup>14</sup> lithium nickel manganese cobalt oxide (LiNiMnCoO<sub>2</sub> or NMC),<sup>15</sup> and lithium iron phosphate (LiFePO<sub>4</sub> or LFP).<sup>16, 17</sup> However, they suffer from a gradual capacity fade during cycling, which is attributed to the dissolution of transition metal ions into the electrolyte, leading to the accumulation on the electrode thus results a high resistive solid electrolyte interphase (SEI) layer on the cathode surface.<sup>18, 19</sup> Furthermore, there are several challenges persist associated with the development of inorganic-based cathode materials:<sup>20-23</sup> Firstly, with the increasing demand of high energy density batteries, there is a limitation in the theoretical capacity and working potential of current inorganic-cathode materials.<sup>24</sup> Secondly, the high cost of raw materials due to its scarcity and environmental burden.<sup>6</sup> Furthermore, such complex and high-temperature synthesis processes are required thus further

enhance the material cost.<sup>25</sup> Thirdly, safety issue associated with unstable cathode materials such as LiCoO<sub>2</sub>, which can pose thermal runaway risks at high voltages, potentially leading to fires or explosions.<sup>26</sup>

Alternatively, organic cathode materials have emerged as promising contenders in the pursuit of next-generation energy storage solutions (Fig. 1c). Organic materials composed of elements such as C, O, N, and S have been recognized as a promising alternative to inorganic materials for battery electrodes.<sup>27</sup> These materials have several advantages, including abundance, light weight, and environmental benignity.<sup>3, 28, 29</sup> They can be used in various types of batteries, including metal-ion,<sup>30</sup> dual-ion,<sup>31, 32</sup> molecular-ion,<sup>33</sup> and anion-shuttle batteries,<sup>34</sup> without being limited by the choice of counterions. Additionally, the flexible intermolecular packing of these materials has the potential to provide higher rate capability than that of inorganic materials.<sup>3, 28</sup> Most importantly, the physicochemical and electrochemical





properties of these materials can be easily tailored through elaborate molecular design.<sup>35</sup>

In general, electroactive organic materials can be broadly classified into three categories based on their charge states during redox reactions, namely p-type, n-type, and bipolar-type (Fig. 1d). As shown in Fig. 1d, the p-type materials undergo oxidation from their neutral state, resulting in a positively charged state, while n-type materials accept an electron and become negatively charged.<sup>36</sup> Bipolar-type materials usually contain both p- and n-type moiety that can utilize both positively and negatively charged states. The specific moiety, or redox center, in the organic molecule governs the electrochemical response and defines the material type. Comparing the organic-based cathode, p-type organic electrodes generally have higher redox potentials than that of n-type materials due to a lower electron energy level, thus results in higher redox potentials.<sup>12</sup> Notably, the type of redox material should be carefully considered in understanding its electrochemical mechanism, as it is sensitive to the nature of the anion and cation dissolved in the electrolyte. For example, the electrochemical activity of p-type materials is affected by the type of anions in the electrolyte. The anions in the electrolyte can coordinate with the redox centers of p-type materials, influencing their electrochemical behavior.<sup>12</sup> Meanwhile, as n-type materials, the positively charged cations (Li<sup>+</sup>, K<sup>+</sup>, Na<sup>+</sup> etc.) determine their electrochemical behavior such as voltage, specific capacity and cyclability.<sup>30, 37-39</sup>

Although organic materials offer many benefits as an alternative electrode material in LIBs, it still faces some challenges that need to be addressed.<sup>28</sup> One major hurdle is their typically low electronic conductivity, which can limit the rate capability and overall performance of the battery.<sup>40, 41</sup> Stability and cyclability are also critical considerations for organic cathode materials. Some organic compounds may suffer from poor stability over repeated charge-discharge cycles, leading to capacity fade and reduced battery life.<sup>42</sup> Additionally, solubility in electrolytes poses a challenge for certain organic cathode materials. The dissolution of active molecules into the electrolyte can result in capacity loss and electrolyte degradation over time.<sup>43, 44</sup> In brief, both inorganic and organic materials have distinct roles to play as cathode materials for LIBs. While inorganic cathodes currently lead in commercial applications, ongoing research into organic cathodes promises advancements that could lead to more sustainable and cost-effective energy storage solutions.

## 1.2 Definition of polymeric electrodes

To improve the stability and cyclability of organic-based electrode materials, several approaches have been explored such as polymerization,<sup>45-47</sup> the use of high-concentration electrolytes,<sup>48, 49</sup> nanostructures,<sup>50-53</sup> and composite formation with advanced carbon materials.<sup>54-57</sup> Among those approaches, polymerization process is considered a significant strategy that could solve the dissolution problem and improve the material stability of an organic-based electrode in an electrolyte.<sup>58-63</sup> Since then, the definitions of polymeric electrodes in LIBs have

emerged as type of electrode material made from polymer-based materials. They are known for their flexibility, conductivity, and chemical stability, making them suitable for use in various electrochemical devices like batteries and capacitors.<sup>29</sup> Their design can be easily customized at the molecular level to meet specific energy storage requirements. Benefiting from organic-based cathode and excellent physical properties, polymeric electrodes emerged as one of new class of electrode materials to replace traditional inorganic electrodes in LIBs. Furthermore, polymeric materials have been proven as the active component that can serve as either the anode or cathode or both electrodes in a LIBs setup.<sup>58, 62-65</sup> Unlike the small-organic molecules which has a major concern on their inherent solubility in organic electrolytes, which limits their widespread use and development, the higher molecular weight of polymer electrode materials often reduces their solubility in organic electrolytes, making them more promising candidates for the next generation of LIBs.<sup>66</sup> One of unique properties of polymer-based electrode is their flexibility, as polymeric electrodes can be made into flexible films thus opening the way for the flexible batteries. Additionally, polymeric materials are generally less expensive than inorganic materials, making them a cost-effective alternative.<sup>67</sup> Furthermore, polymeric materials are more environmentally friendly than inorganic materials, as they do not require the mining and processing of heavy metals. This distinction underscores the potential of these polymers as a favorable trend in advancing LIB technologies. Despite these advantages, polymeric electrodes also face some limitations which need room of improvement. One major limitation is their lower electrical conductivity compared to inorganic materials. This can result in lower charge transfer efficiency and reduced battery performance.<sup>28</sup> Additionally, polymeric materials generally have lower lithium-ion conductivity than inorganic materials, which can lead to slower ion transport and reduced battery performance.<sup>3</sup>

Earlier studies have been shown that conducting polymers (CPs) such as polythiophene (PTh), polypyrrole (PPy), and polyaniline (PANI), can be oxidized by accepting anions, which significantly increases their electrical conductivity, and can be applied in rechargeable batteries.<sup>68-71</sup> However, their use was limited due to their low specific capacity and sloppy voltage profiles. Furthermore, nitroxide radical polymers, which can undergo bipolar-type redox reactions, have also been proposed as an alternative organic cathode material.<sup>72</sup> These polymers can accept an anion or cation, which allows them to undergo single-electron oxidation (p-type) or single-electron reduction (n-type). However, their low electrical conductivity and high solubility made them impractical.<sup>73, 74</sup> Since then, many researchers have focused on n-type organic electrode materials<sup>75-78</sup> such as benzoquinone,<sup>79</sup> anthraquinone,<sup>80</sup> terephthalate,<sup>81</sup> and imide<sup>53, 82</sup> derivatives. However, the redox voltages of these n-type organic materials are typically limited below 3.0 V vs. Li/Li<sup>+</sup>, which is inferior to conventional cathode materials due to their redox mechanism (Fig. 1c).

On the other hand, high redox voltage p-type organic materials such as phenazine,<sup>83, 84</sup> carbazole,<sup>85, 86</sup> and



phenylamine<sup>87, 88</sup> derivatives are gaining attention for their application in LIBs. These materials undergo reversible oxidations to form cationic species, which can lead to faster rate performance. For example, Phenoxazine (**PXZ**) based cathodes offer a specific capacity of 112 mA h g<sup>-1</sup> at 1C with an average discharge voltage of 3.7 V vs. Li/Li<sup>+</sup> and retain 73% capacity at a high rate of 20C.<sup>89</sup> Benzo[*b*]phenazine-based polymer (**p-DPBPZ**) displays initial discharge specific capacities of 151 mA h g<sup>-1</sup>, with energy and power densities reaching 537 Wh kg<sup>-1</sup> and 1,965 W kg<sup>-1</sup>, respectively.<sup>90</sup> Furthermore, indole[3,2-*b*] carbazole (**DEICZ**) shows stable plateaus at high discharge potentials of 3.44 V and 4.09 V vs. Li/Li<sup>+</sup>.<sup>91</sup> Moreover, materials like those based on extended  $\pi$ - $\pi$  conjugation of dioxin have also been reported to surpass the redox potential limit of organic cathode materials, achieving high voltages over 4.1 V.<sup>92</sup> Additionally, on the basis of structural design of polymer electrode, we have successfully combined the triphenylamine (p-type) and naphthalimides (n-type) moieties in a polymer backbone, resulting significant increase on specific capacity and working voltage up to ~202 mA h g<sup>-1</sup> and 4.5 V vs. Li/Li<sup>+</sup>, respectively.<sup>62</sup> Furthermore, our studies also found that conformational structures (isomerism) and bridge functionalization on the imide units impact the electrochemical performance of the polymer electrodes by regulating their intrinsic properties such as charge storage behavior, ion diffusivity, and activation energy.<sup>62-64</sup> These examples underscore the potential of polymer electrode materials and the important of structural design in the polymer structure to achieve high energy density and fast charge-discharge rates as well as high-voltage ability, making them promising candidates for advanced LIBs. In this article, we delve into the cutting-edge advancements in designing high-voltage p-type organic cathode materials for LIBs. We explore a variety of p-type organic materials that have emerged over the last decade, each based on distinct redox-active centers. Our discussion encompasses their electrochemical attributes, such as redox potentials and kinetics, and how these properties influence the overall performance of LIBs. By providing a comprehensive overview of the progress in p-type organic materials, we aim to highlight their potential to revolutionize the design of high-voltage polymer-based cathodes for LIBs applications through a comparison and contrast of the molecular design strategies employed.

## 2. Requirement, properties, and the challenges of polymer electrodes

### 2.1 General requirements of LIBs cathode materials

The cathode plays a pivotal role in LIBs as it serves as both the source and the recipient of lithium ions during the charge and discharge cycles as well as defining the working potential of LIB cells. To ensure optimum performance, several aspects need to be considered on designing next-generation cathode materials such as:<sup>93-95</sup>

i. **Redox-active ion:** The presence of a redox-active ion is crucial as it enables the material to undergo reversible oxidation and reduction processes during charge and

discharge cycles. This redox activity allows for the storage and release of lithium ions, contributing to the overall capacity of the battery. In general, materials with well-defined redox chemistry can exhibit high energy density and excellent cycling stability, making them ideal candidates for high-performance battery electrodes.

- ii. **Reversible lithium reaction:** The ability of the material to undergo reversible reactions with lithium ions is essential for maintaining the integrity of the host structure throughout multiple charge and discharge cycles. This reversible process ensures that the active material can efficiently accommodate and release lithium ions without significant structural degradation. Furthermore, a stable host structure not only prolongs the cycle life of the battery but also helps maintain its energy storage capacity over time.
- iii. **High free energy of reaction:** A high free energy reaction with lithium ions is desirable as it directly correlates with the capacity of the battery electrode material. Materials with a high capacity can store a greater number of lithium ions per unit mass, leading to enhanced energy storage capabilities. Achieving a voltage around 4 V, while considering the stability of the electrolyte, is crucial for maximizing the energy density of LIBs and meeting the demands of high-energy storage applications.
- iv. **Ionic electrical conductivity:** High-power density in LIBs relies on rapid kinetics of lithium-ion insertion/extraction and fast electronic conductivity within the electrode material. Fast lithium diffusion rates and low activation energies enable swift ion transport, ensuring efficient electrochemical reactions. This facilitates rapid energy transfer, ideal for applications such as electric vehicles and portable electronics. Additionally, high electrical conductivity could minimize resistance and voltage losses during electrochemical process thus further enhancing overall energy density and efficiency.
- v. **Structural stability:** Maintaining structural stability is crucial to prevent mechanical deformation, pulverization, or structural collapse of the electrode material during prolonged cycling. Structural stability ensures that the active material retains its integrity and functionality, contributing to the long-term performance and cycle life of the battery. Materials with robust structures exhibit excellent mechanical strength and resistance to degradation, even under extreme operating conditions, enhancing the reliability and safety of LIB systems.
- vi. **Cost-effectiveness and environmental challenges:** Cost-effectiveness and environmental considerations play pivotal roles in the development of LIB materials. Economically feasible materials not only enable widespread adoption by reducing manufacturing costs but also contribute to the competitiveness of LIBs in various markets, fostering innovation and advancement in battery technology. Addressing environmental concerns by utilizing non-toxic, recyclable, and sustainably sourced materials helps minimize the ecological footprint of batteries, aligning with global efforts towards a cleaner



and more sustainable future. Furthermore, promoting the use of environmentally benign materials encourages the development of greener battery technologies, supporting the transition to renewable energy systems and reducing dependence on finite resources.

## 2.2 Properties of p-type polymer electrode

The redox potential of a material is a critical factor in determining its suitability for use in energy storage devices. The redox potential is influenced by the molecular structure of the material and the nature of the electrolyte used.<sup>96</sup> In the case of p-type materials, their redox potential is higher than that of n-type materials, making them more suitable for use as cathodes in energy storage devices (Fig. 2a). At the core of their functionality, their conjugated molecular structure, featuring alternating single and double bonds along the polymer backbone, enables the delocalization of electrons thus facilitates the movement of charge carriers through the material.<sup>97, 98</sup> Furthermore, the p-type polymers offer tunable energy levels through chemical modifications which allows precise engineering of their electronic properties to match specific device requirements.<sup>99, 100</sup> Moreover, p-type polymers have also been recognized to provide good thermal and structural stability, which is essential for withstanding the processing and operational conditions of electronic devices.<sup>101</sup> Some p-type polymers could be designed to be air-stable thus eliminating the need for stringent inert atmospheres during device fabrication.<sup>102, 103</sup> Additionally, their high charge carrier mobility, compatibility with other materials used in device architectures, and relatively low bandgap further contribute to their versatility and suitability for a wide range of applications.<sup>104-106</sup>

Furthermore, in p-type organic cathode materials, the performance is significantly affected by factors such as redox voltage and energy levels, as well as the impact of counter ions.<sup>12, 89</sup> The redox potential of p-type organic cathode materials is crucial for their electrochemical performance, determined by their highest occupied molecular orbital (HOMO) energy level (Fig. 2b).<sup>12</sup> Therefore, adjusting this HOMO level of p-type organic cathode materials through heteroatoms and functionalization could further optimize their performance in energy storage applications.<sup>107</sup> Meanwhile, the counter ions, such as  $\text{BF}_4^-$ ,  $\text{PF}_6^-$ ,  $\text{FSI}^-$ , and  $\text{TFSI}^-$ , also significantly impact p-type organic cathode materials' performance on their charge transport properties, ionic conductivity, and ultimately effecting their storage capacity and power density (Fig. 2c).<sup>108</sup> Overall, p-type polymers offer a combination of properties that make them promising candidates for cathode materials in LIBs.<sup>12, 109</sup>

## 2.3 Challenges and limitations

P-type polymers possess unique properties that make them attractive for various applications, including energy storage such as LIBs. These polymers are characterized by their ability to accept and transport charge ions, within their structure. This property stems from the presence of electron-deficient units or dopants within the polymer backbone. Apart from the

outstanding properties that have been elaborate in previous section, the development of p-type polymers electrode faces challenges such as:<sup>12, 66, 110-116</sup>

- i. **Susceptibility to degradation:** Since the p-type polymer cathode offers high voltage operation, maintaining redox reversibility at higher potential becomes critical during operation. This high voltage operation coupled with electrolyte incompatibility could pose irreversible reactions, structural changes or degradation during charge and discharge cycles which can result in capacity fading and reduced cycling stability. Therefore, enhancing materials stability and electrolyte compatibility is required to ensure long operation p-type polymer cathode in LIBs.
- ii. **Low specific capacity:** Many p-type polymers exhibit lower specific capacities compared to traditional inorganic cathode materials due to minimum redox active sites. This lower specific capacity limits the energy density of LIBs utilizing p-type polymers as cathodes, impacting their overall performance and suitability for certain applications. Additionally, due to the fact that the p-type polymers operate by incorporating anions from the electrolyte during electrochemical process, therefore the corresponding anions play an important role on the defining specific capacity. Furthermore, this anions involvement during electrochemical process along with the organic solvent instability in the electrolyte at high-voltage ( $> 4.0$  V) could result electrolyte degradation and consumption over the cycles leading to lower energy density. Consequently, providing more redox active sites in the polymer backbone through material design and electrolyte optimization is essential to enhance the storage.
- iii. **Minimum rate capability:** The rate capability of p-type polymers refers to their ability to deliver and accept mobile ions at high charge and discharge rates. Some p-type polymers may exhibit limited rate capability as a result of slow ionic diffusion kinetics due to poor electronic conductivity. Hence, enhancing the electronic conductivity of p-type polymer cathodes is crucial to provide rapid ion mobility during electrochemical process.
- iv. **Interfacial issues:** The interface between the p-type polymer cathode and electrolyte plays a crucial role in ion transport and overall battery performance. Poor electrolyte wetting properties, resistive electrode-electrolyte interphase, or unwanted interface reactions significantly hinder ion diffusion and consequently decrease battery efficiency. Therefore, addressing these interfacial issues is essential to improve ion transport kinetics and enhance battery performance.
- v. **Electrode preparation issues:** Although polymer-based cathodes has minimum solubility in electrolytes, it often suffers from aggregation during electrode fabrication thus reducing effective surface area for ion transport and electrochemical reactions. This problem is worse in high-mass-loading electrodes, leading to uneven current distribution, increased resistance, and reduced capacity. In large-scale preparation, low electrical conductivity further hinders performance. Therefore, proper solvent selection



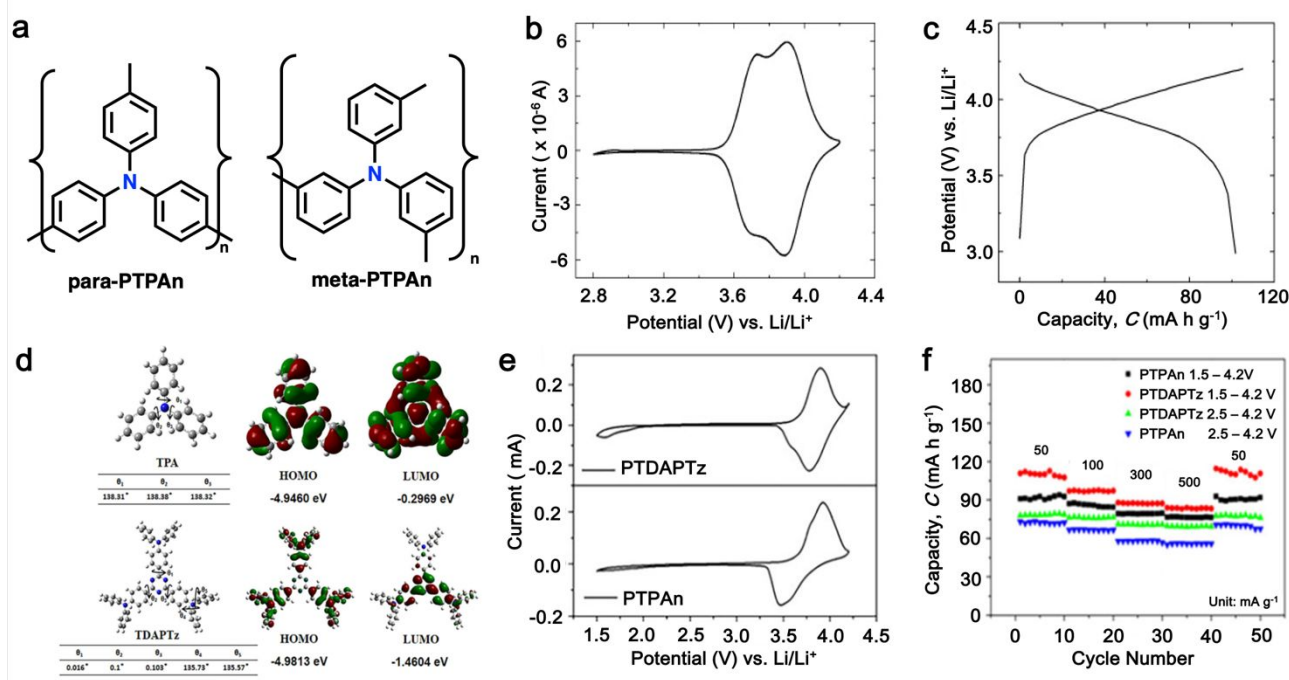


Fig.3 (a) Two possible isomers of **PTPA**, (b) The cyclic voltammetry (CV) curve of **PTPA** in 1 M LiPF<sub>6</sub> EC/DMC (1:1 v/v) measured at a scan rate 1 mV s<sup>-1</sup>, (c) The Charge–discharge curves of Li–**PTPA** test cells at a constant current of 50 mA g<sup>-1</sup>. Reproduced with permission from ref. <sup>117</sup>. Copyright 2008 Elsevier. (d) The molecular orbital (HOMO and LUMO) and geometric structure of **TPA** and **TDAPTz** monomers calculated theoretically by using the DFT calculation at the B3LYP/6-31 g level performed via Gaussian 09. (e) CVs of **PTDAPTz** and **PTPA** in 1 M LiPF<sub>6</sub> EC/DMC (v/v 1:1) measured at 1 mV s<sup>-1</sup> between 1.5 and 4.2 V. (f) Rate performances of the **PTDAPTz** and **PTPA** electrodes at various current rates. Reproduced with permission from ref. <sup>118</sup>. Copyright 2018 John Wiley and Sons.

and structural design are crucial for improving processability. Furthermore, adding conductive additives like carbon black, nanotubes, or graphene can be introduced to enhance electrical and ionic conductivity of the polymer electrode.

vi. **Cost and Scalability:** The production cost and scalability of p-type polymers are important considerations for their practical application in large-scale energy storage systems. Polymers with rare or expensive dopants, complex synthesis, and low processability may face challenges in cost-effective production and scalability, hindering their practical application for commercial viability. Therefore, developing cost-effective synthesis methods, utilizing abundant and sustainable raw materials are essential for realizing the widespread adoption of p-type polymer cathodes in LIBs and other energy storage devices.

### 3. Current progress of p-type polymer cathode materials

#### 3.1 Polytriphenylamine

As a p-type compound, the structural specificity of the polytriphenylamine (**PTPA**) is recognized from the radical nitrogen redox centers that are stabilized by the phenyl groups, which facilitates the radical redox reaction and charge-

transporting processes. This structural feature allows for high power capability and high energy density at prolonged cycling. Additionally, the porous polymer structure with abundant interconnected holes due to a rigid phenyl groups, provides sufficient surface area and ionic channels for rapid ion mobility.<sup>119</sup> Additionally, as promising organic cathode material for LIBs, the redox activity of **PTPA** is recognized from doped/de-doped process of anionic species on the nitrogen radical, providing specific capacity of ~109 mA h g<sup>-1</sup>.<sup>62, 88, 120, 121</sup> However, some issue related to low theoretical capacity, conductivity and processability still hindered **PTPA**-based polymer for practical application. In this regard, Feng and his co-workers reported a simple **PTPA** (Fig. 3a) as organic cathode material for LIBs.<sup>117</sup> The charge-discharge curves of the **PTPA** electrode exhibit an approximately linear relationship between voltage and capacity at 4.2 – 3.6 V, resembling an electrochemical doped/de-doped process (Fig. 3b). At a moderate discharge rate of 0.5 C, the discharge capacity reaches 103 mA h g<sup>-1</sup>, approximately 94% of the theoretical capacity of 109 mA h g<sup>-1</sup>, which is much lower than the conventional electrodes Fig. 3c.<sup>117</sup> Additionally, to enhance the specific capacity, the combination of different redox centers could be made to provide more electron transfer thus extend their storage capability. In the similar fashion, Chen and





colleagues successfully synthesized a novel micro-/mesoporous polymer, **PTDAPTz**, containing triazine units.<sup>118</sup> As shown in Fig. 3d, the energy gap between the lowest unoccupied molecular orbital (LUMO) and HOMO of **TDAPTz** was found to be stronger than that of **TPA** due to the stronger electron-withdrawing effect of the triazine unit, resulting in a lower band gap. This characteristic reflected in their electrochemical response as the redox peaks of triphenylamine units in **PTDAPTz** shifted towards higher potential than that of **PTPA** (Fig. 3e) due to electron-withdrawing effect of the triazine units, thus decreased electron cloud density nearby nitrogen atom of triphenylamine and resulting it difficult to the gain and loss of the radical electron. This unique feature led to improved cell performance as shown in Fig. 3f. Furthermore, higher free radical density of **PTPA** organic cathode, **PTDATA**, has been synthesized to enhance specific capacity via multiple electron transfer.<sup>121</sup> As shown in Fig. 4a, the **PTDATA** exhibited multiple redox peaks than that of **PTPA** cathode. These multiple peaks of **PTDATA** could be associated with the four free radical center structure in the **TDATA** unit of **PTDATA**, which undergoes the four-electron transfer reaction during the charge-discharge process. These multiple electrons transfer successfully improved the cycling performance of **PTDATA** cathode with initial capacity of  $\sim 131$  mA h g<sup>-1</sup>, and maintained at 98 mA h g<sup>-1</sup> after 100 cycles at current density of 20 mA g<sup>-1</sup> (Fig. 4b).

Moreover, different strategies such as formation of hyperbranched and microporous **PTPA** polymer have also been applied to further improve the processability and structural stability.<sup>122, 123</sup> Yamamoto, et. al. reported that hyperbranched phenylamine-based (**PHTPA**), prepared by Buchwald–Hartwig reaction (C–N coupling), exhibits high processability and delivered ultrafast charge-discharge process (Fig. 4c).<sup>122</sup> The high processability is proven as the **PHTPA** could easily dissolved in most of organic solvent such as N-methyl-2-pyrrolidone (NMP), THF, chloroform, and toluene even though the polymer has all aromatic structures. Meanwhile, it remains insoluble in electrolyte solution of 1 M LiPF<sub>6</sub> EC:DEC (30:70), indicating that **PHTPA** can be applied to LIBs. Furthermore, **PHTPA** cathode delivered stable specific capacity of  $\sim 60$  and  $\sim 40$  mA h g<sup>-1</sup> at 20 and 100 C rate, respectively, up to 5000 cycles (Fig. 4c), demonstrating ultralong stability and ultrafast charge-discharge ability due to formation microspheres morphology of the hyperbranched polymer.<sup>122</sup> Additionally, a star-shaped triphenylamine-based monomer with the benzene core has been prepared to form conjugated microporous polymer poly[1,3,5-tris(4-diphenylamino-phenyl)benzene] (**PTTPAB**) by chemical oxidative polymerization (Fig. 4d).<sup>123</sup> This study found that the microporous structure is beneficial on providing fast ion transport thus significantly improve its rate capability. As depicted in Fig. 4e, the **PTTPAB** cathode delivered specific capacity of  $\sim 80$  mA h g<sup>-1</sup> without significant capacity dropped as the current density increased up to 500 mA g<sup>-1</sup>.

In addition, copolymer formation has also been introduced in **PTPA** organic cathode to improve the specific capacity. For instance, a novel conjugated radical copolymer, poly(triphenylamine-co-*N,N'*-bis(4-carbamoyl-2,2,5,5-tetramethyl-pyrrolin-1-oxyl)-*N,N'*-diphenyl-1,4-

phenylenediamine) (**P(TPA-co-DDP-PROXYL)**), has been synthesized through chemical oxidative polymerization and utilized as a cathode material.<sup>124</sup> This polymer incorporates both a crosslinking conjugated backbone and **PROXYL** nitroxide radical side chains. As shown in Fig. 4f, the presence of triphenylamine and nitroxide radicals within the polymeric backbone is expected to provide numerous active sites to improve the specific capacity. In this regard, series of redox couples can be monitored on the CV profile of **P(TPA-co-DDP-PROXYL)** at potential window of 2.5 – 4.2 V vs. Li/Li<sup>+</sup> (Fig. 4g). The two pairs of reversible redox peaks at 3.73/3.78 V (R1/O1) and 3.6/3.64 V (R2/O2), respectively, correspond to the para-substitution and meta-substitution redox reactions of the triphenylamine unit, while R3/O3 (3.37/3.39 V) redox couple associated with transition from nitroxide radicals to the oxoammonium cations.<sup>124</sup> The resulting **P(TPA-co-DDP-PROXYL)** cathode material exhibited superb electrochemical performance and an ultralong cycle life with 72% capacity retention at 2000 mA g<sup>-1</sup> over 3000 cycles (Fig. 4h).<sup>124</sup> This ultralong stability could be attributed to the rigid molecular structure and exceptional resistance when immersed in the electrolyte for extended periods. Moreover, Table 1 summarizes recent development of phenylamine-based cathode for organic LIBs. Overall, the phenylamine-based electrodes have been explored and demonstrated superior high-rate capability, cycling stability, and energy density, making it a promising cathode material for next-generation organic LIBs operated at high voltage.

### 3.2 Thioether polymers

Organosulfur compounds have been recognized as potential cathode materials for LIBs due to their high theoretical capacities (1675 mA h g<sup>-1</sup>) and energy densities, (2600 Wh kg<sup>-1</sup>) via reversible formation/deformation of S-S bond formation.<sup>29</sup> However, despite its abundance and low cost, the challenges such as its non-conductivity and the polysulfide shuttle effect limit its practical use.<sup>125, 126</sup> Although organosulfur cathodes with diverse macromolecular structures could offer an improvement on its stability and kinetics, some issues associated with S-S bond recovery appeared thus impacting its cycling stability.<sup>127-129</sup> Alternatively, thioether polymers with a distinct from organosulfur compounds containing single S-S bonds offer a different redox mechanism, involving the loss of electrons and formation of stable oxidation states.<sup>130</sup> This characteristic makes them potential candidates for cathodes with high voltage outputs, corresponding to the intercalation of anions (ClO<sub>4</sub><sup>-</sup>, PF<sub>6</sub><sup>-</sup>, BF<sub>4</sub><sup>-</sup>, and TFSI<sup>-</sup>).<sup>131, 132</sup> Additionally, the charge storage mechanism of thioether polymers differs from the organosulfur polymers, as it does not involve chain breaking, potentially leading to higher cyclability.<sup>133</sup> Over the past decades, numerous polymeric organosulfide materials have been developed, categorized into four types: main-chain-type, side-chain-type, polysulfides with -S<sub>x</sub>- groups where x > 2, and thioether-type organosulfur polymers.<sup>126</sup> Ren et al. synthesized two polyacetylene derivatives, **P1** and **P2**, containing pendant thianthrene groups through polymerization using [(2,5-norbornadiene)RhCl]<sub>2</sub>/Et<sub>3</sub>N catalyst with thianthrene-1-



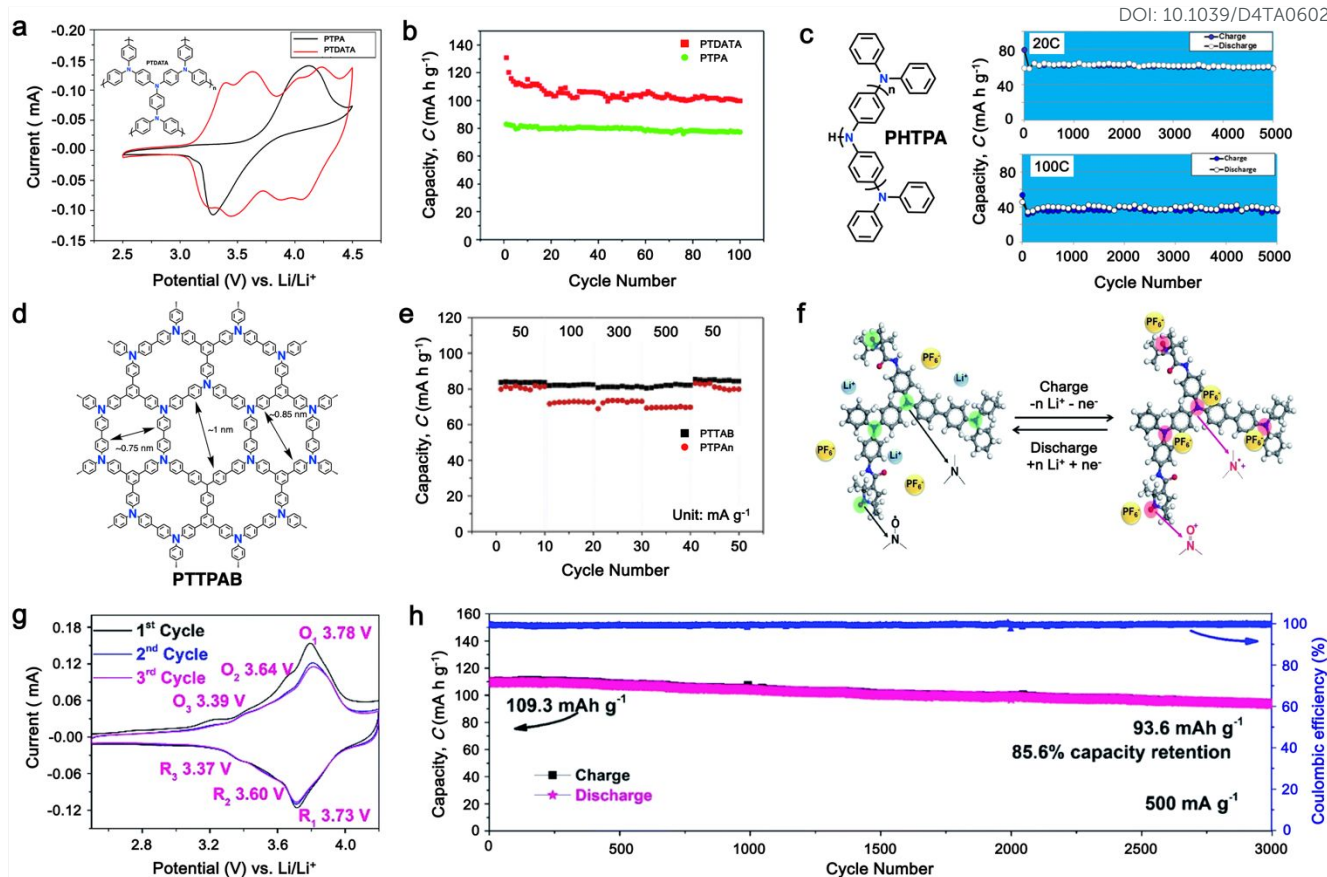


Fig.4 (a) and (b) CV at scan rate of  $1 \text{ mV s}^{-1}$  and cycling performance under  $20 \text{ mA g}^{-1}$  current density of **PTDATA** cathode, respectively. Reproduced with permission from ref. <sup>121</sup>. Copyright 2017 Royal Society of Chemistry. (c) Chemical structure and cycling performance of hyperbranched **PHTPA** cathode under high current rate. Reproduced with permission from ref. <sup>122</sup>. Copyright 2018 American Chemical Society. (d) and (e) Chemical structure and rate performance of microporous **PTTPAB** cathode. Reproduced with permission from ref. <sup>123</sup>. Copyright 2018 Elsevier. (f) Schematic electrochemical reaction mechanism of **P(TPA-co-DDP-PROXYL)**. (g) and (h) CV curve at a scan rate of  $0.5 \text{ mV s}^{-1}$  and long cycling performance of **P(TPA-co-DDP-PROXYL)** at  $500 \text{ mA g}^{-1}$ . Reproduced with permission from ref. <sup>124</sup>. Copyright 2022 Royal Society of Chemistry.

ylmethyl 4-ethynylbenzoate (**M1**) or bis(thianthrene-1-ylmethyl)-4-ethynylphthalate (**M2**) as shown in Fig. 5a.<sup>134</sup> Both **P1** and **P2** exhibited reversible redox activity with a high oxidation potential of  $4.16 \text{ V vs. Li/Li}^+$  due to the presence of p-type thioethers groups.<sup>134</sup> Notably, **P2** showed a higher specific capacity of  $100 \text{ mA h g}^{-1}$  compared to **P1** ( $33 \text{ mA h g}^{-1}$ ) (Fig. 5b and c), attributed to the more active units within the **P2** molecule. Moreover, adopting the same redox behavior, Vaid et al. reported a polythianthrene cathode with an impressive working potential up to  $4.1 \text{ V vs. Li/Li}^+$ , which is comparable to inorganic cathodes.<sup>135</sup>

Additionally, Misaki et. al. demonstrated tris-fused tetrathiafulvalene (**TTF**) analogues, including unsubstituted and bis(ethylenedioxy) derivatives as cathode LIB (Fig. 5d and 5e).<sup>136</sup> As shown in Fig. 5d and 5e, these compounds delivered voltage window up to  $3.6 \text{ V}$  with high capacity of  $192$  and  $160 \text{ mA h g}^{-1}$ . These distinct electrochemical performances were associated with the typical p-type reaction mechanism and six-electron electron transfer as illustrated in Fig. 5f. However,

these materials suffered from rapid capacity decay in the initial cycles, indicating the need to address poor cycling stability (Fig. 5d and 5e). Furthermore, inspired from polymer as presented in Fig. 5g (i and ii), polyphenyls with dithiolane moieties, Fig. 5g (iii) have been prepared and shown promising stability and a stable capacity of up to  $300 \text{ mA h g}^{-1}$ .<sup>137, 138</sup> However, these materials often exhibit large polarization due to their low conductivity, thus limiting their stability. Moreover, the incorporation of two sulfur atoms into a six-membered ring, as seen in thianthrene, results in exceptional stability.<sup>139</sup> Thianthrene-based polymers can lose two electrons alongside the intercalation of anions, leading to a high discharge plateau around  $4.0 \text{ V}$  without significant overpotential.<sup>31</sup> The (iv) polymer exhibited highly reversible charge-discharge curves at  $4.05 \text{ V}$  for charging and  $3.95 \text{ V}$  for discharging, with a capacity of  $105 \text{ mA h g}^{-1}$  after the first cycle and  $81\%$  capacity retention after 250 cycles.<sup>31</sup> Taking the similar strategy, Schubert et al. utilized 1,3-dithiane in a five-membered ring polymer and resulted in a discharge potential of



## ARTICLE

## Journal Name

Table 1. Summarizes recent development of PTPA-based cathode for organic LIBs.

No.	Polymer Material	Chemical structure	Electrolyte	Voltage (V) vs. Li/Li <sup>+</sup>	Capacity (mA h g <sup>-1</sup> )	Current Applied	Ref.
<b>Phenylamine-based cathodes</b>							
1	PDPA		1 M LiPF <sub>6</sub> in EC/DMC (1:1, v/v)	2.5 – 4.5	116	0.1 A g <sup>-1</sup>	140
2	PTPA		1 M LiPF <sub>6</sub> in EC/DMC (1:1, v/v)	2.5 – 4.2	69.7	0.05 A g <sup>-1</sup>	141
4	PDPA-AQ		1 M LiPF <sub>6</sub> in EC/DMC (1:1, v/v)	1.5 – 4.5	159	0.1 C	142
5	PTPAn		1 M LiPF <sub>6</sub> in EC/DMC (1:1, v/v)	2.5 – 4.2	100.4	0.02 A g <sup>-1</sup>	143
	PTPA-CN				85.4		



Journal Name

ARTICLE

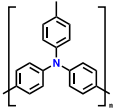
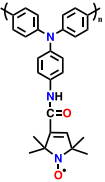
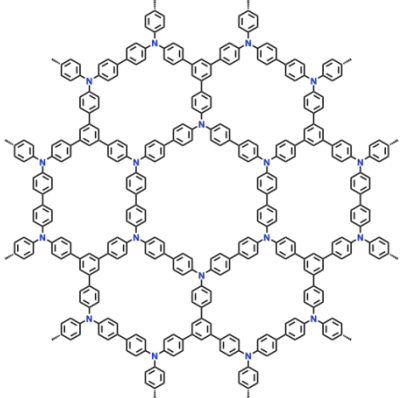
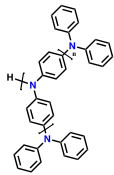
No.	Polymer Material	Chemical structure	Electrolyte	Voltage (V) vs. Li/Li <sup>+</sup>	Capacity (mA h g <sup>-1</sup> )	Current Applied	Ref.
6	poly(4-cyano)triphenylamine		1 M LiPF <sub>6</sub> in EC/DMC/EMC (1:1:1, v/v/v)	3.0 – 4.2	75	0.08 A g <sup>-1</sup>	144
7	PDDP		1 M LiPF <sub>6</sub> in EC/DMC (1:1, v/v)	2.5 – 4.2	110.6	0.02 A g <sup>-1</sup>	88
8	PTPA		1 M LiPF <sub>6</sub> in EC/DMC (1:1, v/v)	2.5 – 4.2	80	0.02 A g <sup>-1</sup>	88
9	PFTP		1 M LiPF <sub>6</sub> in EC/DMC (1:1, v/v)	2.5 – 4.2	74.2	0.02 A g <sup>-1</sup>	145
10	PTPA-PO		1 M LiPF <sub>6</sub> in EC/DEC (1:1, v/v)	2.0 – 4.2	134.5	0.02 A g <sup>-1</sup>	146





## ARTICLE

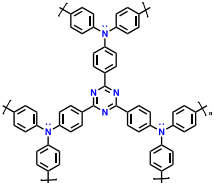
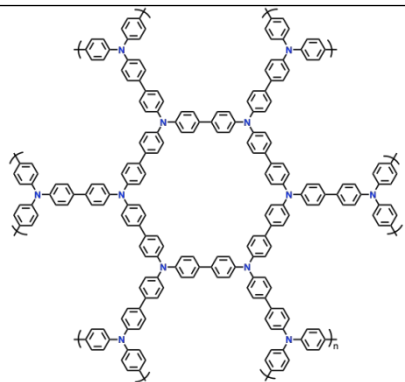
## Journal Name

No.	Polymer Material	Chemical structure	Electrolyte	Voltage (V) vs. Li/Li <sup>+</sup>	Capacity (mA h g <sup>-1</sup> )	Current Applied	Ref.
11	PTPA-CNT		1 M LiPF <sub>6</sub> in EC/DMC (1:1, v/v)	2 – 4.2	103.1	0.02 A g <sup>-1</sup>	147
	PTPO-CNT				128		
12	PTTPAB		1 M LiPF <sub>6</sub> in EC/DMC/DEC (1:1:1, v/v/v)	2.5 – 4.2	86.5	0.02 A g <sup>-1</sup>	123
13	PHTPA		1 M LiPF <sub>6</sub> in EC/DEC (3:7, v/v)	2.8 – 4.0	60	20 C (1 C = 0.06 A g <sup>-1</sup> )	122



Journal Name

ARTICLE

No.	Polymer Material	Chemical structure	Electrolyte	Voltage (V) vs. Li/Li <sup>+</sup>	Capacity (mA h g <sup>-1</sup> )	Current Applied	Ref.
14	PTDAPTz		1 M LiPF <sub>6</sub> in EC/DMC (1:1, v/v)	1.5 – 4.2	123	0.02 A g <sup>-1</sup>	118
15	YPTPA		1 M LiPF <sub>6</sub> in EC/DMC (1:1, v/v)	2.5 – 4.2	100	0.1 A g <sup>-1</sup>	87



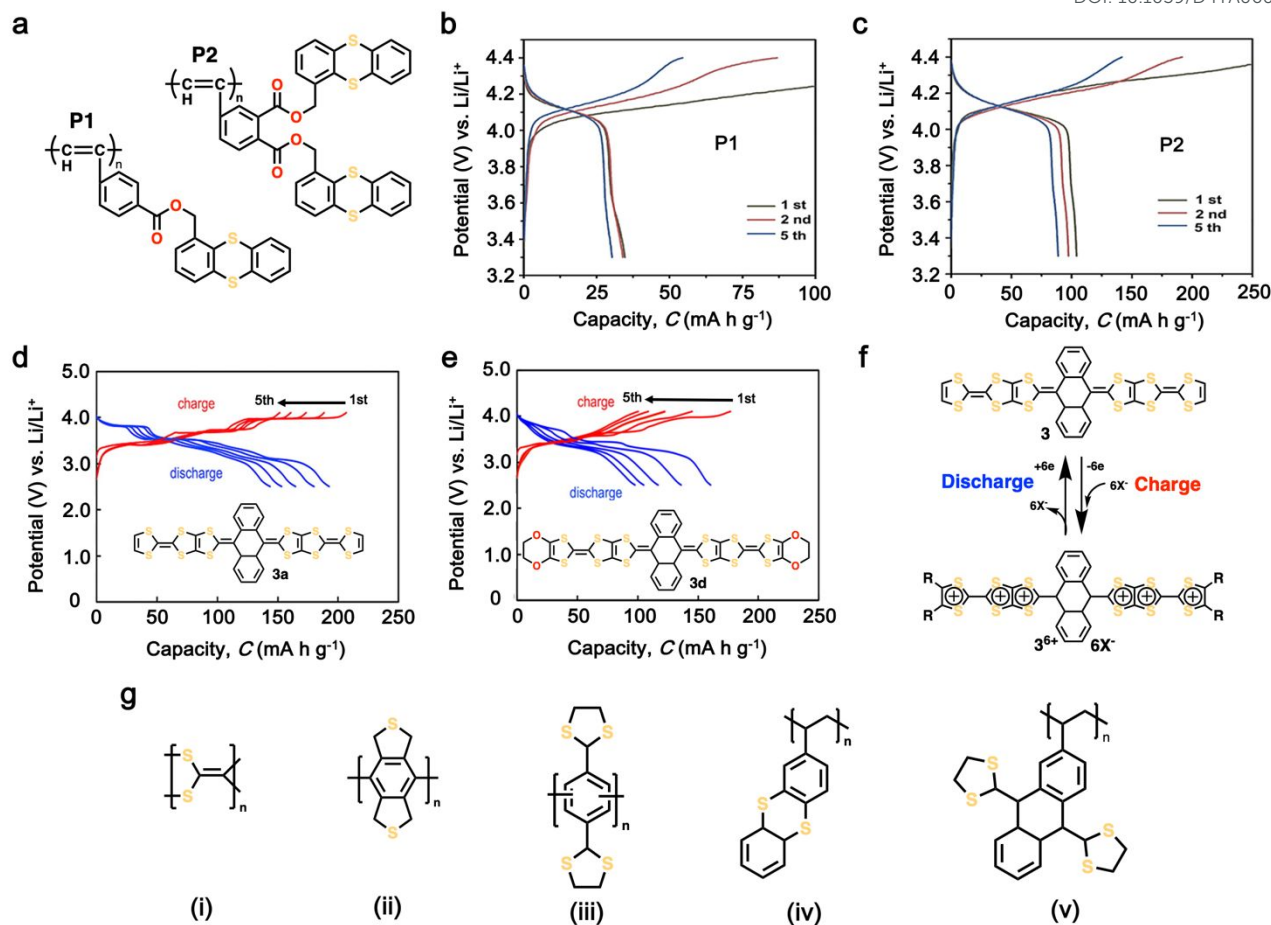


Fig.5 (a) Chemical structure of polyacetylene derivatives containing thioether-based cathode, namely **P1** and **P2**. (b) and (c) The charge-discharge profiles of thioether-based cathode **P1** and **P2**. Reproduced with permission from ref. <sup>148</sup>. Copyright 2020 Elsevier. (d) and (e) The charge-discharge profile and chemical structure of tetrathiafulvalenes (TTFs) based cathode **3a** and **3d**, respectively. (f) Possible redox reaction of TTFs-based cathode. Reproduced with permission from ref. <sup>149</sup>. Copyright 2019 John Wiley and Sons. (g) Examples of representative p-type organosulfur polymers. Reproduced with permission from ref. <sup>130</sup>.

about 3.2 V, where the charge storage mechanism involved anion intercalation (Fig. 5g (v)).<sup>150</sup> These findings highlight the potential of p-type thioether-based cathodes for high-potential LIBs, offering improved capacity, voltage, and cycle stability. Furthermore, Table 2 provides the recent trends of thioether-based cathode for organic LIBs.

### 3.3 Dihydrophenazine-based polymer

In the preceding section, we explored how organic electrodes derived from triphenylamine-based polymer exhibit notably high redox potentials, though their specific capacities typically range around 100 mA h g<sup>-1</sup>. This restriction arises from the fact that the triphenylamine unit tends to undergo a single-electron redox reaction, depending solely on a single nitrogen heteroatomic redox center on their polymer backbone. To overcome this limitation, recent studies have focused on developing p-type organic electrodes that are capable of multi-electron redox reactions to achieve higher capacities. In this regard, dihydrophenazine and its derivatives have been

explored as a new alternative p-type polymer with multi-electron redox reaction. These organic electrodes feature two heteroatomic redox centers (N, S, O) in the core six-membered ring, fused by two respective benzene rings, allowing for two single-electron redox reactions and a significantly higher theoretical specific capacity (~270 mA h g<sup>-1</sup>) than that of triphenylamine-based electrodes. The redox potentials of these phenazines range from 3.1 to 4.2 V vs. Li/Li<sup>+</sup> based on the electron-donating/withdrawing strength of the heteroatoms.

Among phenazines, *N,N'*-substituted phenazine derivatives have captured interest due to their ability to undergo two successive one-electron transfer reactions, categorizing them as p-type molecules with higher redox potentials.<sup>151</sup> As shown in Fig. 6a, the reversibility of these electron transfer reactions depends on the substituted groups on the two N atoms. A significant challenge in applying polymeric materials lies in their insufficient electrical and/or ionic conductivity, especially for those employing an anion-exchange mechanism.<sup>23, 152-154</sup>



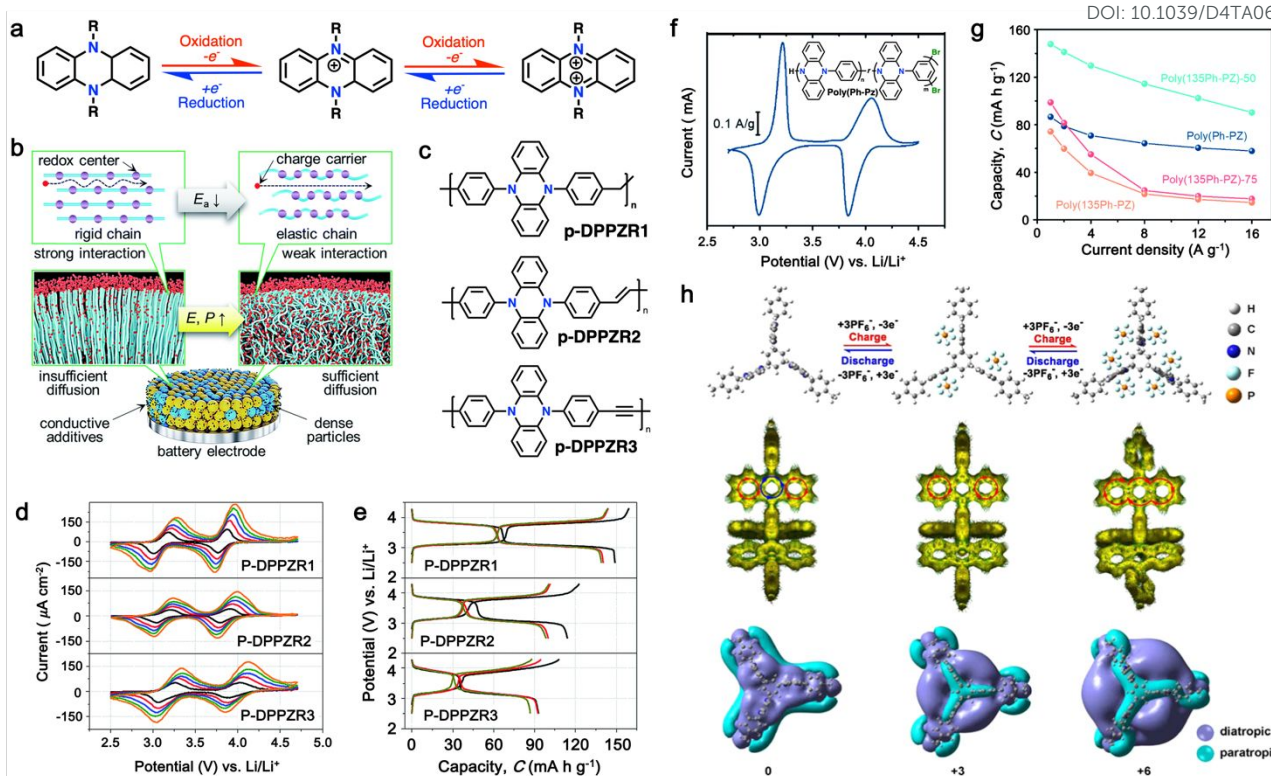


Fig. 6 (a) Chemical structure and redox mechanism of *N,N'*-substituted phenazine derivatives. Reproduced with permission from ref. <sup>84</sup>. Copyright 2019 Elsevier. (b) Schematic demonstration of enhancing power density by decreasing the rigidity of polymer chains. (c) Proposed polymers with variable chain rigidity based on **DPPZ**. (d) CV profiles of **p-DPPZR1**, **p-DPPZR2**, and **p-DPPZR3** cells at sweeping rates of 0.2, 0.4, 0.6, 0.8, and 1 mV s<sup>-1</sup>. (e) Typical charge/discharge profiles of **p-DPPZR1**, **p-DPPZR2**, and **p-DPPZR3** at 1C rate. Reproduced with permission from ref. <sup>155</sup>. Copyright 2019 Royal Society of Chemistry. (f) CV profiles of **poly(Ph-PZ)** at 0.25 mV s<sup>-1</sup> in Li metal half cells. (g) Rate capability of **poly(135Ph-PZ)-50** based cathode. Reproduced with permission from ref. <sup>156</sup>. Copyright 2021 Royal Society of Chemistry. (h) Redox mechanism and DFT calculation of **TPZB** cathode. Reproduced with permission from ref. <sup>157</sup>. Copyright 2020 American Chemical Society.

In this regard, Niu and colleagues have explored manipulating the rigidity of polymer chains to alter ion diffusion behavior in polymeric materials.<sup>155</sup> The study reveals that introducing a suitable twisted group in the phenazine-based polymer significantly enhances the ionic diffusion coefficient, leading to improved power densities despite lower surface area and electrical conductivity.<sup>158</sup> This approach emphasized on the different structural packing of the polymer chains, where rigid chains often hinder ion diffusion through polymer chain due to increased activation energy, while more elastic chains could accelerate ion diffusion via formation of an amorphous phase (Fig. 6b).<sup>159,160</sup> To validate this approach, three polymers based on redox-active *N,N'*-diphenyl-5,10-dihydrophenazine (**DPPZ**) have been synthesized with varying chain rigidities, namely: **p-DPPZR1** (-CH<sub>2</sub>- bridging), **p-DPPZR2** (-CH=CH- trans-isomer), and **p-DPPZR3** (-C≡C-) (Fig. 6c).<sup>155</sup> As shown Fig. 6d, two pairs of redox peaks can be observed, corresponding to the two successive two-steps of one-electron redox reactions of **DPPZ**. In term of specific capacity, **p-DPPZR1** delivered a specific capacity of approximately 145.9 mA h g<sup>-1</sup> (Fig. 6e), surpassing **p-DPPZR2** (112.1 mA h g<sup>-1</sup>) and **p-DPPZR3** (93.7 mA h g<sup>-1</sup>).<sup>155</sup>

Additionally, to address the limitations posed by strong  $\pi$ - $\pi$  interactions narrowing the internal free volume, Gannet et al. developed a network polymer of **PZ** by incorporating a phenylene linker (Ph) with three points of connectivity as shown in Fig. 6f.<sup>156</sup> This modification aimed to enhance the rate performance of the polymer system. Among the copolymers, **poly(135Ph-PZ)-50** demonstrated the highest performance due to its optimal characteristics shown by redox reactions from cyclic voltammetry (Fig. 6f). The polymer electrode achieved a specific capacity of up to 135 mA h g<sup>-1</sup> at 1.0 A g<sup>-1</sup>, retaining 65% of the low-rate capacity at a high rate of 16 A g<sup>-1</sup> (Fig. 6g).<sup>156</sup> Furthermore, the optimized geometries of poly(1,3,5-tris(10-(4-vinylphenyl)phenazin-5(10H)-yl)benzene) (**TPZB**) at 0, +3, and +6 valence states were investigated, revealing a twist angle formed by the dihydrophenazine group with a centered benzene ring, creating storage space for PF<sub>6</sub><sup>-</sup> ions resembling piers (Fig. 6h).<sup>157</sup> This configuration facilitates their diffusion and intercalation/deintercalation. The calculation of isochemical shielding surfaces (ICSSs) further explored the aromaticity of the redox intermediates and their impact on electrode performance (Fig. 6h).<sup>157</sup>





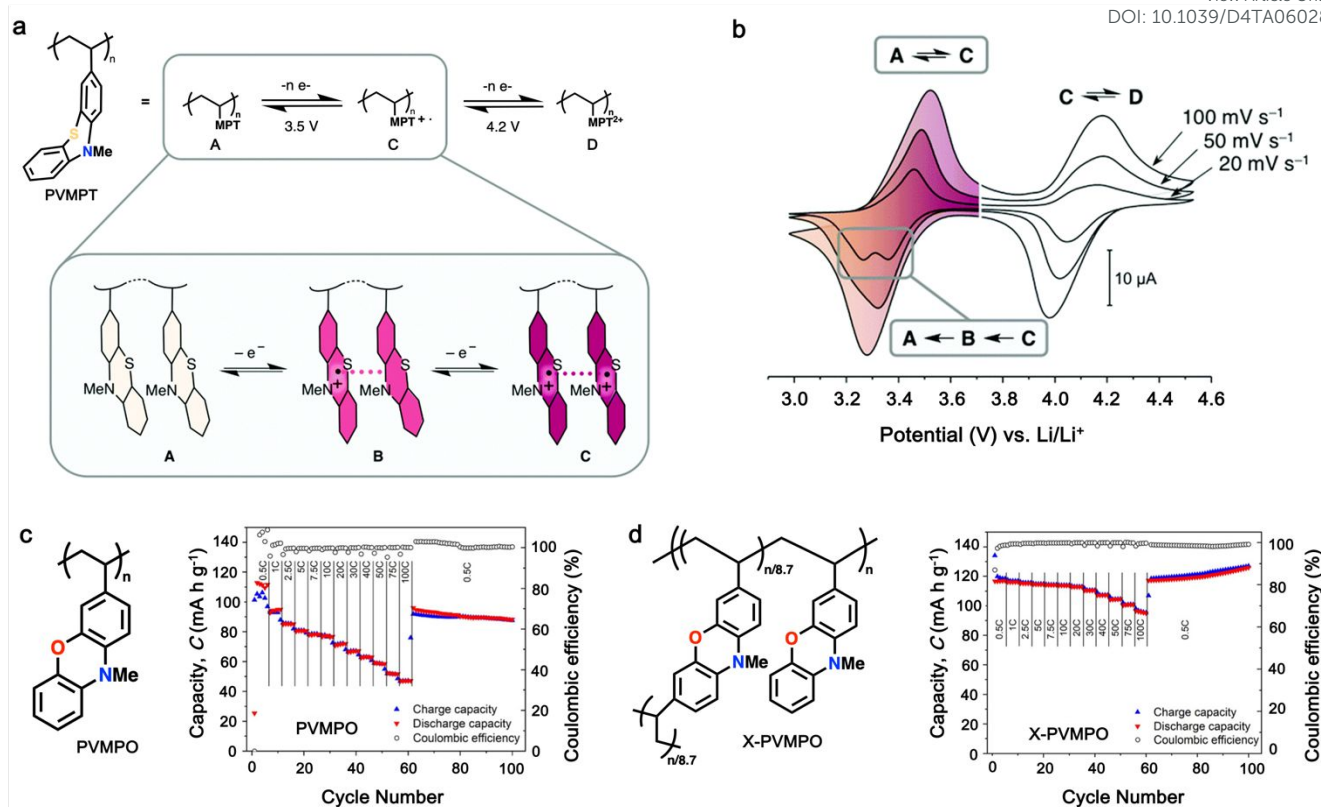


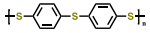
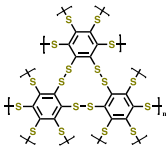
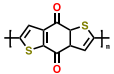
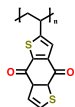
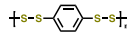
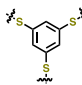
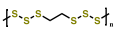
Fig. 7 (a) Schematic representation of the redox processes in **PVMPT** cathode. (b) Cyclic voltammograms of **PVMPT** in solution (1 mM in CH<sub>2</sub>Cl<sub>2</sub>, 0.1 M n-Bu<sub>4</sub>NPF<sub>6</sub>, glassy carbon working electrode). Reproduced with permission from ref. <sup>161</sup>. Copyright 2017 Royal Society of Chemistry. (c) Chemical structure and rate performance of **PVMPO** cathode. (d) Chemical structure and rate performance of **X-PVMPO** cathode. Reproduced with permission from ref. <sup>162</sup>. Copyright 2020 American Chemical Society.

Additionally, substituting one of the N atoms with S or O atom in the phenazine ring would result into further two types of redox active compounds known as phenothiazine and phenoxazine, respectively. This substitution has been reported to increase the redox potential of phenazine-based cathodes, due to the weaker electron-donating strength. For instance, Kolek et al. introduced a phenothiazine (PTZ)-based polymer cathode, **PVMPT**, where *N*-methylated PTZ (MPT) units were attached to a vinyl backbone as pendant groups.<sup>161</sup> In this study, each MPT unit underwent two single-electron oxidations sequentially at 3.44 V (from the neutral state A to the radical cation state C) and 4.18 V vs. Li/Li<sup>+</sup> (to the di-cationic state D), respectively (Fig. 7a). Interestingly, as shown in Fig. 7b, the oxidation of **PVMPT** resulted in strong π–π interactions between neighboring MPT dimers, leading to the formation of the intermediate oxidation state at potentials of 3.44 and 4.18 V vs. Li/Li<sup>+</sup>. Upon oxidation, the PTZ units in **PVMPT** could associate intra- or intermolecularly, stabilizing the oxidized states B and C as depicted in Fig. 7b. These interactions became evident in the CV curves measured at a slow scan rate (20 mV s<sup>-1</sup>), where the second cathodic peak, corresponding to the reduction of the radical cation to the neutral species (C → A), split into two peaks separated by 95 mV.<sup>161</sup>

Furthermore, phenoxazine (PXZ), a phenazine derivative, features an oxygen/nitrogen pair in its core ring and has been explored for cathode LIBs.<sup>163</sup> Otteny et al. replaced the MPT unit in the **PVMPT** polymer with *N*-methylphenoxazine (MPO) to create a poly(3-vinyl-*N*-methylphenoxazine) (**PVMPO**) polymer (Fig. 7c).<sup>162</sup> Similar electrochemical behavior with **PVMPT**, the **PVMPO** electrode exhibited two single-electron oxidation reactions at 3.35 and 4.22 V vs. Li/Li<sup>+</sup>, although the second reaction was not entirely reversible. Notably, **PVMPO** displayed inferior cycle stability due to the lack of π–π interactions between the MPO dimers compared to that of **PVMPT**. Additionally, the cross-linked formation of **PVMPO** to form **X-PVMPO** polymer (Fig. 7d) effectively enhanced cycle stability by preventing dissolution.<sup>161, 164</sup> This strategy has significantly improved the cycling and rate capability performance of PXZ-based polymers. In addition, Table 3 illustrates the recent development of phenazine-based cathodes for organic LIBs.



Table 2. Summarizes recent development of thioether-based cathode for organic LIBs.

No.	Polymer Material	Chemical structure	Electrolyte	Voltage (V) vs. Li/Li <sup>+</sup>	Capacity (mA h g <sup>-1</sup> )	Current Applied	Ref.
<b>Thioether-based polymers</b>							
1	PPPS-14		1 M LiTFSI in DOL/DME (1:1 v/v)	1.8 – 3.0	382.5	1 C (1 C = 0.622 A g <sup>-1</sup> )	<a href="#">165</a>
2	Crosslinked polybenzenhexasulfide		1 M LiTFSI in DOL/DME (1:1 v/v)	0.75 – 3.2	150	0.1 C	<a href="#">166</a>
3	PBDTD		1 M LiClO <sub>4</sub> in DOL/DME (1:1 v/v)	1.9 – 3.2	180	5C (1 C = 0.214 A g <sup>-1</sup> )	<a href="#">167</a>
4	PVBDT		1 M LiClO <sub>4</sub> in EC/DMC (1:1 v/v)	1.5 – 3.25	116	1 C	<a href="#">168</a>
5	PPTS		1 M LiTFSI in DOL/DME (1:1 v/v) with 0.2 M LiNO <sub>3</sub>	1.8 – 3.0	633	1 C (1 C = 0.778 A g <sup>-1</sup> )	<a href="#">169</a>
6	PBTTS		1 M LiTFSI in DOL/DME (1:1 v/v) with 0.2 M LiNO <sub>3</sub>	1.8 – 3.0	616.6	0.1 C (1 C = 0.901 A g <sup>-1</sup> )	<a href="#">170</a>
7	PEHS		1 M LiTFSI in DOL/DME (1:1 v/v) with 0.2 M LiNO <sub>3</sub>	1.8 – 3.0	774	1 C (1 C = 1.217 A g <sup>-1</sup> )	<a href="#">171</a>



## ARTICLE

## Journal Name

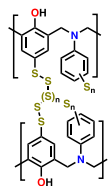
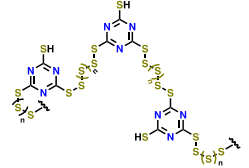
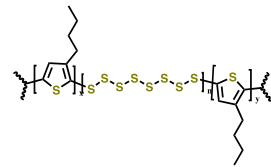
No.	Polymer Material	Chemical structure	Electrolyte	Voltage (V) vs. Li/Li <sup>+</sup>	Capacity (mA h g <sup>-1</sup> )	Current Applied	Ref.
8	S-BOP		1 M LiTFSI in DIOX/TEGDME (0.67:0.33 v/v) with 0.2 M LiNO <sub>3</sub>	1.7 – 2.7	630	1 C (1 C = 0.72 A g <sup>-1</sup> )	<a href="#">172</a>
9	S-TTCA		1 M LiTFSI in DIOX/TEGDME (0.67:0.33 v/v) with 0.2 M LiNO <sub>3</sub>	1.7 – 2.7	813	0.2 C (1 C = 1.675 A g <sup>-1</sup> )	<a href="#">173</a>
10	CP(S3BT)		1 M LiTFSI in DOL/DME (1:1 v/v) with 0.1 M LiNO <sub>3</sub>	1.5 – 3.0	682	1 C	<a href="#">174</a>



Table 3. Summarizes recent development of phenazine-based cathode for organic LIBs.

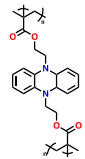
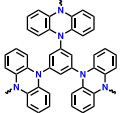
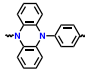
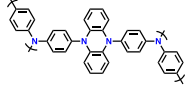
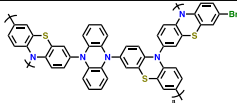
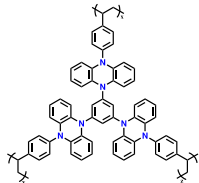
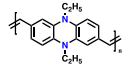
No.	Polymer Material	Chemical structure	Electrolyte	Voltage (V) vs. Li/Li <sup>+</sup>	Capacity (mA h g <sup>-1</sup> )	Current Applied	Ref.
<b>Dihydrophenazine-based polymer</b>							
1	<b>p-DPPZ</b>		1 M LiPF <sub>6</sub> in EC/DEC (1:1, v/v)	2.5 – 4.5	150	0.25 C (1 C = 0.209 A g <sup>-1</sup> )	84
2	<b>p-DPPZS</b>		1 M LiPF <sub>6</sub> EC/DEC	2.9 – 4.3	133	5 C (1 C = 0.147 A g <sup>-1</sup> )	175
3	<b>p-DPPZR-1</b>		1 M LiPF <sub>6</sub> in EC/DEC (1:1, v/v)	2.5 – 4.3	140	1 C (1 C = 0.153 A g <sup>-1</sup> )	155
	<b>p-DPPZR-2</b>				102	1 C (1 C = 0.148 A g <sup>-1</sup> )	
	<b>p-DPPZR-3</b>				88	1 C (1 C = 0.149 A g <sup>-1</sup> )	
4	<b>poly(135Ph-PZ)</b>		1 M LiPF <sub>6</sub> in EC/DEC (1:1, v/v)	2.6 – 4.5	158	1 A g <sup>-1</sup>	156
	<b>poly(135Ph-PZ)-X</b>				180		
5	<b>poly(Ph-PZ)</b>		1 M LiPF <sub>6</sub> in EC/DEC (1:1, v/v)	1.5 – 4.3	209	5 C	176





## ARTICLE

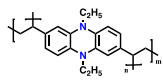
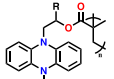
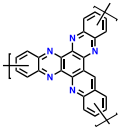
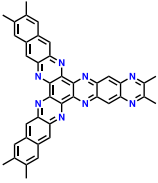
## Journal Name

No.	Polymer Material	Chemical structure	Electrolyte	Voltage (V) vs. Li/Li <sup>+</sup>	Capacity (mA h g <sup>-1</sup> )	Current Applied	Ref.
6	PBEMP		1 M LiPF <sub>6</sub> in EC/DEC (1:1, v/v)	2 – 4.5	101	1 A g <sup>-1</sup>	177
7	p-TPPZ		1 M LiPF <sub>6</sub> in EC/DEC (1:1, v/v)	2.5 – 4.5	171.9	0.5 C (1 C = 0.233 A g <sup>-1</sup> )	178
	p-DPPZ				169.7		
8	PDPAPZ		1 M LiPF <sub>6</sub> in EC/DMC	2.5 – 4.2	107	0.1 A g <sup>-1</sup>	179
	PPTZPZ				83		
9	p-TPZB		1 M LiPF <sub>6</sub> in EC/DEC (1:1, v/v)	2.5 – 4.5	145	2 C	157
10	CPP		1 M LiPF <sub>6</sub> in EC/DEC (1:1, v/v)	2.5 – 4.2	184	0.2 A g <sup>-1</sup>	180



Journal Name

ARTICLE

No.	Polymer Material	Chemical structure	Electrolyte	Voltage (V) vs. Li/Li <sup>+</sup>	Capacity (mA h g <sup>-1</sup> )	Current Applied	Ref.
	<b>NCPP</b>				149		
11	<b>R = Me , PMPPZ</b>		1 M LiPF <sub>6</sub> in EC/DMC (1:1, v/v)	1.5 – 4.2	99	0.2 A g <sup>-1</sup>	181
	<b>R = H , PMPEZ</b>	<b>R = Me , PMPPZ</b> <b>R = H , PMPEZ</b>			130		
12	<b>HAT</b>		1 M LiPF <sub>6</sub> in EC/DMC (1:1, v/v)	1.0 – 3.5	99	10 A g <sup>-1</sup>	182
13	<b>N<sup>2</sup>-HATN</b>		LiCF <sub>3</sub> SO <sub>3</sub> in G4	1.2 – 4.0	183	0.5 A g <sup>-1</sup>	183



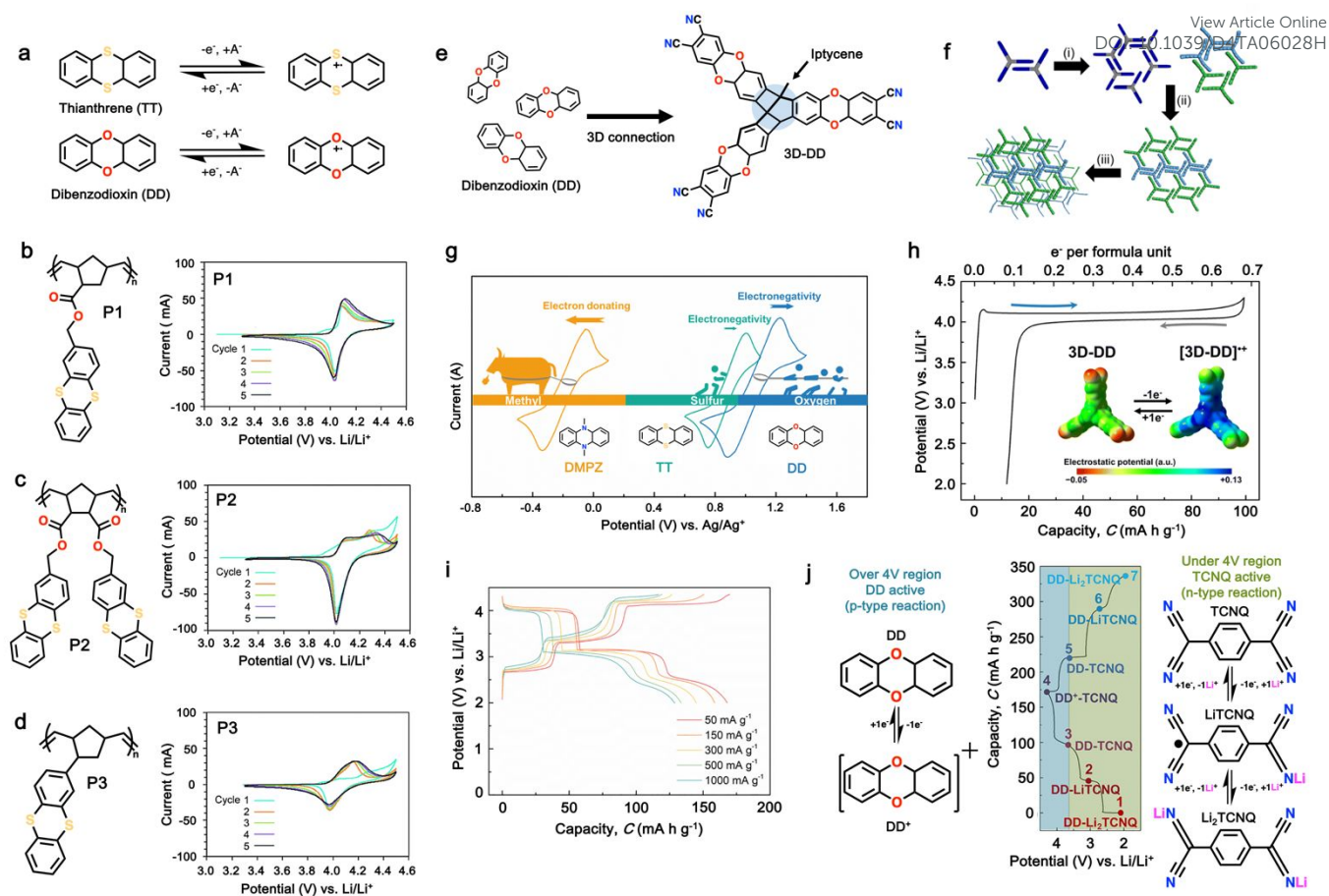


Fig.8 (a) Redox mechanism of Thianthrene (TT) and Dibenzodioxin (DD). Chemical structure and cyclic voltammogram of TT-substituted polynorbornenes (b) P1, (c) P2, and (d) P3, respectively. Reproduced with permission from ref.<sup>139</sup>. Copyright 2015 Royal Society of Chemistry. (e) Schematic illustration of the synthesis and (f) Crystallographically determined solid-state structure of hyperjunction 3D-DD cathode. (g) Cyclic voltammograms and the design scheme of DMPZ, TT, and DD. (h) Charge-discharge profiles of 3D-DD. Inset figure shows MEP maps of 3D-DD and [3D-DD]<sup>+</sup> showing charge delocalization over the three blade components. Reproduced with permission from ref.<sup>92</sup>. Copyright 2023 Royal Society of Chemistry. (i) Rate capability of DD-TCNQ cathode. (j) Redox mechanism of DD-TCNQ cathode. Reproduced with permission from ref.<sup>184</sup>. Copyright 2019 Elsevier.

### 3.4 Thianthrene and dibenzodioxin

Sharing the similar foundational structure with phenazine-based cathode, thianthrene (TT) and dibenzodioxin (DD) have been considered as next-generation high-voltage cathodes for LIBs by replacing nitrogen atoms with sulfur atom (TT) and oxygen atom (DD) that resulting redox reaction at higher voltage ~4.1 V. These heteroatoms play a vital role by providing multiple redox-active sites, enabling the essential multi-electron transfer reactions necessary for efficient charge and discharge processes in batteries. This characteristic is fundamental for achieving high specific capacities and ensuring stable cycling performance, making both compounds highly attractive candidates for high-energy-density LIBs. A notable difference between TT and DD lies in the specific heteroatoms incorporated into their molecular structures. As shown in Fig. 8a, the redox mechanism of TT- and DD-based molecules demonstrates how each unit accommodates a single electron transfer reaction. Recently, Speer and colleagues reported on

three norbornene polymers, namely P1 – P3, featuring one or two TT pendant groups as organic cathodes (Fig. 8b - d).<sup>139</sup> During CV measurement, the first oxidation of the polymers showed a high redox potential (~4.1 V vs. Li/Li<sup>+</sup>), but the second one was irreversible for P2 polymer (Fig. 8b). With only one electron utilized during electrochemical process, it limits their theoretical specific capacity to 73 mA h g<sup>-1</sup> and practically delivered a specific capacity of ~66 mA h g<sup>-1</sup>, accounting for almost 90% of the total specific capacity. However, rapid decay over 100 cycles was observed due to irreversible anion intercalation (Fig. 8c). Importantly, the P1 electrode still delivered a specific energy of 274 Wh kg<sup>-1</sup>, highlighting its potential for high potential and high energy materials. Recently, Wild and his group developed an all-organic battery consisting of poly(2-vinylthianthrene) cathode and poly(2-methacrylamide-TCAQ) anode.<sup>185</sup>



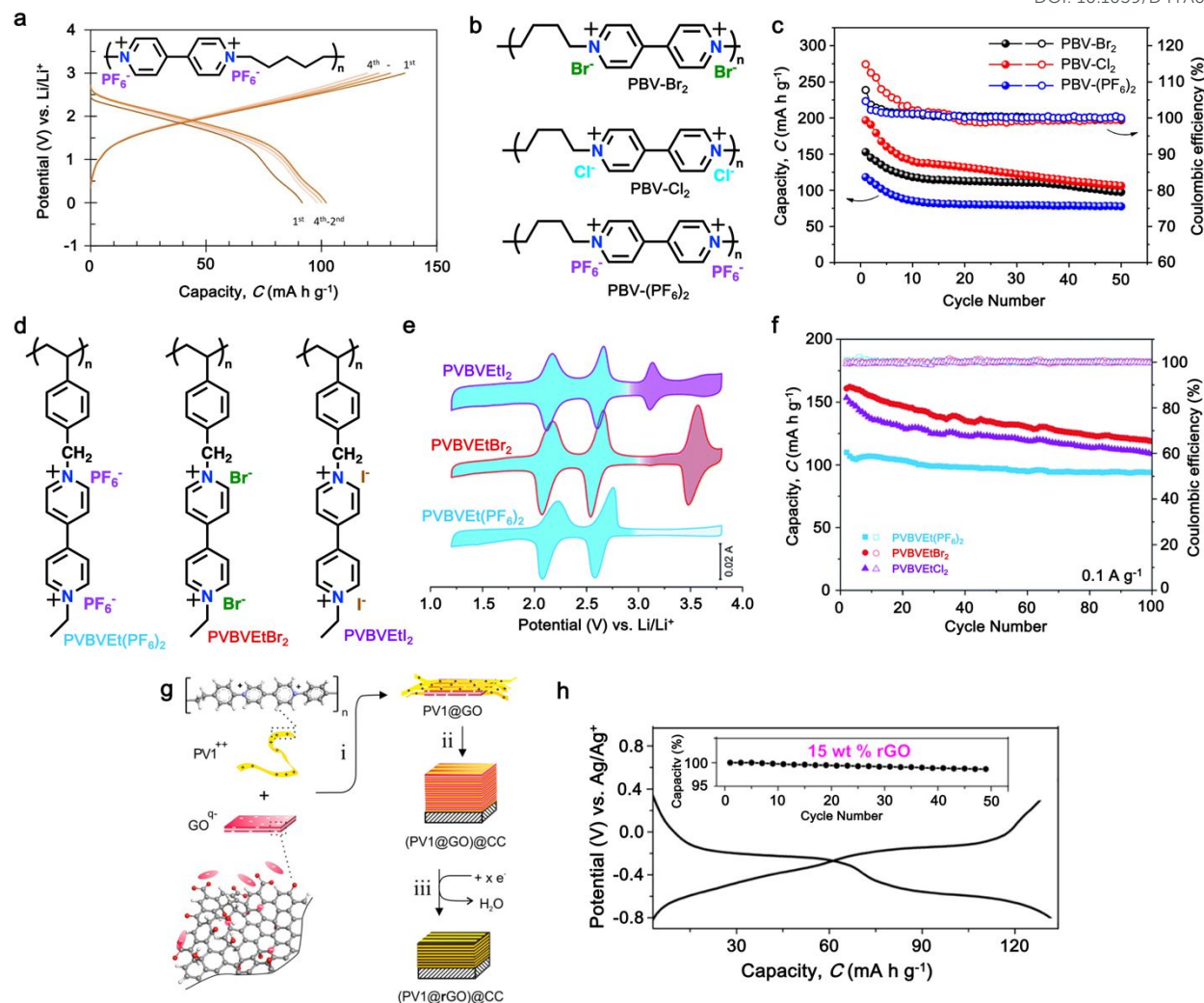


Fig. 9 (a) Galvanostatic charge-discharge profile of full-cell **PBPy**. Reproduced with permission from ref.<sup>186</sup>. Copyright 2015 Springer Nature. (b) Chemical structure and (c) cycling performance under 50 mA g<sup>-1</sup> in 1 M LiPF<sub>6</sub> EC:DEC electrolyte (voltage window of 1.4 – 3.1 V) of poly(butyl viologen)-based cathode. Reproduced with permission from ref.<sup>187</sup>. Copyright 2022 Elsevier. (d) Chemical structures of viologen-based ionic polymers **PVBVEtX<sub>2</sub>** (X = PF<sub>6</sub><sup>-</sup>, Br<sup>-</sup> or I<sup>-</sup>). (e) and (f) CV curves at 0.1 mV s<sup>-1</sup> scan rate and cycling performance under 0.1 A g<sup>-1</sup> current density of **PVBVEt(PF<sub>6</sub>)<sub>2</sub>**, **PVBVEtBr<sub>2</sub>**, and **PVBVEtI<sub>2</sub>** electrodes. Reproduced with permission from ref.<sup>188</sup>. Copyright 2022 Royal Society of Chemistry. (g) An overview on preparation of poly-viologen/rGO composite electrode, **(PV1@rGO)@CC**. (h) Chronopotentiometric measurements of **(PV1@rGO)@GC** in 3 M KCl/H<sub>2</sub>O at cutoff voltages of 0.3 – 0.8 V, at rate of 5 A g<sup>-1</sup>. Reproduced with permission from ref.<sup>189</sup>. Copyright 2017 American Chemical Society.

The cathode material of poly(2-vinylthianthrene) displays a discharging plateau at 3.95 V vs. Li/Li<sup>+</sup> and a discharge capacity of 105 mA h g<sup>-1</sup>, corresponding to a specific energy of about 415 mWh g<sup>-1</sup>.

Despite the remarkable cell potential, **DD**-based cells suffer from severe capacity loss reaching almost 50% during the first 10 cycles, due to the high solubility of **DD** molecules in carbonate-based electrolytes system. In early investigation of **DD**-based cathode, Lee and group devised a modification strategy for the low-solubility **DD** analogue using a rigid iptycene scaffold to maximize intermolecular interactions and form **3D-DD** design incorporates with three **DD(CN)<sub>2</sub>** units

supported by the iptycene scaffold via facile nucleophilic aromatic substitution reactions (Fig. 8e).<sup>92</sup> Methyl-substituted quaternary carbon centers at the bridgehead positions prevent C-H activation reactions during the redox cycle. The stacked **3D-DD** structures are reported to form a complex structure by accommodating large lattice deformation through sliding motions of neighboring  $\pi$ -faces (Fig. 8f). Fig. 8g shows voltage distribution of phenazine derivatives. As depicted in Fig. 8g, it shows that the **DD** electrode (blue line) displays a redox peak at around 1.1 V vs. Ag/Ag<sup>+</sup>, which is much higher than that of **PNZ** (orange line) or thianthrene (**TT**) (green line).<sup>83, 185</sup> Notably, the increase in the redox potential of **DD** molecules was achieved





without the addition of any redox-inactive functional groups, which generally accompany the reduction in the specific capacity.<sup>190, 191</sup> Consequently, when oxygen atoms were introduced in the core structure, it has shown a remarkable increase in the cell potential (4.1 V) against lithium and in turn delivering a discharge capacity of 90 mA h g<sup>-1</sup> at 50 mA g<sup>-1</sup> (Fig. 8h).<sup>92</sup> Besides formation of complex structure, different approach has also been made by incorporating conductive molecules. In this regards, Lee et al. synthesized a charge-transfer complex by combining **DD** with tetracyanoquinodimethane (**TCNQ**).<sup>184</sup> This **DD-TCNQ** complex demonstrated decreased solubility compared to pristine **DD** and **TCNQ** molecules, attributed to robust  $\pi$ - $\pi$  interactions and Coulombic attraction between their layers. Consequently, the **DD-TCNQ** electrode achieved a specific capacity of approximately 170 mA h g<sup>-1</sup> at 50 mA g<sup>-1</sup> within the voltage range of 2.6–4.2 V (Fig. 8i). Spectroscopic analysis unveiled that **DD** undergoes a single-electron redox reaction above the 4 V region, while **TCNQ** undergoes a two-electron redox reaction below the 4 V region during battery cycling. Throughout the charge and discharge process, it's hypothesized that the initial **DD-TCNQ** state transitions into **DD-LiTCNQ**, **DD-Li<sub>2</sub>TCNQ**, and **DD<sup>+</sup>-TCNQ** (Fig. 8j). Their shared capability for multi-electron transfer reactions, coupled with the distinct advantages offered by their respective heteroatoms, underscores their potential for next-generation high-voltage cathodes. In brief, besides the **TT** and **DD**-based compounds capability of providing higher redox activity > 4.0 V, addressing related issue of high solubility due to solvent interaction and side reaction associate with C-S-C bond cleavage during the cycling could pave the way of its practical application as LIBs cathode with enhanced energy density, extended cycle life, and improved overall performance. Moreover, Table 4 present the recent advance of **TT** and **DD**-based cathode for organic LIBs.

### 3.5 Polyviologen

Polyviologens, also known as poly(4,4'-bipyridinium) compounds, are a class of organic materials that have gained significant attention for their potential applications in high-performance LIBs.<sup>192-194</sup> These materials as cathode LIBs are characterized by their unique redox-active viologen units, which consist of anion doped/de-doped process on the two nitrogen-containing pyridinium rings connected by a conjugated bridge leading to the formation of stable radical cations and dications.<sup>187, 189, 195-200</sup> Additionally, polyviologens-based cathode offer several desirable properties for use in LIBs, including high electrochemical stability, good conductivity, and excellent cycling performance.<sup>201</sup> To further explore the potential of viologen, in 2015, Yao and colleagues introduced the first solid-type electrode based on viologen, presenting a viologen polymer poly(1,1'-pentyl-4,4'-bipyridinium dihexafluorophosphate (**PBPY**)) as shown in Fig. 9a (inset). The **PBPY** electrode exhibited two voltage plateaus at 2.6 and 2.1 V vs. Li/Li<sup>+</sup>, delivering a specific capacity of 79 mA h g<sup>-1</sup> in the initial cycle.<sup>186</sup> However, the low degree of polymerization led to rapid capacity degradation to 36 mA h g<sup>-1</sup> after 20 cycles. Nonetheless, when utilized as an anode, **PBPY** enabled the

fabrication of an all-organic full-cell with poly(*N*-vinylcarbazole) (**PVK**) as a cathode, achieving a specific capacity of 100 mA h g<sup>-1</sup> at a voltage of 1.8 V, relying on the PF<sub>6</sub><sup>-</sup> anion charge carrier (Fig. 9a).<sup>186</sup> Furthermore, to improve the specific capacity and cycling performance, an anion insertion approach has been reported effectively increased of viologen-based cathode. For instance, Wang et. al. have been reported the first Cl<sup>-</sup>-insertable p-type polymer, namely poly(butyl viologen dichloride) (**PBV-Cl<sub>2</sub>**) as cathode LIB (Fig. 9b).<sup>187</sup> As shown in Fig. 9c, **PBV-Cl<sub>2</sub>** demonstrated significant capacity improvement up to 200 mA h g<sup>-1</sup> at initial cycles, than that of **PVB(PF<sub>6</sub>)<sub>2</sub>** at 50 mA g<sup>-1</sup> current density. The improved specific capacity is associated to the present inserted Cl<sup>-</sup> ion in the structure which contributed to the ion storage mechanism during charge/discharge process. However, rapid capacity decay is monitored during cycling in the first 50 cycles due to the dissolution of **PBV-A<sub>2</sub>** polymer in the carbonate-ether-based electrolyte and the inevitable anion exchange during discharge-charge process (for **PBV-Br<sub>2</sub>** and **PBV-Cl<sub>2</sub>**) on the other hand.<sup>187</sup>

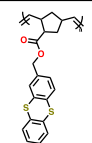
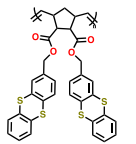
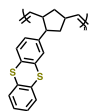
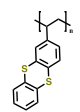
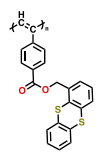
Similarly, series of viologen-based cathode have been prepared to investigate the impact of counter anion in the polymer structure.<sup>197</sup> As shown in Fig. 9d, poly(viologen halide)-based cationic polymers with Br<sup>-</sup> and I<sup>-</sup> as counter anions were prepared and nominated as **PVBVetBr<sub>2</sub>** and **PVBVetI<sub>2</sub>**. Notably, additional redox peak can be monitored when counter anion of Br<sup>-</sup> and I<sup>-</sup> were introduced in the viologen-based cathode. As shown in Fig. 9e, a strong and reversible redox peak is presented at 3.53 V for **PVBVetBr<sub>2</sub>**, assignable to the one-step reaction of Br<sup>-</sup>/Br<sub>3</sub><sup>-</sup> redox couple; and two redox peaks centered at 3.12 and 3.66 V for **PVBVetI<sub>2</sub>**, corresponding to oxidation of I<sup>-</sup> to I<sub>3</sub><sup>-</sup> (3.12 V) and then to I<sub>2</sub> (3.66 V). This involvement of counter anion significantly improved specific capacity of viologen-based cathode at initial cycles, before gradually decaying up to 100 cycles (Fig. 9f). The capacity loss of **PVBVetBr<sub>2</sub>** and **PVBVetI<sub>2</sub>** electrodes was mostly caused by the slight diffusion of Br<sub>3</sub><sup>-</sup>, I<sub>3</sub><sup>-</sup> and I<sub>2</sub> species from the electrodes during the charge/discharge process.<sup>197</sup> In addition, composite electrode formation have been reported could improve the cycling stability of viologen-based polymer during electrochemical process (Fig. 9g).<sup>189</sup> As shown Fig. 9h, the composite formation of viologen-based polymer with 15 wt% reduced graphene oxide (rGO) significantly enhanced cycling performance, as neglectable capacity loss up to 50 cycles. Overall, the unique electrochemical properties and tunable structures of polyviologens make them promising candidates for high-performance LIBs and other energy storage technologies, with ongoing research aimed at further optimizing their performance and expanding their applications in the future. Moreover, Table 4 shows the recent development of viologen-based cathode for organic LIBs.

### 3.6 Nitroxide radical polymers

During the past decade, radical organic compounds have garnered significant attention in the realm of polymer-based batteries.<sup>72, 202-204</sup> They feature polymers with pendant stable organic radicals, characterized by an unpaired electron in their uncharged state. These polymers offer superior redox



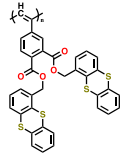
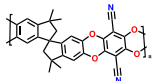
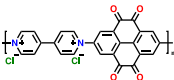
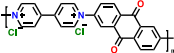
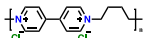
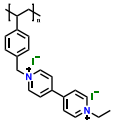
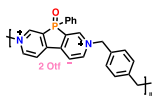
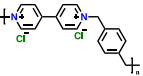
Table 4. Summarizes recent development of thianthrene, dibenzodioxin, and viologen-based cathode for organic LIBs.

No.	Polymer Material	Chemical structure	Electrolyte	Voltage (V) vs. Li/Li <sup>+</sup>	Capacity (mA h g <sup>-1</sup> )	Current Applied	Ref.
<b>Thianthrene-based polymers</b>							
1	P1		1 M LiPF <sub>6</sub> in EC/DMC (1:1, v/v)	3.3 – 4.5	73	1 C	139
	P2						
	P3						
2	poly(2-vinylthianthrene)		1 M LiClO <sub>4</sub> in EC/DMC (3:7 v/v)	3.2 – 4.2	105	1 C	185
3	P1		1 M LiPF <sub>6</sub> in EC/DMC (1:1, v/v)	3.3 – 4.4	35	0.05 mA cm <sup>-2</sup>	134



## ARTICLE

## Journal Name

No.	Polymer Material	Chemical structure	Electrolyte	Voltage (V) vs. Li/Li <sup>+</sup>	Capacity (mA h g <sup>-1</sup> )	Current Applied	Ref.
	<b>P2</b>				100		
<b>Dibenzodioxin-based polymers</b>							
4	<b>PIM 1</b>		Dried PEO with LiTFSI (0.08 g) in 8 mL CH <sub>3</sub> CN	1.6 – 2.7	1181	0.5 C	205
<b>Polyviologen-based polymers</b>							
5	<b>PVPTOCl<sub>2</sub></b>		1 M LiTFSI in (DOL: DME, 1:1 (v/v))	1.5 – 3.8	235	0.2 A g <sup>-1</sup>	206
	<b>PVAQCl<sub>2</sub></b>				113		
6	<b>PBV-Cl<sub>2</sub></b>		1 M LiPF <sub>6</sub> in EC/DEC, (1:1, v/v)	1.4 – 3.1	177	0.2 A g <sup>-1</sup>	187
7	<b>PVBVetX<sub>2</sub></b>		2 M LiClO <sub>4</sub> in TEGDME	1.2 – 3.8	192	0.1 A g <sup>-1</sup>	197
8	<b>P-MV</b>		1 M LiTFSI in DME	1.8 – 3.2	60	0.33 C	198
9	<b>PXVCl<sub>2</sub></b>		0.5 M tributylmethylamm onium chloride in	1.5 – 3.2	140	0.01 A g <sup>-1</sup>	199



Journal Name

ARTICLE

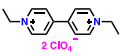
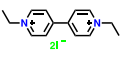
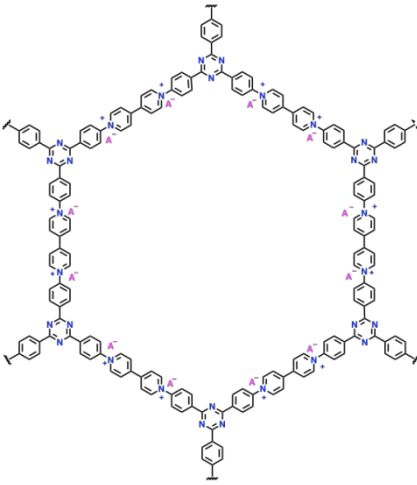
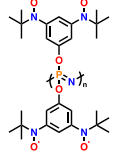
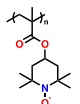
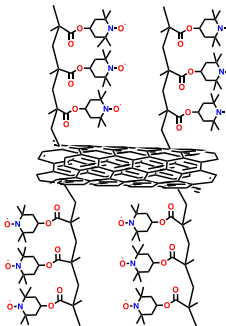
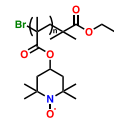
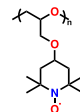
No.	Polymer Material	Chemical structure	Electrolyte	Voltage (V) vs. Li/Li <sup>+</sup>	Capacity (mA h g <sup>-1</sup> )	Current Applied	Ref.
10	<b>EV(ClO<sub>4</sub>)<sub>2</sub></b>		propylene carbonate 2 M LiClO <sub>4</sub> in TEGDME	1.6 – 3.0	176	0.5 C	200
	<b>EVI<sub>2</sub></b>				227		
11	<b>POF</b>		1 M LiPF <sub>6</sub> in EC/DMC (1:1, v/v)	1.5 – 4.5	130	3 A g <sup>-1</sup>	207

Table 5. Summarizes recent development of nitroxide radical-based cathode for organic LIBs.



## ARTICLE

## Journal Name

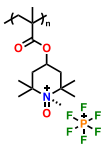
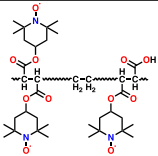
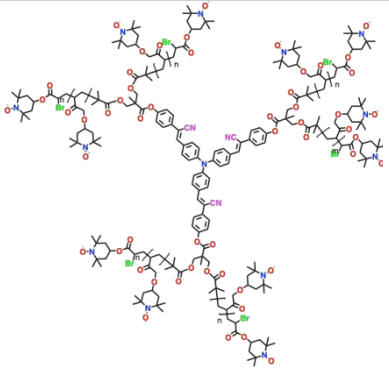
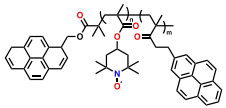
No.	Polymer Material	Chemical structure	Electrolyte	Voltage (V) vs. Li/Li <sup>+</sup>	Capacity (mA h g <sup>-1</sup> )	Current Applied	Ref.
<b>Nitroxide radical-based polymers</b>							
1	PNPP		1 M LiPF <sub>6</sub> in EC:DMC (1:1, v/v)	2.6 – 4.0	100	0.5 C	208
2	PTMA-filled NCNT		1.2 M LiPF <sub>6</sub> in EC:DEC, (1:1, v/v)	1.5 – 4.0	159.6	1 C	209
3	MWNT-g-PTMA		1 M LiPF <sub>6</sub> in (DMC:EC:EMC, 1:1:1 v/v/v)	2.0 – 4.0	243	1 C (1 C = 0.222 A g <sup>-1</sup> )	210
4	PTMA		1 M LiPF <sub>6</sub> in DMC	2.8 – 4.0	67	1 C	211
5	PTEO		1 M LiPF <sub>6</sub> in PC	2.0 – 4.0	220	0.2 C (1 C = 0.24 A g <sup>-1</sup> )	212





Journal Name

ARTICLE

No.	Polymer Material	Chemical structure	Electrolyte	Voltage (V) vs. Li/Li <sup>+</sup>	Capacity (mA h g <sup>-1</sup> )	Current Applied	Ref.
6	PTMA		1 M LiPF <sub>6</sub> in EC:DMC, (1:1, v/v)	1.5 – 4.0	219.8 (2e <sup>-</sup> ) 110.9 (1e <sup>-</sup> )	1 C	213
7	PETM		1 M LiPF <sub>6</sub> in EC:DMC:EMC, (1:1:1 v/v/v)	3.0 – 4.2	90 (binder free) 99.5 (with PVDF)	10 C	214
8	PTMA		1 M LiPF <sub>6</sub> in EC:DEC, (1:1, v/v)	3.0 – 4.2	32	0.025 mA	215
9	P(TMA-r-PyrM)		1 M LiPF <sub>6</sub> in EC:DEC, (1:1, v/v)	3.0 – 4.2	105	0.5 C	216



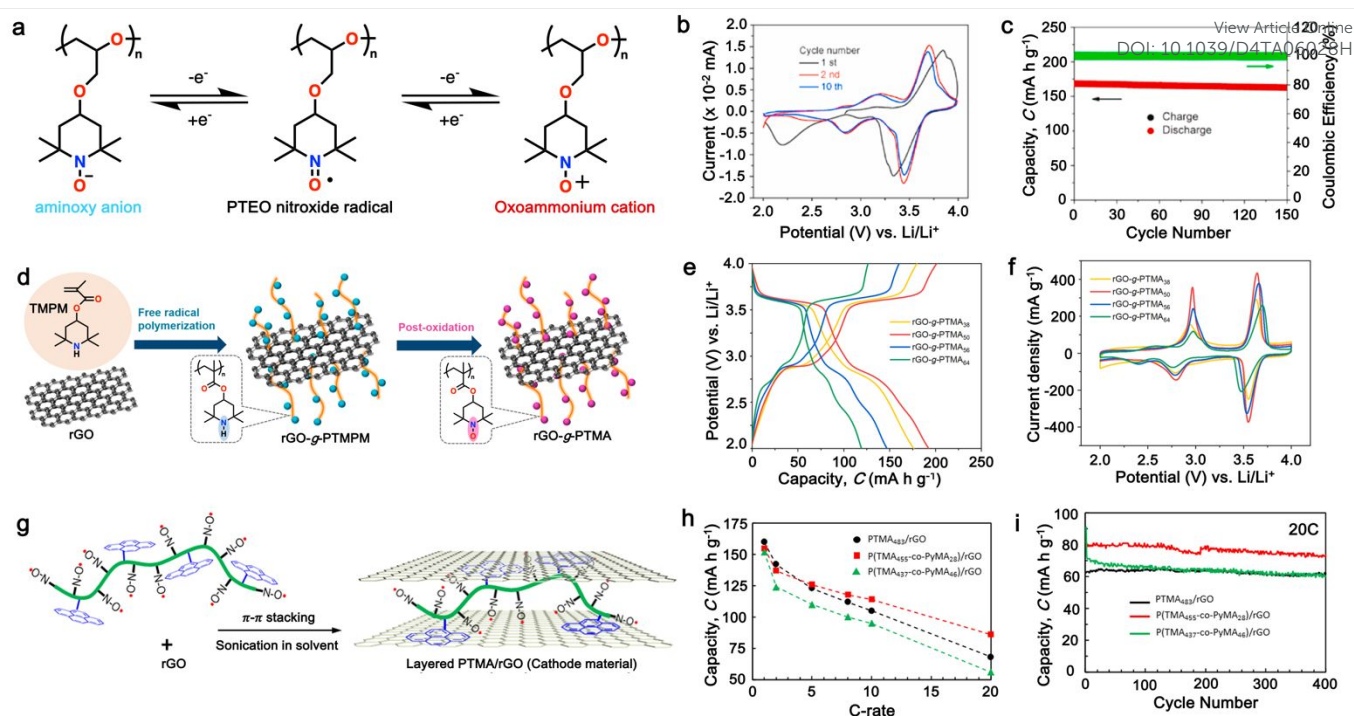


Fig.10 (a) Electrochemical mechanism of PTEO nitroxide radical during charge/discharge cycles. (b) and (c) CV curves at a scan rate of  $0.5 \text{ mV s}^{-1}$  and cycling performance under 1 C rate ( $1 \text{ C} = 240 \text{ mA g}^{-1}$ ) of PTEO nitroxide radical, respectively. Reproduced with permission from ref. <sup>212</sup>. Copyright 2020 Elsevier. (d) Schematic illustration of the preparation of PTMA-grafted graphene sheets via free radical polymerization. (e) Galvanostatic charge-discharge curves (2<sup>nd</sup> cycle) under 1C and (f) CV curves of rGO-g-PTMA with different PTMA loadings. Reproduced with permission from ref. <sup>217</sup>. Copyright 2021 Elsevier. (g) Formation of a layered PTMA/rGO composite through noncovalent  $\pi$ - $\pi$  stacking between pyrene groups and rGO sheets. (h) and (i) Rate performance and cycling stability of layered PTMA/rGO composite, respectively. Reproduced with permission from ref. <sup>218</sup>. Copyright 2017 American Chemical Society.

chemistry with favorable kinetics, facilitated by redox reactions involving the singly occupied molecular orbital, enabling rapid electron transfer and high-rate performance capability. Considering the nonconjugated backbones and stable open-shell pendant groups, nitroxide radical polymers offer charge transport through a series of redox reactions between the pendant open-shell sites. Therefore, stable radicals such as nitroxyl, phenoxy,<sup>202, 219</sup> nitroxylbenzene,<sup>220</sup> nitronylnitroxyl,<sup>221</sup> and hydrazyl<sup>222</sup> groups, with structures like 2,2,6,6-tetramethylpiperidine-*N*-oxy (TEMPO), have been explored as LIBs cathode.<sup>204, 223, 224</sup> Among of those radical polymers, poly (2,2,6,6-tetramethylpiperidinyloxy-4-vinylmethacrylate (PTMA)<sup>54, 153, 225, 226</sup> and 2,2,6,6-tetramethyl-1-piperidinyloxy (PTVE),<sup>224, 227</sup> have been investigated and showed high redox potentials of  $\sim 3.6 \text{ V}$  vs.  $\text{Li/Li}^+$ . In this regard, nitroxide radical polymer based on ethylene oxide backbone, poly (4-glycidyoxy-2,2,6,6-tetramethylpiperidine-1-oxyl) (PTEO), was designed and reported (Fig. 10a). As shown in Fig. 10b, two-step redox reaction of PTEO were observed in the CV curves, which is associated with the formation of aminoxy anion at 2.75/3.20 V and oxoammonium cation at 3.48/3.60 V.<sup>212</sup> Thanks to the super high electrical conductivity of PTEO, due to the unique open-shell site of the monomer as well as the completed

conservation of all of the radical sites in the monomer, this PTEO delivered a specific capacity of  $154 \text{ mA h g}^{-1}$  at 1C rate after 150 cycles, corresponding to 91% capacity retention (Fig. 10c). Additionally, to improve material stability and minimize polymer solubility, Jin et al. grafted PTMA-based polymer onto the surface of reduced graphene oxide (rGO) via in-situ free radical polymerization (FRP) as shown in Fig. 10d. The electrochemical performance of rGO-g-PTMA shows that the specific capacities ranging from 176 to  $119 \text{ mA h g}^{-1}$  can be obtained at a current rate of 1 C by varied PTMA loading from 38 to 54 wt% (Fig. 10e). Notably, the rGO-g-PTMA<sub>50</sub> cathode exhibited the highest specific capacity. Moreover, CV measurement confirmed the electrochemical performance of rGO-g-PTMA, with the rGO-g-PTMA<sub>50</sub> sample demonstrating superior performance as shown in Fig. 10f.<sup>217</sup> Taking a similar approach, Zhang et al. investigated PTMA-based copolymer cathode combined with nanostructured carbon-based electrodes through non-covalent interactions (Fig. 10g). Prior to the additional conductive carbon such as rGO and CNTs, ultrafast single electron transfer-nitroxide radical coupling has been applied to introduce pyrene groups onto PTMA, forming P(TEMPO-co-PyMA) copolymers.



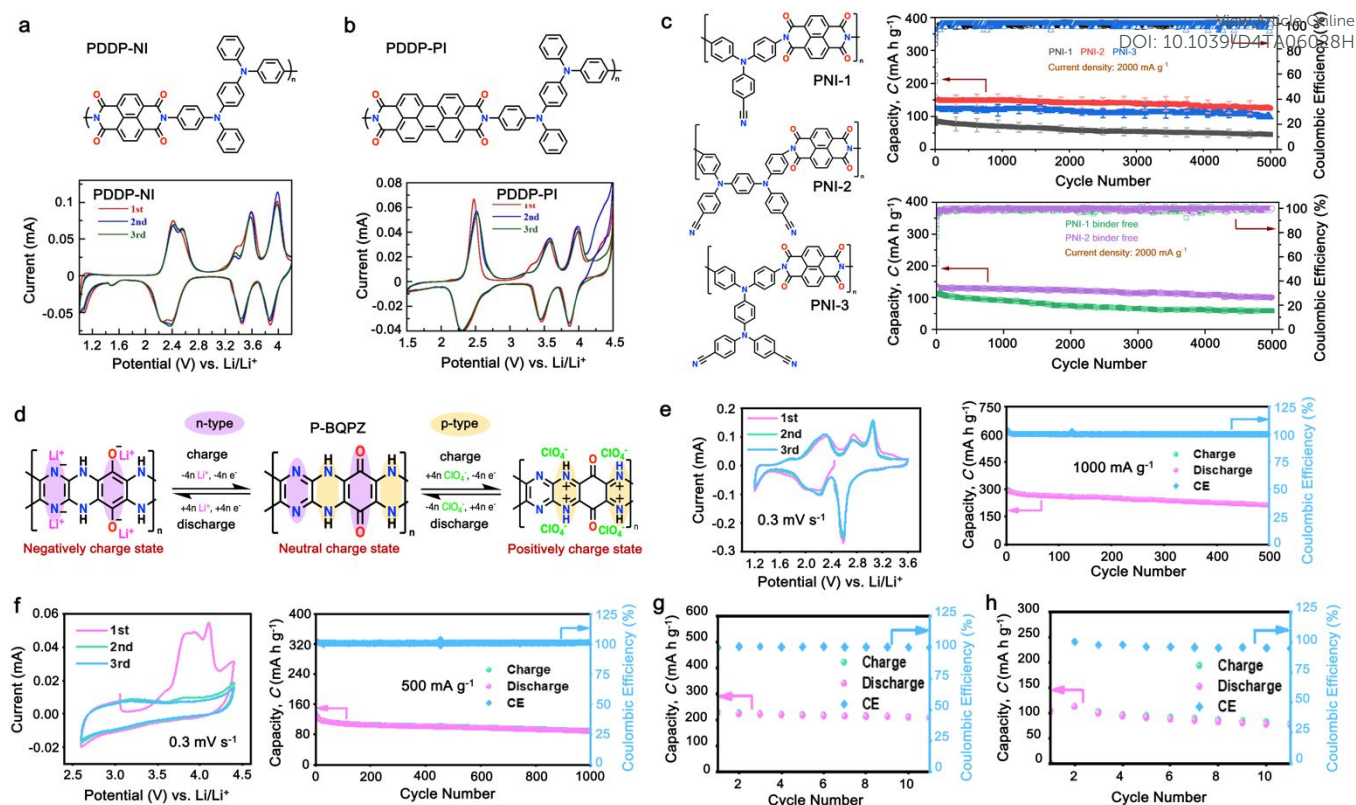


Fig.11 (a) and (b) Chemical structure and cyclic voltammogram of **PDDP-NI** and **PDDP-PI** bipolar polymer. Reproduced with permission from ref.<sup>228</sup>. Copyright 2021 the Electrochemical society. (c) Chemical structures and long cycling performance of redox-active polynaphthalimides (**PNI**s). Reproduced with permission from ref.<sup>62</sup>. Copyright 2023 Royal Society of Chemistry. (d) Chemical structure and redox reaction mechanism of the bipolar polymer **P-BQPZ**. (e) and (f) CV curves and long cycling performance of n-type **P-BQPZ** and p-type **P-BQPZ**, respectively. (g) Cycling performance of the full cell based on n-type redox reaction of **P-BQPZ** at current of  $500 \text{ mA g}^{-1}$  between 0.1 and 2.7 V. (h) Cycling performance of the full cell based on p-type redox reaction of **P-BQPZ** at current of  $50 \text{ mA g}^{-1}$  between 0.1 and 3.4 V. Reproduced with permission from ref.<sup>229</sup>. Copyright 2022 Elsevier.

After that, this **P(TEMPO-co-PyMA)** copolymers were wrapped with **rGO** using ultrasonication and ultracentrifugation. These copolymers were then used to bind to **rGO** flakes, forming electrode composites with a multilayered sandwich-like structure (Fig. 10g). This approach has successfully enhance the performance of **PTMA**-based cathode as it delivered high capacity of  $\sim 150 \text{ mA h g}^{-1}$  at 1C rate (Fig. 10h) and exhibited outstanding stability under high current rate of 20C (Fig. 10i).<sup>218</sup> Table 5 describes the current trends in developing the nitroxyl radical-based cathodes for organic batteries.

## 4. Alternative design of p-type polymer electrodes

### 4.1 Bipolar-type polymers

Bipolar-type polymers have emerged as promising candidates for next-generation high-performance LIBs due to their unique redox properties involving both p-type and n-type charge carriers, enabling an optimum charge storage and transport within the electrode material.<sup>11</sup> Thanks to synergic contribution of p- and n-type charge storage character, the nature of these polymers allows them to store and release both cations and anions during the charging and discharging

processes, leading to enhanced energy storage capabilities.<sup>23</sup> This feature is particularly advantageous for achieving high specific capacities and energy density in LIBs.<sup>230</sup> Bipolar-type polymers have demonstrated impressive electrochemical performance metrics in LIBs, including high specific capacities, excellent rate capabilities, and long-term cycling stability.<sup>231</sup> These polymers hold promise for a wide range of applications in portable electronics, electric vehicles, and grid energy storage systems, where high energy density, fast charging/discharging rates, and durability are critical requirements.<sup>232</sup> Recently, series of bipolar polymers have been reported to significantly improve the specific capacity of LIBs. For instance, Zhang et al. reported two bipolar-type polymers by combining arylamine-based (p-type) and carbonyl-based (n-type) moieties to form poly(arylamine-imide)s, namely poly(*N,N,N',N'*-tetraphenyl-1,4-benzenediamine naphthalenediimide) (**PDDP-NI**) and poly(*N,N,N',N'*-tetraphenyl-1,4-benzenediamine perylenediimide) (**PDDP-PI**), as shown in Fig. 11a – b.<sup>120</sup> The bipolar activity is observed as these polymers exhibited specific redox properties associated with arylamine- and imide-units. As shown in Fig. 11a – b, both of **PDDP-NI** and **PDDP-PI** exhibited three pairs redox peaks at  $\sim 2.46/2.30$ ,  $3.56/3.44$ , and  $3.98/3.87$





V, respectively. The first pair redox peak is ascribed to the redox activity of carbonyl group in imide unit (n-type), while the last two redox couples are associated with doped/de-doped process of arylamine unit (p-type). Furthermore, this strategy successfully improves the cathode specific capacity up to 150.9 (PDDP-NI) and 119.4 (PDDP-PI) mA h g<sup>-1</sup> after 70 cycles at 0.1C.

Taking a similar approach, series of bipolar triphenylamine-based polynaphthalimides (TPA-PNIs) have been reported not only as cathode, but also as anode and binder-free cathode in LIBs.<sup>62</sup> These TPA-PNIs cathode delivered a high specific capacity up to 195 mA h g<sup>-1</sup> after 100 cycles at 50 mA g<sup>-1</sup>, due to synergic contribution from both p- and n-type units. As shown in Fig. 11c, these polymers exhibited outstanding stability up to 5000 cycles under extreme current density of 2000 mA g<sup>-1</sup>. Notably, no significant capacity drop can be monitored even as a binder-free cathode (Fig. 11c), suggesting excellent material stability and dual-role ability as active materials and electrode binder simultaneously. In another study, Labasan et al. developed two polyimide (PI) derivatives, TPA-PMPI and TPA-NTCPI, as electrode materials for LIBs.<sup>58</sup> These polymers exhibit excellent thermal stability and bipolar properties. TPA-NTCPI cathode delivered a reversible specific capacity of 150 mA h g<sup>-1</sup> at 0.1 A g<sup>-1</sup> and showed stability up to 1000 cycles, while TPA-PMPI anode achieved a high specific capacity of up to 1600 mA h g<sup>-1</sup> at 0.1 A g<sup>-1</sup> after 100 cycles.<sup>58</sup> Furthermore, various polymerization methods have also been studied to integrate bipolar moieties. Wang and colleagues successfully polymerized amino-phenyl carbazole naphthalene diimide (APCNDI) using in situ electropolymerization to eliminate the dissolution problem.<sup>233</sup> The electropolymerized cathode demonstrated excellent electrochemical performance, stable cycling performance, and superior rate performance. In addition, taking different strategy, Zhao and colleagues integrated series of n- and p-type redox-active moieties into one stable polymer backbone to minimize redox-inactive moieties (Fig. 11d).<sup>229</sup> As shown in Fig. 11e, the CV curves of P-BQPZ demonstrate clear and reversible redox peaks of n-type redox reactions attributed to C=O at 2.6, 2.7, and 3.0 V (vs. Li/Li<sup>+</sup>) and C=N bonds at 2.3 and 2.2 V (vs. Li/Li<sup>+</sup>). This redox activity contributed to the specific capacity of 213.3 mA h g<sup>-1</sup> up to 500 cycles under current density of 1000 mA g<sup>-1</sup> (Fig. 11e). Additionally, P-BQPZ p-type activity is depicted in Fig. 11f, showing a higher redox activity at 3.1 V (vs. Li/Li<sup>+</sup>) and contributing capacity of ~120 mA h g<sup>-1</sup> up to 1000 cycles at 500 mA h g<sup>-1</sup>. Additionally, the cycling performance of the full cell based on n-type and p-type redox reaction of P-BQPZ has been presented in Fig. 11g and 11h, respectively, depicting successful incorporation of P-BQPZ in full cell LIB system. These findings provide a novel strategy for designing and fabricating high-performance cathode LIBs by combining two different electrochemical characters thus offering potential solutions to improve energy density. Continued research efforts aimed at advancing the synthesis, characterization, and understanding of these polymers as well as minimizing synthetic cost are essential for realizing their full potential in energy storage applications. Furthermore, Table 6 describes the current trends

in developing alternatives design p-types cathodes for organic batteries.

DOI: 10.1039/D4TA06028H

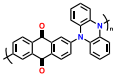
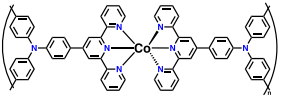
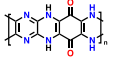
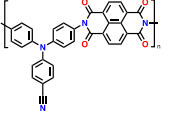
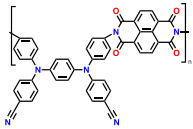
## 4.2 Hybrid organic-inorganic polymer

Hybrid organic-inorganic polymers have emerged as promising alternatives approach to improve electrochemical performance and stability of polymer-based for electrodes. This synergistic combination of both organic and inorganic character offers opportunities to overcome limitations associated with conventional electrode materials and to develop high-performance LIBs with enhanced energy storage capabilities. One common approach in designing organic-inorganic hybrid electrodes involves incorporating polymers matrix into the structure of inorganic materials. For example, organic molecules like conducting polymers, viologens, or redox-active organic compounds can be integrated with inorganic materials such as metal oxides, sulfides, phosphides, or carbon-based materials to form hybrid electrode composites.<sup>234</sup> These composites can exhibit improved electrochemical properties, including high capacity, cycling stability, and rate capability, compared to their individual components. Another strategy involves the synthesis of nanostructured hybrid materials, where organic and inorganic components are intimately intertwined at the nanoscale. This approach enables precise control over the morphology, surface area, and interfacial properties of the electrode materials, leading to enhanced ion diffusion kinetics and electrochemical performance.<sup>235</sup> Nanostructured hybrid materials can be fabricated using techniques such as sol-gel synthesis, hydrothermal synthesis, chemical vapor deposition, or electrodeposition.<sup>236</sup>

Several types of organic-inorganic hybrid materials have been investigated for LIB electrodes, including metal-organic frameworks (MOFs),<sup>235, 237, 238</sup> covalent organic frameworks (COFs),<sup>53, 65, 239-241</sup> conductive polymers/carbon composites,<sup>242, 243</sup> and redox-active organic-inorganic composites.<sup>244, 245</sup> In particular, Zhu et al. developed a composite cathode material by introducing polydiphenylamine (PDPA) on the lithium trivanadate (LiV<sub>3</sub>O<sub>8</sub>, LVO) using an in situ oxidative polymerization method, leading to significant improvements in electrochemical properties and the inhibition of adverse reactions as shown in Fig. 12a.<sup>246</sup> TEM analysis revealed that the surfaces of LiV<sub>3</sub>O<sub>8</sub> were coated with a layer of PDPA, with an average polymer thickness of around 20 nm (Fig. 12b). The 10 wt% LiV<sub>3</sub>O<sub>8</sub>/PDPA composite exhibited a high initial specific discharge capacity of 311 mA h g<sup>-1</sup>, which decreased to 272 mA h g<sup>-1</sup> after 50 cycles at a current density of 60 mA g<sup>-1</sup>. Furthermore, the composite displayed remarkable improvement in rate capability, with discharge capacities at various current densities outperforming those of pure LVO electrodes (Fig. 12c). This increased performance of LVO-based cathode could be ascribed to high conductive coating of PDPA. With a similar aim, LiFePO<sub>4</sub>/poly(3,4-ethylenedioxythiophene) (PEDOT) composites were prepared.<sup>247</sup> Furthermore, poly(aniline) has also been explored to coat LiFePO<sub>4</sub> cathode, resulting hybrid polymer-inorganic composite. It was demonstrated that the polymer serves not only as a conductive



Table 6. Summarizes recent development of alternatives design p-type cathode for organic LIBs.

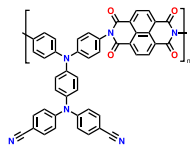
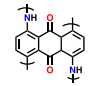
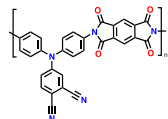
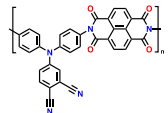
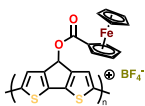
No.	Polymer Material	Chemical structure	Electrolyte	Voltage (V) vs. Li/Li <sup>+</sup>	Capacity (mA h g <sup>-1</sup> )	Current Applied	Ref.
<b>Bipolar-type polymers</b>							
1	<b>PAQDPZ</b>		3 M LiFSI in TEGDME	1.6 – 4.3	105 (Symmetric organic battery)	0.2 A g <sup>-1</sup>	248
			1 M LiPF <sub>6</sub> in EC/DEC	1.5 – 4.2	208 (Li-ion full cell)	0.2 A g <sup>-1</sup>	
			3 M LiFSI in TEGDME	1.6 – 4.3	222 (Li-ion half-cell)	0.2 A g <sup>-1</sup>	
2	<b>poly(CoL)<sub>n</sub></b>		1 M LiPF <sub>6</sub> in EC:DEC, (1:1, v/v)	1.5 – 4.5	125.16	2 A g <sup>-1</sup>	249
3	<b>P-BQPZ</b>		1 M LiTFSI in DOL:DME (1:1, v/v)	2.6 – 4.4	130 (p-type)	0.5 A g <sup>-1</sup>	229
			1 M LiClO <sub>4</sub> in EC:DMC (1:1, v/v)	1.2 – 3.6	298 (n-type)	1 A g <sup>-1</sup>	
4	<b>PNI-1</b>		1 M LiPF <sub>6</sub> in EC:DEC (1:1, v/v)	1.5 – 4.5	125	0.05 A g <sup>-1</sup>	62
	<b>PNI-2</b>				195		





## ARTICLE

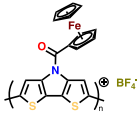
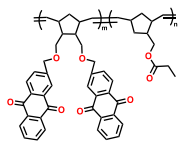
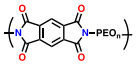
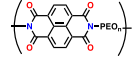
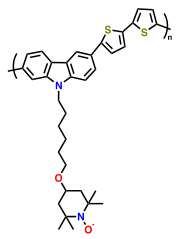
## Journal Name

No.	Polymer Material	Chemical structure	Electrolyte	Voltage (V) vs. Li/Li <sup>+</sup>	Capacity (mA h g <sup>-1</sup> )	Current Applied	Ref.
	<b>PNI-3</b>				170		
5	<b>DAAQ</b>		1 M LiPF <sub>6</sub> in EC:DMC (1:1, v/v)	1.5 – 4.5	311	0.05 A g <sup>-1</sup>	250
6	<b>TPA-PMPI</b>		1 M LiTFSI in DOL:DME (1:1, v/v),	1.5 – 3.5 (cathode)	150	0.1 A g <sup>-1</sup>	58
	<b>TPA-NTCPI</b>						
<b>Hybrid organic-inorganic polymer</b>							
7	<b>LiV<sub>3</sub>O<sub>8</sub>/polythiophene (LiV<sub>3</sub>O<sub>8</sub>/PTh)</b>		1 M LiPF <sub>6</sub> in EC:DMC (1:1, v/v)	1.8 – 4.0	213.3	1 C (1 C = 0.3 A g <sup>-1</sup> )	251
8	<b>LiV<sub>3</sub>O<sub>8</sub>/polydiphenylamine</b>		1 M LiPF <sub>6</sub> in EC:DMC:EMC, (1:1:1, v/v/v)	1.8 – 4.0	311	0.06 A g <sup>-1</sup>	246
9	<b>pCPDT-Fc P1</b>		1 M LiPF <sub>6</sub> in EC:DMC (1:1, v/v)	2.7 – 3.9	59.7	0.1 C (1 C = 0.066 A g <sup>-1</sup> )	252



Journal Name

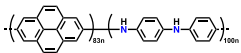
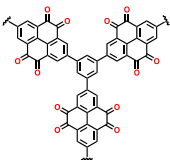
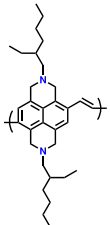
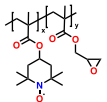
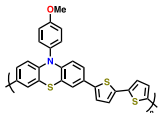
ARTICLE

No.	Polymer Material	Chemical structure	Electrolyte	Voltage (V) vs. Li/Li <sup>+</sup>	Capacity (mA h g <sup>-1</sup> )	Current Applied	Ref.
	<b>pDTP-Fc P2</b>				59.8		
10	<b>NMC/PPy</b>		1 M LiPF <sub>6</sub> in EC:DMC:EMC, (1:1:1 (v/v/v))	2.5 – 4.5	202.2	0.2 C	253
11	<b>LMNC@Li<sub>3</sub>PO<sub>4</sub>&amp;PANI</b>		1 M LiPF <sub>6</sub> in EC:DMC:EMC, (1:1:1 (v/v/v))	2.0 – 4.8	172.60	1 C	254
12	<b>Li<sub>1.2</sub>Ni<sub>0.2</sub>Mn<sub>0.6</sub>O<sub>2</sub>/PEDOT:PSS</b>		1 M LiPF <sub>6</sub> in EC:DMC (1:1, v/v)	2.0 – 4.8	285	0.2 C (1 C = 0.3 A g <sup>-1</sup> )	255
<b>Copolymer materials</b>							
13			2 M LiTFSI in DOL/DME (1:1, v/v)	1.5 - 3.0	127 84	0.1 C 1 C (1 C = 0.172 A g <sup>-1</sup> )	256
14	<b>Pyromellitic polyimide-b-PEO</b>		1 M LiTFSI/MeTHF	1.0 – 3.4	225	0.1 C (1 C = 0.203 A g <sup>-1</sup> )	257
					160		
15	<b>pBTC-TEMPO</b>		1 M LiPF <sub>6</sub> in EC/DMC, (1:1, v/v)	3.0 – 4.0	50	1 C (1 C = 0.06 A g <sup>-1</sup> )	258



## ARTICLE

## Journal Name

No.	Polymer Material	Chemical structure	Electrolyte	Voltage (V) vs. Li/Li <sup>+</sup>	Capacity (mA h g <sup>-1</sup> )	Current Applied	Ref.
16	Poly-PPDA-PYR		1 M LiPF <sub>6</sub> in EC/DMC, (1:1, v/v)	2.0 – 4.2	75	0.5 A g <sup>-1</sup>	<a href="#">259</a>
17	PPh-PTO		1 M LiTFSI in DOL/DME(1:1, v/v)	1.5 – 3.8	235	0.1 A g <sup>-1</sup>	<a href="#">260</a>
18	PENDI		1 M LiPF <sub>6</sub> in EC/DMC, (1:1, v/v)	1.0 – 4.0	110	0.1 C (1 C = 0.202 A g <sup>-1</sup> )	<a href="#">261</a>
19	PTMA-co-GMA		1 M LiPF <sub>6</sub> in EC/DEC (1:1, v/v)	3.0 – 4.0	104	0.1 C	<a href="#">262</a>
20	p(APT-T2)		1 M LiPF <sub>6</sub> in EC/DMC (1:1, v/v)	3.2 – 4.2	68.5	1 C	<a href="#">263</a>



Journal Name

ARTICLE

No.	Polymer Material	Chemical structure	Electrolyte	Voltage (V) vs. Li/Li <sup>+</sup>	Capacity (mA h g <sup>-1</sup> )	Current Applied	Ref.
21	PTPA-HATN		1 M LiPF <sub>6</sub> in EC/DMC/EMC (1:1:1, v/v/v)	1.5 – 4.2	120	0.025 A g <sup>-1</sup>	264
	PDTPA-HATN				103.6		
22	NSHATN		LiCF <sub>3</sub> SO <sub>3</sub> in G4	1.5 – 4.0	337	0.05 A g <sup>-1</sup>	265
23	HATCNO-poly		1 M LiTFSI in TEGDME	1.0 – 2.8	158.6	0.05 A g <sup>-1</sup>	266



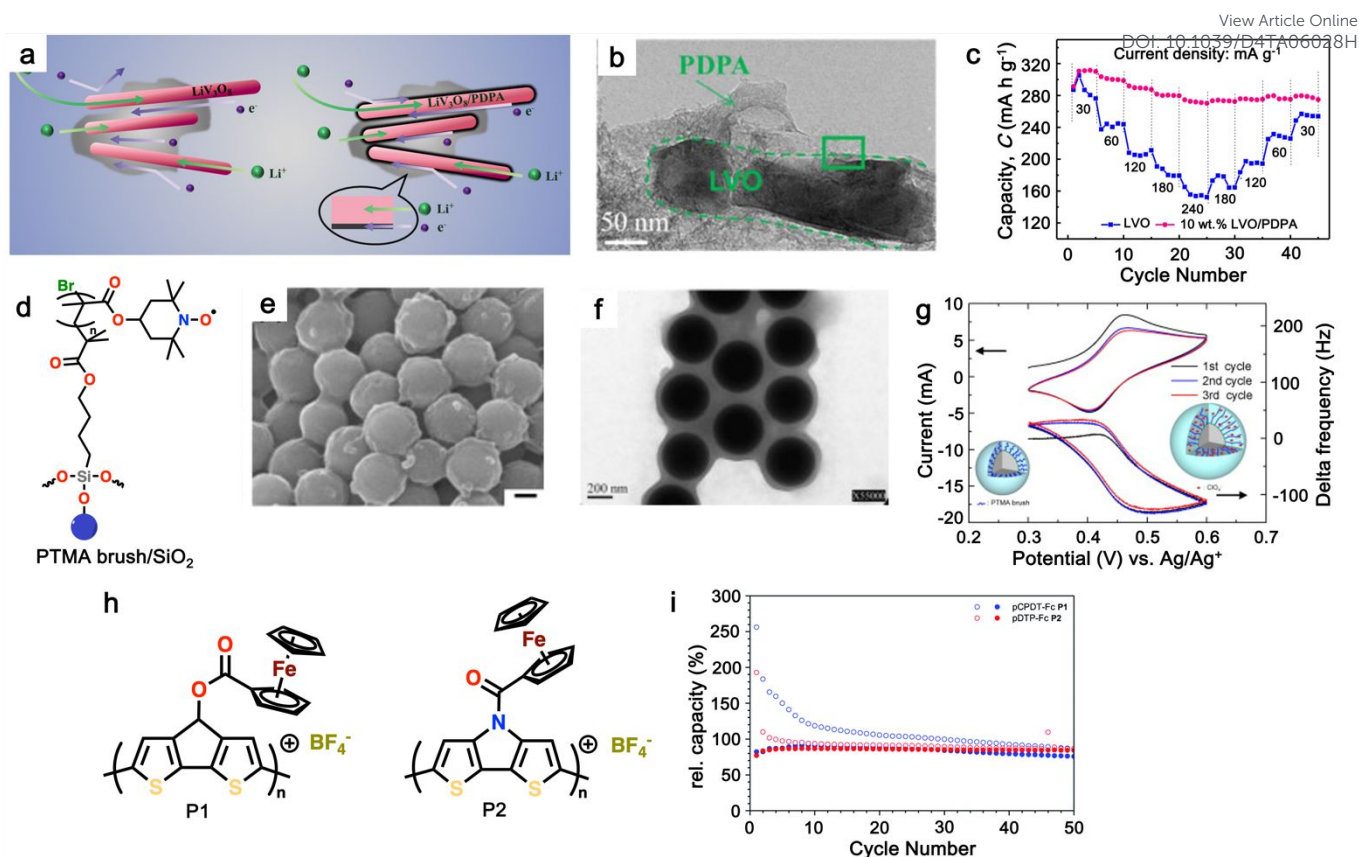


Fig.12 (a) Schematic illustration depicting the Li<sup>+</sup> and electron-transfer pathway for LVO and LVO/PDPA composites. (b) TEM micrographs showing the morphology of 10 wt% LVO/PDPA composite. (c) Rate capabilities comparison between LVO and 10 wt% LVO/PDPA composites at various current densities. Reproduced with permission from ref.<sup>246</sup>. Copyright 2018 American Chemical Society. (d) Chemical structure of PTMA brush/SiO<sub>2</sub> hybrid materials. (e) and (f) SEM and TEM images of PTMA brush/SiO<sub>2</sub>, respectively. (g) Cyclic voltammogram of PTMA brush/SiO<sub>2</sub> on the Au electrode and its corresponding resonance frequency change of EQCM sensor. The electrolyte was 0.1 M (C<sub>4</sub>H<sub>9</sub>)<sub>4</sub>NClO<sub>4</sub> in acetonitrile. Reproduced with permission from ref.<sup>267</sup>. Copyright 2011 Elsevier. (h) Chemical structure of ferrocene-functionalized polyheteroacenes, namely P1 and P2. (i) Cycling performance of P1 and P2 ferrocene-functionalized polyheteroacenes under 0.1 C. Reproduced with permission from ref.<sup>252</sup>. Copyright 2018 Royal Society of Chemistry.

matrix and binder but also as an additional host for lithium-ion intercalation. At 0.2 C rate, it achieved a capacity of 165 mA h g<sup>-1</sup>, which decreased by 25% to 123 mA h g<sup>-1</sup> at 10 C rate. Despite this, the discharging curves remained flat, suggesting a good cycling stability.<sup>268</sup>

In addition, a triphenylamine-based MOF, **Cu-TCA** (H<sub>3</sub>TCA = tricarboxytriphenyl amine), has been reported as a LIB cathode active material.<sup>269</sup> In this framework architecture, the redox activity of **Cu-TCA** is associated with redox activity of both metal clusters (Cu<sup>+/Cu<sup>2+</sup></sup>) and organic ligand radicals (N/N<sup>+</sup>) with separated voltage plateaus and a high working potential up to 4.3 V (vs. Li/Li<sup>+</sup>). Due to its abundant redox-active constituents and highly stable organic ligands, **Cu-TCA** has a theoretical capacity of 145 mA h g<sup>-1</sup>, which is comparable to that of commercial materials such as LiFePO<sub>4</sub> (170 mA h g<sup>-1</sup>). Moreover, **Cu-TCA** achieved long cycling stability over 200 cycles at a 2 C rate, with an average coulombic efficiency of 96.5%, suggesting that **Cu-TCA** is capable of delivering high recharge rate with

high-capacity retention. Inspired by these findings, Lin et al. explored the potential of nitroxide radical-based PTMA as a cathode material (Fig. 12d) by polymerizing a polymer brush over silica nanoparticles.<sup>267</sup> The nitroxide polymer brushes, grafted onto silica nanoparticles via surface-initiated atom transfer radical polymerization, prevented polymer dissolution into organic electrolytes. SEM and TEM images confirm the nitroxide polymer brushes are successfully grafted onto silica nanoparticles (Fig. 12e and 12f). Further, the results of the electrochemical quartz crystal microbalance indicate that the non-crosslinking nitroxide polymer brushes prevent the polymer from dissolving into organic electrolytes (Fig. 12g). These electrodes showed high discharge capacities and excellent cycle-life performance, demonstrating the potential of organic-inorganic hybrid systems for energy storage applications. Similarly, Schwartz et al. synthesized conjugated polymers based on ferrocene-functionalized cyclopentadithiophene and poly(dithieno[3,2-*b*:2',3'-*d*]pyrrole)





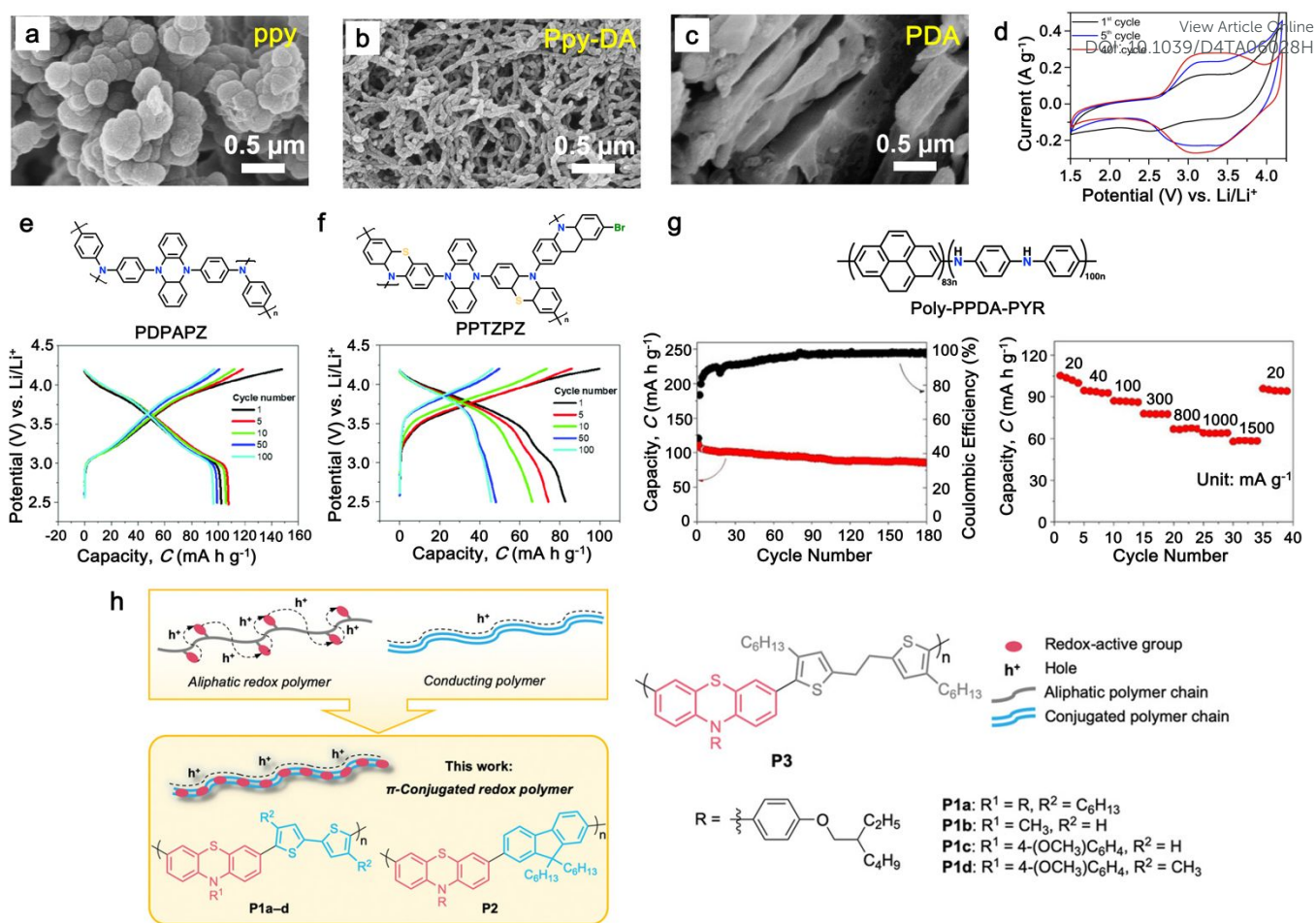


Fig.13 SEM images of (a) PPy, (b) PPy-DA, and (c) PDA. (d) CV curves of PPy-DA at a scan rate of 1 mV s<sup>-1</sup>. Reproduced with permission from ref.<sup>270</sup>. Copyright 2018 Elsevier. (e) and (f) Chemical structure and galvanostatic charge-discharge of PDPAPZ and PPTZPZ copolymers, respectively. Reproduced with permission from ref.<sup>179</sup>. Copyright 2020 John Wiley and Sons. (g) Cycling performance under current density of 20 mA g<sup>-1</sup> and rate performance of poly-PPDA-PYR copolymer. Reproduced with permission from ref.<sup>259</sup>. Copyright 2019 John Wiley and Sons. (h) Schematic π-conjugated redox polymer. Reproduced with permission from ref.<sup>271</sup>. Copyright 2019 John Wiley and Sons.

backbones (Fig. 12h).<sup>252</sup> These polymers exhibited high reversible capacities and excellent capacity retentions over multiple cycles, showcasing their suitability for battery applications (Fig. 12i). Together, these studies highlight the potential of organic-inorganic hybrid materials as electrodes for high-performance LIBs.

### 4.3 Copolymer materials

Recently, copolymerization emerged as an alternative approach to enhance the electrochemical performance of polymer-based electrode. These materials typically consist of two or more different monomer units polymerized together, offering synergistic benefits than that of individual polymers.<sup>272, 273</sup> One notable advantage of copolymer materials is their ability to combine the desirable properties of different polymer components. For example, copolymers can incorporate both electron-rich and electron-deficient monomers, enabling

improved charge transfer kinetics and stability during cycling. Additionally, the incorporation of various functional groups within copolymer structures can be introduced to facilitate rapid lithium-ion diffusion and enhance the number of active sites.<sup>273</sup> Moreover, copolymer materials often offer enhanced mechanical strength and flexibility compared to individual polymer or traditional inorganic electrodes, making them suitable for use in flexible and lightweight battery applications.<sup>274</sup> Furthermore, copolymer-based electrodes can be processed using scalable solution-based techniques, enabling cost-effective and large-scale manufacturing.

Recent research efforts have focused on designing copolymer materials with tailored properties for specific battery applications. For instance, copolymers containing conjugated backbones, such as polythiophenes or polypyrrole, have been investigated for their high electrical conductivity and lithium-ion storage capacity.<sup>92, 275</sup> Additionally, copolymers incorporating redox-active moieties, such as viologen or



anthraquinone, have shown promise for achieving high capacity and long-term cycling stability.<sup>276</sup> Copolymers like the one derived from pyrrole and dopamine (**PPy-DA**) offer distinct advantages in LIB applications by combining the charge storage properties of different monomers.<sup>270</sup> The copolymer presented a porous NFs morphology, which was different from the plate-like structure of **PDA** and the aggregated nanospheres of **PPy** (Fig. 13a – c). **PPy-DA** is produced by the copolymerization of dopamine (n-type) and **PPy** (p-type) monomer, leading to a copolymer with a shorter polaron delocalization length. This reduction in delocalization is effective to enhance its redox potential (around 3 - 3.5 V) and specific capacity ( $\sim 160 \text{ mA h g}^{-1}$ ) (Fig. 13d). Furthermore, two novel copolymers, namely poly(dihydrophenazine-co-diphenylamine) (**PDPAPZ**) and poly(dihydrophenazine-co-phenothiazine) (**PPTZPZ**), have been synthesized and evaluated as cathode materials (Fig. 13e and 13f).<sup>179</sup> These copolymers exhibit a high average discharge potential (3.5 – 3.6 V) in lithium cells. Remarkably, **PDPAPZ**/Li cells demonstrate steady specific capacities of  $\sim 101 \text{ mA h g}^{-1}$  current density of  $0.1 \text{ A g}^{-1}$  up to 100 cycles (Fig. 13e). On the other hand, **PPTZPZ** exhibited a lower capacity of  $80 \text{ mA h g}^{-1}$  and later demonstrated gradual capacity decreased up to 100 cycles (Fig. 13f), due to inactive sulfur species. Similarly, Yao and colleagues have synthesized a new conjugated copolymer for use as an organic cathode material by incorporating both conducting aniline and pyrene units (Fig. 13g).<sup>259</sup> This **poly-PPDA-PYR** achieved a reversible specific capacity of  $113 \text{ mA h g}^{-1}$  under  $20 \text{ mA g}^{-1}$  current density with a high voltage output of 3.2 V and impressive capacity retention of 75.2% after 180 cycles (Fig. 13g). Additionally, the copolymer exhibits excellent rate performance up to  $1500 \text{ mA g}^{-1}$ , and the highest specific capacity  $\sim 100 \text{ mA h g}^{-1}$  could be recovered once the current density switched back to  $20 \text{ mA g}^{-1}$  (Fig. 13g).

In addition to copolymerization of redox-active components, the incorporation of inactive components into copolymers has also been extensively investigated due to their impact on the electrochemical performance. These inactive components serve various functions such as enhancing cycle stability, electrical conductivity, ionic conductivity, cohesiveness, and flexibility, however, the reduced theoretical capacity is often monitored.<sup>277</sup> For instance, Hernández et al. combined a redox-active polyimide (**PI**) with ion-conductive polyether blocks (**PEO**), where **PEO** acted as both a binder and conductive agent.<sup>257</sup> The resulting binder-free and conductive agent-free copolymer electrode exhibited excellent discharge capacity and cycling life. Similarly, Zhang et al. synthesized a copolymer based on poly (2,2,6,6-tetramethylpiperidinyloxy methacrylate) (**PTMA**) with controllable pyrene side groups, which enhanced electron transfer rates and resulted in improved specific capacity and rate capability when uniformly dispersed in a composite with reduced graphene oxide (**rGO**).<sup>218</sup> Additionally, ultra-high-rate capability and long stability have been demonstrated using phenothiazine copolymer.<sup>271</sup> The design of this copolymer cathode is based on combination of high oxidation phenothiazine of 3.6 V (vs. Li/Li<sup>+</sup>) and good hole conductivity of bithiophene and fluorene comonomer (Fig. 13i). The ultra-high-rate capability and long cycling stability is

demonstrated as the  $\pi$ -conjugated copolymer could be operated up to 30000 cycles under extreme current rate of 100C with >97% capacity retention. These studies emphasized the importance of copolymerization strategy in order to enhance electrochemical performance of polymer cathode.

## 5. Conclusions and perspective

Polymeric electrode materials have emerged as a promising alternative cathode material towards high-performance and high-energy-density 4.0 V-class LIBs. By tailoring the chemical structure through functionalization, doping, and incorporating both redox-active and inactive components, researchers are able to optimize the batteries key parameters such as specific capacity, cycling stability, and rate capability. This innovative approach addresses many of the limitations associated with traditional electrode materials, paving the way for more efficient, durable, and high-performing LIBs. As the demand for higher energy storage solutions continues to grow, the advancements in polymeric electrode design are poised to play a crucial role in meeting the energy needs of the future. Thanks to flexibility in design, scalability of synthesis, and compatibility with high-energy-density applications compare to the conventional inorganic cathode materials, series of high-voltage polymer such as arylamine-based, thioether, phenazine, viologen and radical polymer have been explored and discussed in detail. Additionally, alternative approaches such as the bipolar polymer formation, hybrid organic-inorganic, and copolymerization strategies have also shown a promising to enhance electrochemical performance and stability of polymer cathode. By harnessing the unique properties of each polymer, such as tunable redox chemistry, mechanical flexibility, and chemical stability, researchers have unlocked new possibilities for achieving superior electrochemical performance in LIBs. Moving forward, continued research efforts in this field will be essential to further optimize the design and synthesis of polymeric-based electrode materials, paving the way for the next generation of high-performance LIBs.

Looking ahead, the future of polymeric electrode materials for high-energy-density LIBs holds exciting prospects and challenges. First and foremost, there is a need for deeper understanding of the fundamental electrochemical processes occurring within polymer electrodes, including ion transport mechanisms, charge storage mechanisms, and degradation pathways. Advanced characterization techniques, coupled with computational modeling, will play a crucial role in elucidating these complex phenomena and guiding the rational design of next-generation polymer electrodes. Furthermore, efforts should be directed towards the development of scalable synthesis methods for producing polymer materials with well-defined structures and tailored properties. Integration of advanced manufacturing techniques, such as additive manufacturing and roll-to-roll processing, will enable the fabrication of large-area, high-performance polymer electrodes for practical applications. Additionally, research should focus on exploring novel polymer chemistries, functionalization strategies, and electrode architectures to further enhance the



energy density, safety, and lifespan of 4.0 V-class LIBs. Additionally, collaboration between academia, industry, and government institutions will be crucial for accelerating the translation of research findings into commercialized products. Investment in infrastructure, pilot-scale production facilities, and collaborative research initiatives will facilitate the transition of polymeric electrode materials from the laboratory to the marketplace. Ultimately, the continued advancement of polymeric electrode materials holds immense potential to drive innovation in energy storage technology and address the growing demand for high-performance LIBs in a wide range of applications.

### Author contributions

Conceptualization and Methodology: F.B. and H.J.Y. Investigation: F.B., S.U.S and A.L.L. Writing-Original Draft: F.B. and S.U.S. Writing-Review & Editing: F.B. S.U.S., and H.J.Y. Visualization: F.B. Supervision: H.J.Y. All authors discussed the results and reviewed the manuscript.

### Conflicts of interest

There are no conflicts to declare.

### Acknowledgements

F. B. acknowledges the postdoctoral fellowship program supported by Academia Sinica (AS-PD-11201-M04). H.-J. Yen acknowledges the financial support by Ministry of Science and Technology in Taiwan (MOST 110-2124-M-001-001) and National Science and Technology Council (NSTC 112-2113-M-001-012).

### Notes and references

1. Y. Ding, Z. P. Cano, A. Yu, J. Lu and Z. Chen, *Electrochem. Energy Rev.*, 2019, **2**, 1-28.
2. J. Xie and Y.-C. Lu, *Nat. Commun.*, 2020, **11**, 2499.
3. C. N. Gannett, L. Melecio-Zambrano, M. J. Theibault, B. M. Peterson, B. P. Fors and H. D. Abruña, *Mater. Rep. Energy*, 2021, **1**, 100008.
4. T. Wulandari, D. Fawcett, S. B. Majumder and G. E. J. Poinern, *Battery Energy*, 2023, **2**, 20230030.
5. C. P. Grey and D. S. Hall, *Nat. Commun.*, 2020, **11**, 6279.
6. A. Manthiram, *Nat. Commun.*, 2020, **11**, 1550.
7. B. Dunn, H. Kamath and J.-M. Tarascon, *Science*, 2011, **334**, 928-935.
8. J. B. Goodenough and K.-S. Park, *J. Am. Chem. Soc.*, 2013, **135**, 1167-1176.
9. C. Liu, Z. G. Neale and G. Cao, *Mater. Today*, 2016, **19**, 109-123.
10. A. Saxena, N. Gnanaseelan, S. K. Kamaraj and F. Caballero-Briones, in *Rechargeable Lithium-Ion Batteries*, CRC Press, 2020, pp. 260-288.
11. J. M. Tarascon and M. Armand, *Nature*, 2001, **414**, 359-367.
12. H. Kye, Y. Kang, D. Jang, J. E. Kwon and B.-G. Kim, *Adv. Energy Sust. Res.*, 2022, **3**, 2200030.
13. J. Li, C. Lin, M. Weng, Y. Qiu, P. Chen, K. Yang, W. Huang, Y. Hong, J. Li, M. Zhang, C. Dong, W. Zhao, Z. Xu, X. Wang, K. Xu, J. Sun and F. Pan, *Nat. Nanotech.*, 2021, **16**, 599-605.
14. B. Tao, I. J. McPherson, E. Daviddi, C. L. Bentley and P. R. Unwin, *ACS Sust. Chem. Eng.*, 2023, **11**, 1459-1471.
15. D. D. MacNeil, Z. Lu and J. R. Dahn, *J. Electrochem. Soc.*, 2002, **149**, A1332.
16. M. V. Reddy, G. V. Subba Rao and B. V. R. Chowdari, *Chem. Rev.*, 2013, **113**, 5364-5457.
17. F. Wu, J. Maier and Y. Yu, *Chem. Soc. Rev.*, 2020, **49**, 1569-1614.
18. S. Gantenbein, M. Schönleber, M. Weiss and E. Ivers-Tiffée, *Molecules*, 2019, **11**.
19. C. Zeng, F. Fan, R. Zheng, X. Wang, G. Tian, S. Liu, P. Liu, C. Wang, S. Wang and C. Shu, *ACS Appl. Mater. Interfaces*, 2024, **16**, 11377-11388.
20. B. Xu, D. Qian, Z. Wang and Y. S. Meng, *Mater. Sci. Eng. Rep.*, 2012, **73**, 51-65.
21. S. Zhao, K. Yan, J. Zhang, B. Sun and G. Wang, *Angew. Chem. Int. Ed.*, 2021, **60**, 2208-2220.
22. K. Amin, L. Mao and Z. Wei, *Macromol. Rapid Commun.*, 2019, **40**, 1800565.
23. Z. Song and H. Zhou, *Energy Environ. Sci.*, 2013, **6**, 2280-2301.
24. H. Ji, J. Wu, Z. Cai, J. Liu, D.-H. Kwon, H. Kim, A. Urban, J. K. Papp, E. Foley, Y. Tian, M. Balasubramanian, H. Kim, R. J. Clément, B. D. McCloskey, W. Yang and G. Ceder, *Nat. Energy*, 2020, **5**, 213-221.
25. M. Malik, K. H. Chan and G. Azimi, *Mater. Today Energy*, 2022, **28**, 101066.
26. K. Liu, Y. Liu, D. Lin, A. Pei and Y. Cui, *Sci. Adv.*, **4**, eaas9820.
27. B. Häupler, A. Wild and U. S. Schubert, *Adv. Energy Mater.*, 2015, **5**, 1402034.
28. P. Poizot, J. Gaubicher, S. Renault, L. Dubois, Y. Liang and Y. Yao, *Chem. Rev.*, 2020, **120**, 6490-6557.
29. W. Du, X. Du, M. Ma, S. Huang, X. Sun and L. Xiong, *Adv. Funct. Mater.*, 2022, **32**, 2110871.
30. S. Lee, J. E. Kwon, J. Hong, S. Y. Park and K. Kang, *J. Mater. Chem. A*, 2019, **7**, 11438-11443.
31. A. Wild, M. Strumpf, B. Häupler, M. D. Hager and U. S. Schubert, *Adv. Energy Mater.*, 2017, **7**, 1601415.
32. L. M. Zhu, A. W. Lei, Y. L. Cao, X. P. Ai and H. X. Yang, *Chem. Commun.*, 2013, **49**, 567-569.
33. K. Hatakeyama-Sato, T. Tezuka, R. Ichinoi, S. Matsumono, K. Sadakuni and K. Oyaizu, *ChemSusChem*, 2020, **13**, 2443-2448.
34. É. Deunf, P. Moreau, É. Quarez, D. Guyomard, F. Dolhem and P. Poizot, *J. Mater. Chem. A*, 2016, **4**, 6131-6139.
35. D. Larcher and J.-M. Tarascon, *Nat. Chem.*, 2015, **7**, 19-29.
36. M. E. Baumert, V. Le, P.-H. Su, Y. Akae, D. Bresser, P. Théato and M. M. Hansmann, *J. Am. Chem. Soc.*, 2023, **145**, 23334-23345.
37. D. J. Min, K. Lee, S. Y. Park and J. E. Kwon, *ChemSusChem*, 2020, **13**, 2303-2311.
38. X. Liu and Z. Ye, *Adv. Energy Mater.*, 2021, **11**, 2003281.
39. Y. Hu, Y. Gao, L. Fan, Y. Zhang, B. Wang, Z. Qin, J. Zhou and B. Lu, *Adv. Energy Mater.*, 2020, **10**, 2002780.
40. F. Cheng, J. Liang, Z. Tao and J. Chen, *Adv. Mater.*, 2011, **23**, 1695-1715.
41. S. Lee, G. Kwon, K. Ku, K. Yoon, S. K. Jung, H. D. Lim and K. Kang, *Adv. Mater.*, 2018, **30**, 1704682.
42. X. Feng, X. Chen, B. Ren, X. Wu, X. Huang, R. Ding, X. Sun, S. Tan, E. Liu and P. Gao, *ACS Appl. Mater. Interfaces*, 2021, **13**, 7178-7187.





43. R. Chen, D. Bresser, M. Saraf, P. Gerlach, A. Balducci, S. Kunz, D. Schröder, S. Passerini and J. Chen, *ChemSusChem*, 2020, **13**, 2205-2219.
44. J. Heiska, M. Nisula and M. Karppinen, *J. Mater. Chem. A*, 2019, **7**, 18735-18758.
45. Z. Song, H. Zhan and Y. Zhou, *Angew. Chem. Int. Ed.*, 2010, **49**, 8444-8448.
46. T. Nokami, T. Matsuo, Y. Inatomi, N. Hojo, T. Tsukagoshi, H. Yoshizawa, A. Shimizu, H. Kuramoto, K. Komae and H. Tsuyama, *J. Am. Chem. Soc.*, 2012, **134**, 19694-19700.
47. S. Muench, A. Wild, C. Friebe, B. Haupler, T. Janoschka and U. S. Schubert, *Chem. Rev.*, 2016, **116**, 9438-9484.
48. J. Yang, Z. Wang, Y. Shi, P. Sun and Y. Xu, *ACS Appl. Mater. Interfaces*, 2020, **12**, 7179-7185.
49. T. Cai, Y. Han, Q. Lan, F. Wang, J. Chu, H. Zhan and Z. Song, *Energy Storage Mater.*, 2020, **31**, 318-327.
50. F. Wan, X.-L. Wu, J.-Z. Guo, J.-Y. Li, J.-P. Zhang, L. Niu and R.-S. Wang, *Nano Energy*, 2015, **13**, 450-457.
51. Y. Wang, Y. Ding, L. Pan, Y. Shi, Z. Yue, Y. Shi and G. Yu, *Nano Lett.*, 2016, **16**, 3329-3334.
52. M. Lee, J. Hong, J. Lopez, Y. Sun, D. Feng, K. Lim, W. C. Chueh, M. F. Toney, Y. Cui and Z. Bao, *Nat. Energy*, 2017, **2**, 861-868.
53. Q. Dong, T. Naren, L. Zhang, W. Jiang, M. Xue, X. Wang, L. Chen, C.-S. Lee and Q. Zhang, *Angew. Chem. Int. Ed.*, 2024, **63**, e202405426.
54. W. Guo, Y.-X. Yin, S. Xin, Y.-G. Guo and L.-J. Wan, *Energy Environ. Sci.*, 2012, **5**, 5221-5225.
55. Z. Song, T. Xu, M. L. Gordin, Y.-B. Jiang, I.-T. Bae, Q. Xiao, H. Zhan, J. Liu and D. Wang, *Nano Lett.*, 2012, **12**, 2205-2211.
56. C. Luo, Y. Zhu, Y. Xu, Y. Liu, T. Gao, J. Wang and C. Wang, *J. Power Sources*, 2014, **250**, 372-378.
57. C. Peng, G.-H. Ning, J. Su, G. Zhong, W. Tang, B. Tian, C. Su, D. Yu, L. Zu, J. Yang, M.-F. Ng, Y.-S. Hu, Y. Yang, M. Armand and K. P. Loh, *Nat. Energy*, 2017, **2**, 17074.
58. K. B. Labasan, H.-J. Lin, F. Baskoro, J. J. H. Togonon, H. Q. Wong, C.-W. Chang, S. D. Arco and H.-J. Yen, *ACS Appl. Mater. Interfaces*, 2021, **13**, 17467-17477.
59. J. Wang, H. Liu, C. Du, X. Zhang, Y. Liu, H. Yao, Z. Sun and S. Guan, *Chem. Eng. J.*, 2022, **444**, 136598.
60. X.-y. Han, C.-x. Chang, L.-j. Yuan, T.-l. Sun and J. Sun, *Adv. Mater.*, 2007, **19**, 1616-1621.
61. J. Kim, J. H. Kim and K. Ariga, *Joule*, 2017, **1**, 739-768.
62. F. Baskoro, A. L. Lubis, H. Q. Wong, G.-S. Liou and H.-J. Yen, *J. Mater. Chem. A*, 2023, **11**, 11210-11221.
63. F. Baskoro, H.-J. Lin, C.-W. Chang, C.-L. Wang, A. L. Lubis and H.-J. Yen, *J. Mater. Chem. A*, 2023, **11**, 569-578.
64. A. L. Lubis, F. Baskoro, T.-H. Lin, H. Q. Wong, G.-S. Liou and H.-J. Yen, *ACS Appl. Mater. Interfaces*, 2024, **16**, 48722-48735.
65. J. Sun, Y. Xu, Y. Lv, Q. Zhang and X. Zhou, *CCS Chem.*, 2023, **5**, 1259-1276.
66. M. Majumder, A. K. Thakur, A. S. Patole and S. P. Patole, in *Organic Electrodes: Fundamental to Advanced Emerging Applications*, ed. R. K. Gupta, Springer International Publishing, Cham, 2022, pp. 171-188.
67. Z. Yang, F. Wang, P. Meng, J. Luo and C. Fu, *Energy Storage Mater.*, 2022, **51**, 63-79.
68. F. Goto, K. Abe, K. Ikabayashi, T. Yoshida and H. Morimoto, *J. Power Sources*, 1987, **20**, 243-248.
69. M. Kobayashi, N. Colaneri, M. Boysel, F. Wudl and A. J. Heeger, *J. Chemical Phys.*, 1985, **82**, 5717-5723.
70. S. Taguchi and T. Tanaka, *J. Power Sources*, 1987, **20**, 249-252.
71. L. W. Shacklette, R. L. Elsenbaumer, R. R. Chance, J. M. Sowa, D. M. Ivory, G. G. Miller and R. H. Baughman, *J. Am. Chem. Soc.*, 1982, **104**, 361-362.
72. K. Nakahara, S. Iwasa, M. Satoh, Y. Morioka, J. Iriyama, M. Suguro and E. Hasegawa, *Chem. Phys. Lett.*, 2002, **359**, 351-354.
73. W. Choi, D. Harada, K. Oyaizu and H. Nishide, *J. Am. Chem. Soc.*, 2011, **133**, 19839-19843.
74. T. Suga, M. Sakata, K. Aoki and H. Nishide, *ACS Macro Lett.*, 2014, **3**, 703-707.
75. Z. Song, Y. Qian, M. L. Gordin, D. Tang, T. Xu, M. Otani, H. Zhan, H. Zhou and D. Wang, *Angew. Chem.*, 2015, **127**, 14153-14157.
76. K. Zhang, C. Guo, Q. Zhao, Z. Niu and J. Chen, *Adv. Sci.*, 2015, **2**, 1500018.
77. J. E. Kwon, C.-S. Hyun, Y. J. Ryu, J. Lee, D. J. Min, M. J. Park, B.-K. An and S. Y. Park, *J. Mater. Chem. A*, 2018, **6**, 3134-3140.
78. W. Huang, Z. Zhu, L. Wang, S. Wang, H. Li, Z. Tao, J. Shi, L. Guan and J. Chen, *Angew. Chem. Int. Ed.*, 2013, **52**, 9162-9166.
79. H. Senoh, M. Yao, H. Sakaebe, K. Yasuda and Z. Siroma, *Electrochim. Acta*, 2011, **56**, 10145-10150.
80. Y. Liang, P. Zhang, S. Yang, Z. Tao and J. Chen, *Adv. Energy Mater.*, 2013, **3**, 600-605.
81. Q. Zhao, J. Wang, C. Chen, T. Ma and J. Chen, *Nano Res.*, 2017, **10**, 4245-4255.
82. Y. Shi, H. Tang, S. Jiang, L. V. Kayser, M. Li, F. Liu, F. Ji, D. J. Lipomi, S. P. Ong and Z. Chen, *Chem. Mater.*, 2018, **30**, 3508-3517.
83. M. Lee, J. Hong, B. Lee, K. Ku, S. Lee, C. B. Park and K. Kang, *Green Chem.*, 2017, **19**, 2980-2985.
84. G. Dai, X. Wang, Y. Qian, Z. Niu, X. Zhu, J. Ye, Y. Zhao and X. Zhang, *Energy Storage Mater.*, 2019, **16**, 236-242.
85. J. Kim, H.-S. Park, T.-H. Kim, S. Y. Kim and H.-K. Song, *Phys. Chem. Chem. Phys.*, 2014, **16**, 5295-5300.
86. M. Yao, H. Senoh, T. Sakai and T. Kiyobayashi, *J. Power Sources*, 2012, **202**, 364-368.
87. C. Zhang, X. Yang, W. Ren, Y. Wang, F. Su and J.-X. Jiang, *J. Power Sources*, 2016, **317**, 49-56.
88. C. Su, F. Yang, L. Ji, L. Xu and C. Zhang, *J. Mater. Chem. A*, 2014, **2**, 20083-20088.
89. K. Lee, I. E. Serdiuk, G. Kwon, D. J. Min, K. Kang, S. Y. Park and J. E. Kwon, *Energy Environ. Sci.*, 2020, **13**, 4142-4156.
90. M. Li, R. Wang, T. Wu, Y. Liu, Y. Chen, W. He, S. Feng, X. Zhang, G. Dai and Y. Zhao, *ACS Appl. Energy Mater.*, 2023, **6**, 6834-6841.
91. H. Park, H. Kye, J.-S. Lee, Y.-C. Joo, D. J. Min, B.-G. Kim, S. Y. Park and J. E. Kwon, *Energy Environ. Mater.*, 2024, **7**, e12694.
92. S. Lee, G. Kwon, T. Kang, J. Kim, B. Lee, C. Kim, C. Lee, Y. Kim, J. Noh, Y.-S. Yu, D. Lee and K. Kang, *J. Mater. Chem.*, 2023, **11**, 22441-22448.
93. M. S. Whittingham, *Chem. Rev.*, 2004, **104**, 4271-4302.
94. J. Xu, X. Cai, S. Cai, Y. Shao, C. Hu, S. Lu and S. Ding, *Energy Environ. Mater.*, 2023, **6**, e12450.
95. M. S. Whittingham, *Chem. Rev.*, 2014, **114**, 11414-11443.
96. S. V. Venkatesan, A. Nandy, K. Karan, S. R. Larter and V. Thangadurai, *Electrochem. Energy Rev.*, 2022, **5**, 16.
97. R. Hildner, A. Köhler, P. Müller-Buschbaum, F. Panzer and M. Thelakkat, *Adv. Energy Mater.*, 2017, **7**, 1700314.
98. S. Wang, G. Zuo, J. Kim and H. Siringhaus, *Prog. Polym. Sci.*, 2022, **129**, 101548.
99. H. Sun, F. Chen and Z.-K. Chen, *Mater. Today*, 2019, **24**, 94-118.



100. J.-H. Dou, Z.-A. Yu, J. Zhang, Y.-Q. Zheng, Z.-F. Yao, Z. Tu, X. Wang, S. Huang, C. Liu, J. Sun, Y. Yi, X. Cao, Y. Gao, J.-Y. Wang and J. Pei, *J. Am. Chem. Soc.*, 2019, **141**, 6561-6568.
101. C. Bian, S. Wang, Y. Liu and X. Jing, *RSC Adv.*, 2016, **6**, 55007-55016.
102. A. Onwubiko, W. Yue, C. Jellett, M. Xiao, H.-Y. Chen, M. K. Ravva, D. A. Hanifi, A.-C. Knall, B. Purushothaman, M. Nikolka, J.-C. Flores, A. Salleo, J.-L. Bredas, H. Sirringhaus, P. Hayoz and I. McCulloch, *Nat. Commun.*, 2018, **9**, 416.
103. H. Usta, C. Risko, Z. Wang, H. Huang, M. K. Delimeroglu, A. Zhukhovitskiy, A. Facchetti and T. J. Marks, *J. Am. Chem. Soc.*, 2009, **131**, 5586-5608.
104. S. Fratini, M. Nikolka, A. Salleo, G. Schweicher and H. Sirringhaus, *Nat. Mater.*, 2020, **19**, 491-502.
105. S. Prodhon, J. Qiu, M. Ricci, O. M. Roscioni, L. Wang and D. Beljonne, *J. Phys. Chem. Lett.*, 2020, **11**, 6519-6525.
106. K. H. Hendriks, W. Li, M. M. Wienk and R. A. J. Janssen, *J. Am. Chem. Soc.*, 2014, **136**, 12130-12136.
107. H. Bronstein, C. B. Nielsen, B. C. Schroeder and I. McCulloch, *Nat. Rev. Chem.*, 2020, **4**, 66-77.
108. S. Bitton and N. Tessler, *Adv. Electron. Mater.*, 2024, **n/a**, 2300766.
109. K. D. Fong, J. Self, K. M. Diederichsen, B. M. Wood, B. D. McCloskey and K. A. Persson, *ACS Central Sci.*, 2019, **5**, 1250-1260.
110. T. Junkers, J. Vandenberg, P. Adriaensens, L. Lutsen and D. Vanderzande, *Polym. Chem.* 2012, **3**, 275-285.
111. A. Chamas, H. Moon, J. Zheng, Y. Qiu, T. Tabassum, J. H. Jang, M. Abu-Omar, S. L. Scott and S. Suh, *ACS Sust. Chem. Eng.*, 2020, **8**, 3494-3511.
112. T. L. D. Tam, M. Lin, S. W. Chien and J. Xu, *ACS Macro Lett.*, 2021, **11**, 110-115.
113. A. Dai, A. Wan, C. Magee, Y. Zhang, S. Barlow, S. R. Marder and A. Kahn, *Org. Electron.*, 2015, **23**, 151-157.
114. I. M. Ward and J. Sweeney, *Mechanical properties of solid polymers*, John Wiley & Sons, 2012.
115. H.-Y. Wu, J.-D. Huang, S. Y. Jeong, T. Liu, Z. Wu, T. van der Pol, Q. Wang, M.-A. Stoeckel, Q. Li and M. Fahlman, *Mater. Horiz.*, 2023, **10**, 4213-4223.
116. L. Bondi, C. Marzuoli, E. Gutiérrez-Fernández, G. Tullii, J. Martín, B. Fraboni, D. Mecerreyes, M. R. Antognazza and T. Cramer, *Adv. Electron. Mater.*, 2023, **9**, 2300146.
117. J. K. Feng, Y. L. Cao, X. P. Ai and H. X. Yang, *J. Power Sources*, 2008, **177**, 199-204.
118. Z. Chen, C. Su, X. Zhu, R. Xu, L. Xu and C. Zhang, *J. Polym. Sci. Part A: Polym. Chem.*, 2018, **56**, 2574-2583.
119. I. K. Yakushchenko, M. G. Kaplunov, O. N. Efimov, M. Yu. Belov and S. N. Shamaev, *Phys. Chem. Chem. Phys.*, 1999, **1**, 1783-1785.
120. C. Zhang, S. Chen, G. Zhou, Q. Hou, S. Luo, Y. Wang and G. Shi, *J. Electrochem. Soc.*, 2021, **168**, 050548.
121. C. Su, H. He, L. Xu, K. Zhao, C. Zheng and C. Zhang, *J. Mater. Chem. A*, 2017, **5**, 2701-2709.
122. K. Yamamoto, D. Suemasa, K. Masuda, K. Aita and T. Endo, *ACS Appl. Mater. Interfaces*, 2018, **10**, 6346-6353.
123. Z. Chen, W. Li, Y. Dai, N. Xu, C. Su, J. Liu and C. Zhang, *Electrochim. Acta*, 2018, **286**, 187-194.
124. Y. Ou, Y. Xiong, Z. Hu, Y. Zhang and L. Dong, *J. Mater. Chem. A*, 2022, **10**, 10373-10382.
125. X. Zhao, C. Wang, Z. Li, X. Hu, A. A. Razaq and Z. Deng, *J. Mater. Chem. A*, 2021, **9**, 19282-19297.
126. Y. Liang, Z. Tao and J. Chen, *Adv. Energy Mater.*, 2012, **2**, 742-769. DOI: 10.1039/D4TA06028H
127. P. Sang, Q. Chen, D.-Y. Wang, W. Guo and Y. Fu, *Chem. Rev.*, 2023, **123**, 1262-1326.
128. X. Zhang, W. Guo and Y. Fu, *Acc. Mater. Res.*, 2024, **5**, 316-328.
129. M. A. Weret, C.-F. J. Kuo, W.-N. Su, T. S. Zeleke, C.-J. Huang, N. A. Sahalie, T. A. Zegeye, Z. T. Wondimkun, F. W. Fenta, B. A. Jote, M.-C. Tsai and B. J. Hwang, *J. Power Sources*, 2022, **541**, 231693.
130. Y. Chen, S. Zhuo, Z. Li and C. Wang, *EnergyChem*, 2020, **2**, 100030.
131. D.-Y. Wang, W. Guo and Y. Fu, *Acc. Chem. Res.*, 2019, **52**, 2290-2300.
132. W. Guo, D. Y. Wang, Q. Chen and Y. Fu, *Adv. Sci.*, 2022, **9**, 2103989.
133. M. J. H. Worthington, R. L. Kucera and J. M. Chalker, *Green Chem.*, 2017, **19**, 2748-2761.
134. J. Ren, X. Wang, H. Liu, Y. Hu, X. Zhang and T. Masuda, *React. Funct. Polym.*, 2020, **146**, 104365.
135. T. P. Vaid, M. E. Easton and R. D. Rogers, *Synth. Met.*, 2017, **231**, 44-50.
136. D. Ogi, Y. Fujita, M. Kato, T. Yamauchi, T. Shirahata, M. Yao and Y. Misaki, *Eur. J. Org. Chem.*, 2019, **2019**, 2725-2728.
137. J. Tang, L. Kong, J. Zhang, L. Zhan, H. Zhan, Y. Zhou and C. Zhan, *React. Funct. Polym.*, 2008, **68**, 1408-1413.
138. L. Zhan, Z. Song, N. Shan, J. Zhang, J. Tang, H. Zhan, Y. Zhou, Z. Li and C. Zhan, *J. Power Sources*, 2009, **193**, 859-863.
139. M. E. Speer, M. Kolek, J. J. Jassoy, J. Heine, M. Winter, P. M. Bieker and B. Esser, *Chem. Commun.*, 2015, **51**, 15261-15264.
140. F. A. Obrezkov, A. F. Shestakov, S. G. Vasil'ev, K. J. Stevenson and P. A. Troshin, *J. Mater. Chem. A*, 2021, **9**, 2864-2871.
141. I. Kang, T. Lee, Y. R. Yoon, J. W. Kim, B.-K. Kim, J. Lee, J. H. Lee and S. Y. Kim, *Mater.*, 2021, **14**, 7885.
142. W. Huang, T. Jia, G. Zhou, S. Chen, Q. Hou, Y. Wang, S. Luo, G. Shi and B. Xu, *Electrochim. Acta*, 2018, **283**, 1284-1290.
143. C. Su, X. Zhu, L. Xu, N. Zhou, H. He and C. Zhang, *Electrochim. Acta*, 2016, **196**, 440-449.
144. L. Zhu and X. Cao, *Mater. Lett.*, 2015, **150**, 16-19.
145. C. Su, L. Ji, L. Xu, N. Zhou, G. Wang and C. Zhang, *RSC Adv.*, 2016, **6**, 22989-22995.
146. J. Xiong, Z. Wei, T. Xu, Y. Zhang, C. Xiong and L. Dong, *Polym.*, 2017, **130**, 135-142.
147. T. Xu, J. Xiong, X. Du, Y. Zhang, S. Song, C. Xiong and L. Dong, *J. Phys. Chem. C*, 2018, **122**, 20057-20063.
148. J. Ren, X. Wang, H. Liu, Y. Hu, X. Zhang and T. Masuda, *React. Funct. Polym.*, 2020, **146**, 104365.
149. D. Ogi, Y. Fujita, M. Kato, T. Yamauchi, T. Shirahata, M. Yao and Y. Misaki, *Eur. J. Org. Chem.*, 2019, **2019**, 2725-2728.
150. B. Häupler, R. Burges, C. Friebe, T. Janoschka, D. Schmidt, A. Wild and U. S. Schubert, *Macromol. Rapid Commun.*, 2014, **35**, 1367-1371.
151. R. F. Nelson, D. W. Leedy, E. T. Seo and R. N. Adams, *Fresenius' Z. Anal. Chem.*, 1966, **224**, 184-196.
152. S. Muench, A. Wild, C. Friebe, B. Häupler, T. Janoschka and U. S. Schubert, *Chem. Rev.*, 2016, **116**, 9438-9484.
153. T. Janoschka, M. D. Hager and U. S. Schubert, *Adv. Mater.*, 2012, **24**, 6397-6409.
154. J. Xie, P. Gu and Q. Zhang, *ACS Energy Lett.*, 2017, **2**, 1985-1996.
155. Z. Niu, H. Wu, L. Liu, G. Dai, S. Xiong, Y. Zhao and X. Zhang, *J. Mater. Chem. A*, 2019, **7**, 10581-10588.





156. C. N. Gannett, B. M. Peterson, L. Melecio-Zambrano, C. Q. Trainor, B. P. Fors and H. D. Abruña, *J. Mater. Chem. A*, 2021, **9**, 5657-5663.
157. L. Huang, Y. Chen, Y. Liu, T. Wu, H. Li, J. Ye, G. Dai, X. Zhang and Y. Zhao, *ACS Sust. Chem. Eng.*, 2020, **8**, 17868-17875.
158. L. J. Fetters, D. J. Lohse, D. Richter, T. A. Witten and A. Zirkel, *Macromol.*, 1994, **27**, 4639-4647.
159. D. Golodnitsky, E. Strauss, E. Peled and S. Greenbaum, *J. Electrochem. Soc.*, 2015, **162**, A2551.
160. E. B. Trigg, T. W. Gaines, M. Maréchal, D. E. Moed, P. Rannou, K. B. Wagener, M. J. Stevens and K. I. Winey, *Nat. Mater.*, 2018, **17**, 725-731.
161. M. Kolek, F. Otteny, P. Schmidt, C. Mück-Lichtenfeld, C. Einholz, J. Becking, E. Schleicher, M. Winter, P. Bieker and B. Esser, *Energy Environ. Sci.*, 2017, **10**, 2334-2341.
162. F. Otteny, V. Perner, D. Wassy, M. Kolek, P. Bieker, M. Winter and B. Esser, *ACS Sust. Chem. Eng.*, 2020, **8**, 238-247.
163. H. Kye, Y. Kang, D. Jang, J. E. Kwon and B.-G. Kim, *Adv. Energy Sustain. Res.*, 2022, **3**, 2200030.
164. M. Kolek, F. Otteny, J. Becking, M. Winter, B. Esser and P. Bieker, *Chem. Mater.*, 2018, **30**, 6307-6317.
165. P. Sang, Y. Si and Y. Fu, *Chem. Commun.*, 2019, **55**, 4857-4860.
166. M. B. Preefer, B. Oschmann, C. J. Hawker, R. Seshadri and F. Wudl, *Angew. Chem. Int. Ed.*, 2017, **56**, 15118-15122.
167. Y. Jing, Y. Liang, S. Gheyhani and Y. Yao, *Nano Energy*, 2017, **37**, 46-52.
168. B. Häupler, T. Hagemann, C. Friebe, A. Wild and U. S. Schubert, *ACS Appl. Mater. Interfaces*, 2015, **7**, 3473-3479.
169. A. Bhargav, M. E. Bell, Y. Cui and Y. Fu, *ACS Appl. Energy Mater.*, 2018, **1**, 5859-5864.
170. P. Sang, J. Song, W. Guo and Y. Fu, *Chem. Eng. J.*, 2021, **415**, 129043.
171. A. Bhargav, C.-H. Chang, Y. Fu and A. Manthiram, *ACS Appl. Mater. Interfaces*, 2019, **11**, 6136-6142.
172. S. H. Je, T. H. Hwang, S. N. Talapaneni, O. Buyukcakir, H. J. Kim, J.-S. Yu, S.-G. Woo, M. C. Jang, B. K. Son, A. Coskun and J. W. Choi, *ACS Energy Lett.*, 2016, **1**, 566-572.
173. H. Kim, J. Lee, H. Ahn, O. Kim and M. J. Park, *Nat. Commun.*, 2015, **6**, 7278.
174. S. Zeng, L. Li, D. Zhao, J. Liu, W. Niu, N. Wang and S. Chen, *J. Phys. Chem. C*, 2017, **121**, 2495-2503.
175. G. Dai, Y. Liu, Z. Niu, P. He, Y. Zhao, X. Zhang and H. Zhou, *Matter.*, 2019, **1**, 945-958.
176. C. N. Gannett, B. M. Peterson, L. Shen, J. Seok, B. P. Fors and H. D. Abruña, *ChemSusChem*, 2020, **13**, 2428-2435.
177. Y. Wang, Y. Huang, Y. Hua, Y. Du and H. Yang, *New J. Chem.*, 2022, **46**, 14314-14317.
178. S. Xu, H. Dai, S. Zhu, Y. Wu, M. Sun, Y. Chen, K. Fan, C. Zhang, C. Wang and W. Hu, *eScience*, 2021, **1**, 60-68.
179. F. A. Obrezkov, A. I. Somova, E. S. Fedina, S. G. Vasil'ev, K. J. Stevenson and P. A. Troshin, *Energy Technol.*, 2021, **9**, 2000772.
180. X. Zhao, X. Qiu, H. Xue, S. Liu, D. Liang, C. Yan, W. Chen, Y. Wang and G. Zhou, *Angew. Chem.*, 2023, **135**, e202216713.
181. Q. He, S. Lv, Y. Huang, J. Guo, X. Peng, Y. Du and H. Yang, *RSC Adv.*, 2023, **13**, 12464-12468.
182. R. R. Kapaev, I. S. Zhidkov, E. Z. Kurmaev, K. J. Stevenson and P. A. Troshin, *J. Mater. Chem. A*, 2019, **7**, 22596-22603.
183. J. Wang, J. C. Z. En, S. N. Riduan and Y. Zhang, *Chem. Eur. J.*, 2020, **26**, 2581-2585.
184. S. Lee, J. Hong, S.-K. Jung, K. Ku, G. Kwon, W. M. Seong, H. Kim, G. Yoon, I. Kang, K. Hong, H. W. Jang and K. Kang, *Energy Storage Mater.*, 2019, **20**, 462-469.
185. A. Wild, M. Strumpf, B. Häupler, M. D. Hager and U. S. Schubert, *Adv. Energy Mater.*, 2017, **7**, 1601415.
186. M. Yao, H. Sano, H. Ando and T. Kiyobayashi, *Sci. Rep.*, 2015, **5**, 10962.
187. F. Wang, J. Wang, G. Li, Z. Guo, J. Chu, X. Ai and Z. Song, *Energy Storage Mater.*, 2022, **50**, 658-667.
188. Z. Wang, A. Duan, W. Jin, X. Huang and Y. Li, *J. Mater. Chem. A*, 2022, **10**, 10026-10032.
189. S. M. Beladi-Mousavi, S. Sadaf, A. M. Mahmood and L. Walder, *ACS Nano*, 2017, **11**, 8730-8740.
190. M. Lee, J. Hong, D.-H. Seo, D. H. Nam, K. T. Nam, K. Kang and C. B. Park, *Angew. Chem. Int. Ed.*, 2013, **52**, 8322-8328.
191. H. Banda, D. Damien, K. Nagarajan, A. Raj, M. Hariharan and M. M. Shaijumon, *Adv. Energy Mater.*, 2017, **7**, 1701316.
192. T. Škorjanc, D. Shetty, M. A. Olson and A. Trabolsi, *ACS Appl. Mater. Interfaces*, 2019, **11**, 6705-6716.
193. K. Madasamy, D. Velayutham, V. Suryanarayanan, M. Kathiresan and K.-C. Ho, *J. Mater. Chem. C*, 2019, **7**, 4622-4637.
194. M. Kathiresan, B. Ambrose, N. Angulakshmi, D. E. Mathew, D. Sujatha and A. M. Stephan, *J. Mater. Chem. A*, 2021, **9**, 27215-27233.
195. V. Kolivoška, M. Gál, L. Pospíšil, M. Valášek and M. Hromadová, *Phys. Chem. Chem. Phys.*, 2011, **13**, 11422-11429.
196. W. Haiss, H. van Zalinge, H. Höbenreich, D. Bethell, D. J. Schiffrin, S. J. Higgins and R. J. Nichols, *Langmuir*, 2004, **20**, 7694-7702.
197. Z. Wang, A. Duan, W. Jin, X. Huang and Y. Li, *J. Mater. Chem. A*, 2022, **10**, 10026-10032.
198. M. Stolar, C. Reus and T. Baumgartner, *Adv. Energy Mater.*, 2016, **6**, 1600944.
199. T. Xia, T. Zhu, Y. Miao and X. Zhao, *ACS Appl. Energy Mater.*, 2022, **5**, 6980-6985.
200. T. Ma, L. Liu, J. Wang, Y. Lu and J. Chen, *Angew. Chem. Int. Ed.*, 2020, **59**, 11533-11539.
201. M. J. Lacey, J. T. Frith and J. R. Owen, *Electrochem. Commun.*, 2013, **26**, 74-76.
202. H. Nishide and K. Oyaizu, *Science*, 2008, **319**, 737-738.
203. J. Qu, T. Katsumata, M. Satoh, J. Wada, J. Igarashi, K. Mizoguchi and T. Masuda, *Chem. Eur. J.*, 2007, **13**, 7965-7973.
204. H. Nishide, S. Iwasa, Y.-J. Pu, T. Suga, K. Nakahara and M. Satoh, *Electrochim. Acta*, 2004, **50**, 827-831.
205. Y. Ji, K. Yang, M. Liu, S. Chen, X. Liu, B. Yang, Z. Wang, W. Huang, Z. Song and S. Xue, *Adv. Funct. Mater.*, 2021, **31**, 2104830.
206. A. Yu, C. Li, X. Chen, C. Zhang, S. Mei and C. J. Yao, *ChemSusChem*, 2024, **17**, e202301809.
207. W. Sun, C. Zhou, Y. Fan, Y. He, H. Zhang, Z. Quan, H. Kong, F. Fu, J. Qin and Y. Shen, *Angew. Chem.*, 2023, **135**, e202300158.
208. S. Yeşilot, F. Hacivelioglu, S. Küçükköylü, E. Demir, K. B. Celik and R. Demir-Cakan, *Polym. Adv. Technol.*, 2019, **30**, 2977-2982.
209. H. Byeon, B. Gu, H.-J. Kim, J. H. Lee, I. Seo, J. Kim, J. W. Yang and J.-K. Kim, *Chem. Eng. J.*, 2021, **413**, 127402.
210. T. Zhou, W. Jin, W. Xue, B. Dai, C. Feng, X. Huang, P. Théato and Y. Li, *J. Power Sources*, 2021, **483**, 229136.
211. K. Zhang, Y. Hu, L. Wang, J. Fan, M. J. Monteiro and Z. Jia, *Polym. Chem.*, 2017, **8**, 1815-1823.
212. W. Deng, W. Shi, Q. Liu, J. Jiang, Q. Wang and C. Guo, *J. Power Sources*, 2020, **479**, 228796.
213. J.-K. Kim, *J. Power Sources*, 2020, **477**, 228670.



214. Y. Chen, Y. Zhang, X. Liu, X. Fan, B. Bai, K. Yang, Z. Liang, Z. Zhang and K. Mai, *Macromol. Rapid Commun.*, 2018, **39**, 1800195.
215. A. Gopinath and A. S. Nasar, *Polym.*, 2019, **178**, 121601.
216. N. Hergué, B. Ernoult, A. Minoia, R. Lazzaroni, J.-F. Gohy, P. Dubois and O. Coulembier, *Batter. Supercaps*, 2018, **1**, 102-109.
217. W. Jin, T. Zhou, Z. Wang, W. Xue, C. Feng, F. Zhang, X. Huang, D. Yang, P. Théato and Y. Li, *J. Power Sources*, 2021, **511**, 230363.
218. K. Zhang, Y. Hu, L. Wang, M. J. Monteiro and Z. Jia, *ACS Appl. Mater. Interfaces*, 2017, **9**, 34900-34908.
219. Y. Xie, K. Zhang, Y. Yamauchi, K. Oyaizu and Z. Jia, *Mater. Horiz.*, 2021, **8**, 803-829.
220. T. Suga, Y.-J. Pu, S. Kasatori and H. Nishide, *Macromol.*, 2007, **40**, 3167-3173.
221. T. Suga, S. Sugita, H. Ohshiro, K. Oyaizu and H. Nishide, *Adv. Mater.*, 2011, **6**, 751-754.
222. J. C. Barbosa, A. Fidalgo-Marijuan, J. C. Dias, R. Gonçalves, M. Salado, C. M. Costa and S. Lanceros-Méndez, *Energy Storage Mater.*, 2023, **60**, 102841.
223. H. Nishide and T. Suga, *Electrochem. Soc. Interface*, 2005, **14**, 32.
224. M. Suguro, S. Iwasa, Y. Kusachi, Y. Morioka and K. Nakahara, *Macromol. Rapid Commun.*, 2007, **28**, 1929-1933.
225. K. Nakahara, J. Iriyama, S. Iwasa, M. Suguro, M. Satoh and E. J. Cairns, *J. Power Sources*, 2007, **165**, 398-402.
226. J.-K. Kim, Y. Kim, S. Park, H. Ko and Y. Kim, *Energy Environ. Sci.*, 2016, **9**, 1264-1269.
227. K. Koshika, N. Sano, K. Oyaizu and H. Nishide, *Macromol. Chem. Phys.*, 2009, **210**, 1989-1995.
228. C. Zhang, S. Chen, G. Zhou, Q. Hou, S. Luo, Y. Wang and G. Shi, *J. Electrochem. Soc.*, 2021, **168**, 050548.
229. Y. Zhao, M. Wu, H. Zhang, Z. Ge, C. Li, Y. Ma and Y. Chen, *Energy Storage Mater.*, 2022, **47**, 141-148.
230. P. G. Bruce, S. A. Freunberger, L. J. Hardwick and J.-M. Tarascon, *Nat. Mater.*, 2012, **11**, 19-29.
231. B. Dunn, J.-M. Kamath, H. Fau - Tarascon and J. M. Tarascon, *Science*, 2011, **334**(6058), 928-35.
232. V. Etacheri, R. Marom, R. Elazari, G. Salitra and D. Aurbach, *Energy Environ. Sci.*, 2011, **4**, 3243-3262.
233. W. Wang, C. Zhao, J. Yang, P. Xiong, H. Su and Y. Xu, *Sci. China Mater.*, 2021, **64**, 2938-2948.
234. N. Cheng, L. Ren, X. Xu, Y. Du and S. X. Dou, *Mater. Today Phys.*, 2020, **15**, 100289.
235. T. Mehtab, G. Yasin, M. Arif, M. Shakeel, R. M. Korai, M. Nadeem, N. Muhammad and X. Lu, *J. Energy Storage*, 2019, **21**, 632-646.
236. G. Zhang, C. Xie, P. You and S. Li, in *Introduction to Organic Electronic Devices*, eds. G. Zhang, C. Xie, P. You and S. Li, Springer Nature Singapore, Singapore, 2022, pp. 283-307.
237. L. Wang, Y. Han, X. Feng, J. Zhou, P. Qi and B. Wang, *Coord. Chem. Rev.*, 2016, **307**, 361-381.
238. G. Xu, P. Nie, H. Dou, B. Ding, L. Li and X. Zhang, *Mater. Today*, 2017, **20**, 191-209.
239. X. Chen, W. Sun and Y. Wang, *ChemElectroChem*, 2020, **7**, 3905-3926.
240. Y. Deng, Y. Wang, X. Xiao, B. J. Saucedo, Z. Zhu, M. Xie, X. Xu, K. Yao, Y. Zhai and Z. Zhang, *Small*, 2022, **18**, 2202928.
241. H. Kong, Y. Guan, J. Wang, W. Sun, L. Chen, J. Ou, L. Xie, F. Fu, H. Zhang and H. Chen, *J. Mater. Chem. A*, 2022, **10**, 20866-20873.
242. X. Du, Z. Zhang, W. Liu and Y. Deng, *Nano Energy*, 2017, **35**, 299-320. DOI: 10.1039/D4TA06028H
243. X. Yao and Y. Zhao, *Chem.*, 2017, **2**, 171-200.
244. P. Sengodu and A. D. Deshmukh, *RSC Adv.*, 2015, **5**, 42109-42130.
245. S. Maiti, A. Pramanik, T. Dhawa and S. Mahanty, *Mater. Lett.*, 2017, **209**, 613-617.
246. L. Zhu, L. Xie and X. Cao, *ACS Appl. Mater. Interfaces*, 2018, **10**, 10909-10917.
247. J.-Y. Shi, C.-W. Yi and K. Kim, *Bull. Korean Chem. Soc.*, 2010, **31**, 2698-2700.
248. B. Wei, Y. Hong, W. Tang, M. Guo, X. He, C. Tang, J. Hu and C. Fan, *Chem. Eng. J.*, 2023, **451**, 138773.
249. C.-x. Zhang, X.-h. Chen, W.-s. Zhang, Y. Wang, S.-l. Mei, Y.-W. Zhong and C.-J. Yao, *Chem. Eng. J.*, 2024, **483**, 149198.
250. T. Liu, K. C. Kim, B. Lee, S. Jin, M. J. Lee, M. Li, S. Noda, S. S. Jang and S. W. Lee, *ACS Appl. Energy Mater.*, 2020, **3**, 3728-3735.
251. H. Guo, L. Liu, H. Shu, X. Yang, Z. Yang, M. Zhou, J. Tan, Z. Yan, H. Hu and X. Wang, *J. Power Sources*, 2014, **247**, 117-126.
252. P.-O. Schwartz, S. Förtsch, E. Mena-Osteritz, D. Weirather-Köstner, M. Wachtler and P. Bäuerle, *RSC Adv.*, 2018, **8**, 14193-14200.
253. L. Zhu, L. Xie, C. Bao, X. Yan and X. Cao, *Int. J. Energy Res.*, 2020, **44**, 298-308.
254. X. Li, X. Tang, K. Ouyang, P. Deng, L. Huang and W. Dang, *Ionics*, 2021, **27**, 4649-4661.
255. F. Wu, J. Liu, L. Li, X. Zhang, R. Luo, Y. Ye and R. Chen, *ACS Appl. Mater. Interfaces*, 2016, **8**, 23095-23104.
256. J. Yang, Y. Shi, M. Li, P. Sun and Y. Xu, *ACS Appl. Mater. Interfaces*, 2020, **12**, 32666-32672.
257. G. Hernández, N. Casado, R. Coste, D. Shanmukaraj, L. Rubatat, M. Armand and D. Mecerreyes, *RSC Adv.*, 2015, **5**, 17096-17103.
258. L. Assumma, Y. Kervella, J. M. Mouesca, M. Mendez, V. Maurel, L. Dubois, T. Gutel and S. Sadki, *ChemSusChem*, 2020, **13**, 2419-2427.
259. C.-J. Yao, J. Xie, Z. Wu, Z. J. Xu, S. Zhang and Q. Zhang, *Chem. Asian J.*, 2019, **14**, 2210-2214.
260. S. Zheng, L. Miao, T. Sun, L. Li, T. Ma, J. Bao, Z. Tao and J. Chen, *J. Mater. Chem. A*, 2021, **9**, 2700-2705.
261. H. Zhang, Y. Xie, X. Chen, T. Jia, W. Huang, S. Luo, Q. Hou, R. Zeng and Z. Sun, *J. Electrochem. Soc.*, 2017, **164**, A290.
262. S. Wang, A. M. G. Park, P. Flouda, A. D. Easley, F. Li, T. Ma, G. D. Fuchs and J. L. Lutkenhaus, *ChemSusChem*, 2020, **13**, 2371-2378.
263. P. Acker, J. S. Wössner, G. Desmaizieres and B. Esser, *ACS Sust. Chem. Eng.*, 2022, **10**, 3236-3244.
264. Z. Chen, S. Mei, W. Li, N. Xu, Y. Dong, Y. Jin, M. Ouyang and C. Zhang, *J. Mater. Chem. A*, 2021, **9**, 27010-27018.
265. J. Wang, Y. Lee, K. Tee, S. N. Riduan and Y. Zhang, *Chem. Commun.*, 2018, **54**, 7681-7684.
266. R. Akiyoshi, M. Fujiwara, Y. Kamakura, T. Shimizu, R. Inoue, Y. Morisaki, A. Saeki, H. Yoshikawa and D. Tanaka, *ACS Appl. Energy Mater.*, 2022, **5**, 12760-12767.
267. H.-C. Lin, C.-C. Li and J.-T. Lee, *J. Power Sources*, 2011, **196**, 8098-8103.
268. W.-M. Chen, L. Qie, L.-X. Yuan, S.-A. Xia, X.-L. Hu, W.-X. Zhang and Y.-H. Huang, *Electrochim. Acta*, 2011, **56**, 2689-2695.
269. Z. Peng, X. Yi, Z. Liu, J. Shang and D. Wang, *ACS Appl. Mater. Interfaces*, 2016, **8**, 14578-14585.
270. C. Liedel, X. Wang and M. Antonietti, *Nano Energy*, 2018, **53**, 536-543.



## ARTICLE

Journal Name

271. P. Acker, L. Rzesny, C. F. N. Marchiori, C. M. Araujo and B. Esser, *Adv. Funct. Mater.*, 2019, **29**, 1906436.
272. J. Wang, W. Zhang, H. Wei, X. Zhai, F. Wang, Y. Zhou, F. Tao, P. Zhai, W. Liu and Y. Liu, *Sust. Energy Fuels*, 2022, **6**, 2901-2923.
273. S. Lei, Y. Dong, Y. Dou, X. Zhang, Q. Zhang and Y. Yang, *Mater. Adv.*, 2021, **2**, 5785-5790.
274. P. Das and B. C. Thompson, *Polym. J.*, 2023, **55**, 317-341.
275. K.-L. Wang, K.-T. Chen, Y.-H. Yi, Y.-H. Hung, H.-Y. Tuan and M. Horie, *ACS Sust. Chem. Eng.*, 2020, **8**, 1043-1049.
276. V. V. Kondratiev and R. Holze, *Chem. Pap.*, 2021, **75**, 4981-5007.
277. P. Acker, L. Rzesny, C. F. N. Marchiori, C. M. Araujo and B. Esser, *Adv. Funct. Mater.*, 2019, **29**, 1906436.

View Article Online  
DOI: 10.1039/D4TA06028H

Open Access Article. Published on 12 November 2024. Downloaded on 11/22/2024 6:55:32 PM.  
This article is licensed under a Creative Commons Attribution 3.0 Unported Licence.



Journal of Materials Chemistry A Accepted Manuscript

## Data Availability Statement

View Article Online  
DOI: 10.1039/D4TA06028H

The data supporting this article have been included as **Notes and references**.

